Improvements in the PLC Systems for Smart Grids Environments

PhD Candidate:
Javier Matanza Domingo

Directed by:
Dr. Sadot Alexandres Fernández
Dr. Carlos Rodríguez-Morcillo García

Universidad Pontificia Comillas

Abstract

During recent past years there has existed an international effort to develop Smart Grid's technologies to help achieving more efficient ways of energy management. However, even though it seems clear that new smart grids should also include an information technology (IT) infrastructure, it is not so clear under what type of technologies it should be developed. One of the promising communication's technologies for smart grid's implementation is Power Line Communications (PLC). The main reason of PLC' suitability is that, since it uses the power cables as communication medium, this technology reaches all places where energy is present.

However, PLC has to deal with the fact that power lines present a very harmful environment for signal transmission due to the presence of several noisy sources and severe attenuations. These two effects reduce communications' quality.

The two main objectives of this PhD thesis are: first, propose modifications and techniques that increase the performance of current narrowband PLC standards; and second, develop a simulation tool that, considering all physical phenomena, provide the expected system's performance in terms of end-to-end communication's latencies.

In order to achieve those objectives, this PhD thesis analyses the performance of the two main narrowband PLC solutions endorsed by the industry: PRIME and G3-PLC. In general terms both solutions are very similar: both are Orthogonal Frequency Division Multiplexing-based (OFDM) and use the CENELEC-A band to modulate the information. As a main difference, G3-PLC introduces extra redundancy in the transmitted bits, which increases the quality of the communications. PRIME, however, uses a less robust scheme, which allows for higher transmission rates compared to G3-PLC (up to 7 times faster).

To obtain the communication's performance of both PRIME and G3-PLC, a Matlab simulation framework has been developed. It includes the main physical phenomena present in the PLC channel and the implementation of the transceivers following PRIME and G3-PLC specifications.

Thanks to these simulations, a considerable weaker performance of PRIME can be observed when compared to G3-PLC in terms of number of bit errors. This difference

is incremented in environments where impulsive noise is present, which is a common scenario in PLC networks. This kind of noise is very damaging in OFDM systems. The main reason for this is that the energy of the impulses is spread over all frequencies in the transmission band due to the Discrete Fourier Transform (DFT) mechanism used in the receiver.

So as to decrease the effect of impulsive noise in narrowband PLC transmissions, a compressed sensing technique modification is proposed. Thanks to a reordering of the subcarriers used for data transmission in the OFDM spectrum, an enhanced reconstruction of the impulsive component is achieved. This reordering follows a difference set pattern. This proposal is tested in the PRIME transceiver's model implemented. There, an almost complete cancellation of the impulsive noise effect is observed. An additional advantage of this technique is that redundancy included in the message is not incremented, thus data bit rates are not decreased.

Following the second objective, a network simulator is used to emulate an Advanced Meter Infrastructure (AMI) system's behaviour in terms of communications. Due to its good performance with respect to runtime and memory consumption, OMNeT++ network simulator is chosen for this task. The network simulation software uses physical performance from the previous Matlab analysis. This combined simulation framework creates an accurate modelling by taking into account both the whole communication's layer stack and the channel's effects. To the best knowledge of the author, this kind of approach has never been addressed in the literature before.

Main results obtained from network simulations show that, under impulsive environments, communication's latencies are too high to implement a tele-metering application using narrow band PLC over a low voltage network. By introducing the proposed modifications to PRIME in an impulsive noise environment, latencies are considerably reduced.

Finally, the author finds the use of this kind of simulation tools be very helpful to companies that are currently deploying their AMI systems. These simulations can provide the average number of meters that can be polled in a given period of time, which is an important parameter in the dimensioning of the network.

Resumen

En los últimos años ha existido un esfuerzo internacional en desarrollar tecnologías encaminadas a una gestión más eficiente de la energía dentro del paradigma conocido como Smart Grid (Redes Inteligentes). Sin embargo, a pesar de que existe un conseso en la idea de que las nuevas Redes Inteligentes deberían de contar con una infraestructura basada en diferentes tecnologías de la información (IT), no está tan claro cuál sería la mejor arquitectura para interconectarlas. Un tecnología prometedora para el desarrollo de estas redes inteligentes es la de comunicación a través de los cables eléctricos, conocida popularmente por sus siglas en inglés: PLC (o Power Line Communications). Una de las principales razones por las que PLC se presupone como una tecnología adecuada para el escenario en cuestión es que, debido a que usa los cables de potencia como medio de comunicación, es capaz de alcanzar todos los lugares donde la energía está presente.

No obstante, la tecnología PLC ha de enfrentarse al hecho de que los cables eléctricos presentan un entorno muy dañino para la transmisión de señales. Esto se debe a la existencia de diferentes fuentes de ruido y atenuación que introduce el canal. Ambos efectos merman la calidad de las comunicaciones.

En este contexto, la tesis persigue dos objetivos principales: en primer lugar, proponer modificaciones en los actuales estándares para PLC encaminadas a obtener una transmisión más robusta; y, en segundo lugar, desarrollar una herramienta de simulación que, teniendo en cuenta todos los fenómenos físicos de las comunicaciones, sea capaz de obtener valores de latencia punto a punto en una red PLC donde participan diferentes dispositivos.

Para conseguir los objetivos definidos anteriormente, la tesis se centra en el análisis del rendimiento de dos de las principales tecnologías de PLC de banda estrecha desarrolladas por la industria: PRIME y G3-PLC. En líneas generales los dos estándares son muy similares: se trata de un transceptor basado en una modulación OFDM que usa la banda CENELEC-A para transmitir información. La gran diferencia de G3-PLC frente a PRIME es que el primero introduce redundancia extra en el mensaje enviado para conseguir una mayor calidad en la comunicación. Sin embargo, PRIME utiliza un esquema menos robusto, apostando por una mayor tasa de transmisión que la alcanzada

por G3-PLC (aproximadamente 7 veces superior).

El análisis del rendimiento de la comunicación para PRIME y G3-PLC se ha llevado a cabo mediante la implementación de una plataforma de simulación desarrollada con Matlab. En dicho entorno se han codificado el diseño de ambos transceptores de acuerdo a la especificación. Así mismo, se han implementado los diferentes fenómenos físicos que ocurren en el canal de comunicaciones para emular un entorno tan realista como sea posible.

Tras el análisis de los resultados obtenidos con dicha plataforma, se ha observado un peor comportamiento de PRIME respecto a G3-PLC. Esta diferencia se ve incrementada en entornos donde el ruido impulsivo es dominante en el canal de comunicaciones, hecho que es común en redes PLC. Este tipo de ruido es muy dañino en comunicaciones basadas en OFDM puesto que la energía de los impulsos se propaga a toda la banda de transmisión debido al efecto de la Transformada Discreta de Fourier (Discrete Fourier Transform o DFT).

Este peor comportamiento de PRIME sirve como argumento para motivar la búsqueda de técnicas que mejoren el rendimiento de dicho estándar al mismo tiempo que no mermen su valor añadido respecto a G3-PLC: la mayor tasa de transmisión. En concreto se ha observado una mejora en el rendimiento utilizando los conceptos de *compressed sensing* para estimar la componente impulsiva del ruido. Así mismo, en el presente documento, se propone una reordenación de la posición de las portadoras utilizadas para transmitir información en el espectro OFDM que mejora notablemente dicha estimación. Como consecuencia, se consigue eliminar casi por completo el efecto de los impulsos.

Respecto al segundo objetivo perseguido en esta tesis, se ha usado un simulador de red para reproducir el comportamiento de un sistema de telemedida (Advanced Meter Infrastructure o AMI) desde un punto de vista de comunicaciones. Debido a su buen rendimiento en términos de consumo de memoria y tiempo de ejecución, el simulador de redes OMNeT++ ha sido elegido para esta tarea. La implementación llevada a cabo hace uso de los resultados de capa física obtenidos mediante Matlab en la etapa anterior. De esta manera, se consigue generar un entorno lo más realista posible donde se tienen en cuenta los efectos de toda la pila de comunicaciones y del canal de transmisión.

Uno de los principales resultados obtenidos con la plataforma descrita es que, en entornos de ruido impulsivo, la latencia en las comunicaciones de PLC es demasiado alta para implementar aplicaciones de tele-medida. Este comportamiento se consigue mejorar mediante el uso de la técnica de cancelación de ruido impulsivo descrita anteriormente, y así lo muestran las simulaciones.

Este tipo de herramientas de simulación son de gran utilidad para las empresas que se encuentren en el proceso de despliegue de redes de AMI. El uso de este tipo de herramien-

tas podría usarse en el proceso de dimensionamiento de dichas redes, ya que indicaría el número de dispositivos que pueden ser encuestados en un determinado intervalo temporal.

Contents

List of Figures

List of Tables

List of Acronyms

8PSK	8-Phase Shift Keying
AMI	Advanced Meter Infrastructure
BER	Bit Error Rate
BPDU	Beacon Packet Data Unit
BPSK	Binary Phase Shift Keying
Cenelec	Comité Européen de Normalisation Electrotechnique
CFP	Contention Free Period
CS	Compressed Sensing
CSMA-CA	Carrier Sense Multiple Access - Collision Avoidance
D/A	Digital to Analog Converter
D8PSK	Differential 8-Phase Shift Keying
DBPSK	Differential Binary Phase Shift Keying
DFT	Discrete Fourier Transform
DLL	Data Link Layer
DPSK	Differential Phase Shift Keying
DQPSK	Differential Quadrature Phase Shift Keying
DR	Demand Reponse
DS	Difference Set
DVB-T	Digital Video Broadcasting - Terrestrial
FCC	Federal Communications Commission
FCH	Frame Control Header
FEC	Forward Error Correction
FFT	Fast Frourier Transform
HV	High Voltage
IDFT	Inverse Discrete Fourier Transform
IEEE	Institute of Electrical and Electronics Engineers
IFFT	Inverse Fast Fourier Transform
IT	Information Technologies
LCID	Local Connection Identifier

LLC	Logical Link Control
LNID	Local Node Identifier
LV	Low Voltage
MAC	Medium Access Control
MV	Medium Voltage
OFDM	Orthogonal Frequency Division Multiplexing
P/S	Parallel to Serial
PDU	Packet Data Unit
PFH	PHY Frame Header
PHY	Physical Layer
PLC	Power Line Communication
PRIME	Powerline Intelligent Metering Evolution
PRN	Promotion Needed
PSD	Power Spectrum Density
PSK	Phase Shift Keying
QAM	Quadrature Amplitude Modulation
QPSK	Quadrature Phase Shift Keying
ROBO	Robust orthogonal frequency division multiplexing (OFDM)
Rx	Receiver
S/P	Serial to Parallel
SCP	Shared Contention Period
SID	Switch Identifier
SNA	Subnetwork Address
SNR	Signal to Noise Ratio
Super-ROBO	Super robust orthogonal frequency division multiplexing (OFDM)
Tx	Transmitter

List of Symbols

α	Attenuation constant.
β	Phase constant.
Δf	Frequency separation.
ϵ_0	Vacuum's permittivity.
ϵ_r	Relative permittivity.
μ	Vacuum permeability.
Γ	Gaussian to impulsive variance ratio.
γ	Propagation constant.
A	Impulsive noise index.
C	Per-unit-length capaticance.
F_s	Sampling frequency.
f	Continuous frequency.
G	Per-unit-length admitance.
$\boldsymbol{I} = (I_1, \cdots, I_N)$	Impulsive noise in frequency domain.
$\boldsymbol{i} = (i_1, \cdots, i_N)$	Impulsive noise in time domain.
j	Square root of -1.
L	Per-unit-length inductance.
M	Dimension of the compressed signal.
N	Dimension of the measured signal.
N_{DFT}	DFT Length.
N_{OFDM}	DFT length + Cyclic prefix.
N_{subc}	Number of data subcarriers in an OFDM symbol.
n	Discrete time index.
P_X	Power of signal x.
R	Per-unit-length resistance.
$\boldsymbol{R} = (R_1, \cdots, R_N)$	Received signal in frequency domain.
$\boldsymbol{r} = (r_1, \cdots, r_N)$	Received signal in time domain.
$\boldsymbol{S} = (S_1, \cdots, S_N)$	Transmitted signal in frequency domain.
$\boldsymbol{s} = (s_1, \cdots, s_N)$	Transmitted signal in time domain.

T	OFDM Symbol's duration.
t	Continuous time.
$\tan \delta_c$	Loss tangent.
$\boldsymbol{v} = (v_1, \cdots, v_{N-M})$	Data subcarriers decomposition in frequency domain .
$\boldsymbol{w} = (w_1, \cdots, w_M)$	Null subcarriers decomposition in frequency domain .
Z_c	Characteristic impedance.
$\boldsymbol{Z} = (Z_1, \cdots, Z_N)$	Background noise in frequency domain.
$\boldsymbol{z} = (z_1, \cdots, z_N)$	Background noise in time domain.

Chapter 1

Introduction

Smart Grid has become a very popular term in the last few years to refer the new and upgraded generation of power grid characterized by a higher efficiency, reliability and safety. These features are achieved thanks to the existence of two-way communication methods that allow for the interconnection of the different actors present in the network. Smart Grid's actions cover from a traditional central generator to emerging renewal distributed generators through transmission and distributions to industrial customers and home user's appliances.

Two main features are foreseen as *killer applications* within the Smart Grid paradigm. One of them is Demand Response (DR), which will allow users and utilities to interact in order to consume and produce energy in a more cost-effective manner for both parties. The second one is Smart Metering, which will allow utilities to have an accurate value for energy consumption and quality. This consumption can be obtained by polling the devices that are installed at all customer's homes. This smart meter's architecture is commonly referred to as Advanced Meter Infrastructure (AMI).

It seems clear that information technologies need to play an important role in order to build such network. However, it is not so clear under what architecture they should be build up. Several studies have addressed this issue by comparing the main advantages and disadvantages of different communication's medium [1–5]. As stated in some of the studies [3–5], the power line communication's technology is found to be a very suitable technology for smart metering applications.

Due to this use of case, PLC is considered an emerging technology and, as such, is gathering the attraction of the industrial and scientific community because of the promise of a new or alternative way for the transmission of information.

The origins of this technology go back to the beginning of the twentieth century, where power lines were used to control switching operations in substations. Since the decades of the 80's the research on this field has increased, as it can be a transmission medium with almost complete market penetration.

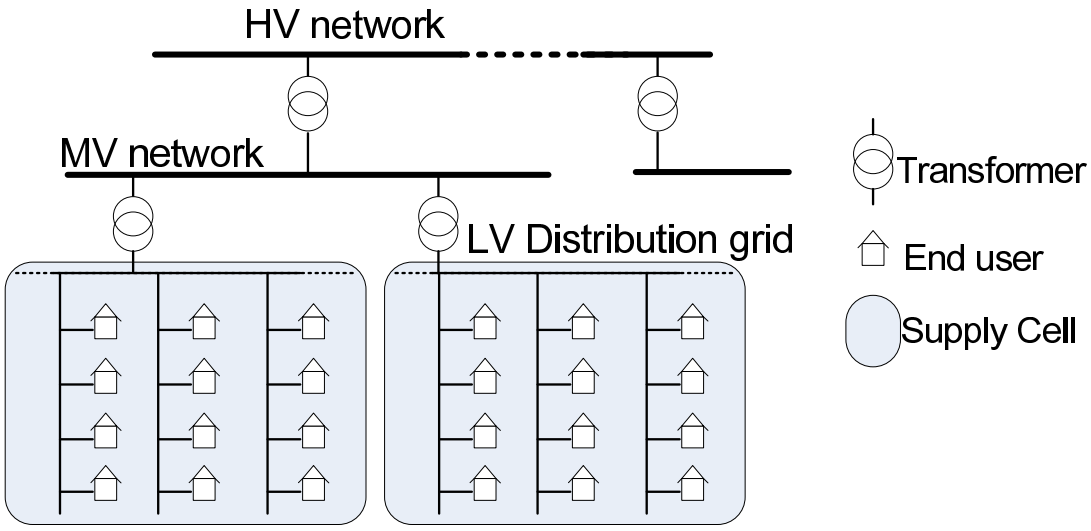

Figure 1.1: *Generic European power supply network structure. Adapted from [6].*

With respect to the the PLC's topology, the electrical power grid is typically divided in three segments: High Voltage networks (HV), with tension over $100kV$; Medium Voltage networks (MV), for tensions in the range of $[10-30kV]$; and Low Voltage networks (LV), where the transported electricity is around $230-400V$. Most of the research efforts regarding PLC are done in this third segment, since it is the most widely spread and has a direct connection to all users. Moreover, in most cases both HV and MV already count with a dedicated communication link. A diagram of the structure of a generic European power supply network is shown in Figure 1.1.

Although power line networks are very efficient in the transmission of energy, they are not well suited for data communications. A power line network is composed of a number of connection points, branches and unmatched impedances that are responsible for the multipath effects induced in the transmitted signal [7]. As a result, the PLC channel is characterized by a frequency-dependent transmission medium. Additionally, several noise sources are also present in the channel, disturbing the sent signals [8]. These noise sources are produced by the supply network itself and the different devices (switches, rectifiers, etc) that are connected to the system. All these effects are the responsible for the low popularity of broadband power line systems in the past.

Additionally, there exists another physical limitation for PLC technologies. Due to the frequency of use (below 500kHz, as it will be detailed later on) and the length of the transmission lines, cables act as antennas, producing electromagnetic radiation on the environment. This radiation interacts with wireless systems working on the same band of the spectrum. In concrete, certain limitations are applied in the transmitted signal in order not to disturb amateur radio transmissions.

Despite of all these effects, both researchers and industry are looking once again to PLC technologies as an ideal way for transmitting information, in part thanks to the popularity of the Smart Grids paradigm. With respect to this, power line communication counts with a major advantage over other means of communications: the network is already deployed and all devices that can be controlled or measured are connected to it [9].

Nevertheless, for the design and correct functioning of such a system, technologies need to be analysed and assessed to guarantee that they can perform in the desired manner.

This thesis addresses the analysis, evaluation and improvement of one of the most popular narrowband powerline communication standards endorsed by the industry: PRIME.

1.1 Motivation

As mentioned in the introduction, power line communication has gathered the attention of the scientific and industrial community due to the important role that it plays in the Smart Grid's paradigm. However, for this technology to behave as expected, an extensive study is needed.

As stated by one of the reports published by the Open Meter Consortium [10], one of the key features that PLC technologies need to address is its performance improvement in impulsive noise environments. As it will be seen in Chapter 4, the performance of one of the studied technologies (PRIME) is considerably poorer in impulsive noise environments when compared with the rest of NB-PLC standards. The reason for this lack of robustness resides in its interleaver's design. As it will be more deeply detailed in Chapter 4, the interleaver block does not scatter the energy of the noise enough and , as a result, it is very difficult for the decoders to correct all the erroneous bits.

Additionally, another important issue that PLC technology needs to solve was mentioned by Dr. Stefano Galli on the International Symposium of Power Line Communications and its Applications (ISPLC) in 2012 [11]. Dr. Galli stressed the lack of planning tools for narrowband power line deployments. In the present, there are pilot projects powered by utility companies where PLC transceivers are installed in determined low voltage networks in order to analyse its behaviour [12,13]. Additionally, there exist plans for the massive roll-out of Smart Meter networks in Europe for the year 2020, as detailed in [14]. However, there has barely been efforts in developing tools that help in the sizing of this kind of networks.

Regarding power line communications, there are several ongoing and finished projects, sponsored by private and public funds, where the Institute for Research in Technology

(in Spanish Instituto de Investigación Tecnológica or IIT), affiliated to the Universidad Pontificia Comillas is or has been present. This fact makes the present job coherent with the line of work followed by the Institute. The following list describes the most important participations:

- Open PLC European Research Alliance (OPERA) [15]. The strategic objective of this project is to offer low-cost broadband access service to all European citizens using the most ubiquitous infrastructure: Power Lines.

  All efforts were focused on obtaining: an improved performance in transmission speed; a ready-to-sell and low-cost product; a complete system specification; a unique international regulation; full inter-operability with existing back haul and in-home technologies; and a higher market share. OPERA contribute to develop the European Information Society in concordance with the proposed objectives in the plan eEurope 2005 [16] by: increase of competition in access network, fostering mass services availability and European Industry Leadership.

- OPERA - Phase 2 [17]. The strategic objective of this Opera proposal was to push PLC technology in all the different and relevant aspects (standardization, technology improvement, installation tools and processes, telecom services, intelligent grid services, dissemination) so as to allow the technology to become a competitive alternative that offers broadband access service to all European citizens using the most ubiquitous infrastructure.

- OPERA-AC [18]. Developing Work Package 1 (WP1) of the OPERA Project. The work consisted of studying common mode current at a point of an electric installation as a function of the differential mode voltage and the common mode current injected at the transmitter, placed at the end of the installation. Funds were provided by the *Ministerio de Educación y Ciencia* of Spain.

- ENERGOS [19,20]. Which pursuits the development of knowledge and technologies that advance the deployment of Intelligent Networks. The consortium is led by Gas Natural Fenosa. It has the presence of leaders in technologies, such as INDRA, and prestigious companies in the electric sector, as ZIV, AIA, ORMAZABAL and SAC, among others.

- ADDRESS [21, 22]. Which targets are the development of new innovative architectures for Active Distribution Networks (ADN) able to balance, in real time, power generation and demand, allowing network operators, consumers, retailers

and stakeholders to benefit from the increased flexibility of the entire system. Important energy companies, such as ENEL, EDF, Iberdrola, have also joined this project which is sponsored by European funds.

- DENISE [23]. The project CENIT-DENISE is a project financed by CDTI. It was developed by a consortium of firms and research centers whose objective is to research about future electricity networks that will enable an intelligent, secure and efficient production and distribution of electricity. The consortium is headed by Endesa Servicios.

  The activities around IEC 61850 within DENISE correspond with subtasks 3.1 and 3.3 integrated in task 3 "Intelligent networks" coordinated by Eliop. Among the participants of the consortium, several research Centers (AICIA and IIT) are participating in the task. The project studied the application of IEC 61850 to power distribution networks, the development of 61850 controllers and configuration software.

1.2 Objectives of this thesis

The general objectives of this thesis are to contribute to the current technologies for narrowband power line communications working in the low voltage network. These objectives are addressed in two lines of work. The first one focuses on increasing the robustness of PLC communications in impulsive noise environments. The second line of work deals with the study of the overall PLC system's performance taking into account physical and networking effects. Concrete pursued scientific objectives can be summed up in:

- Implement a transceiver simulation model for the two main NB-PLC technologies endorsed by the industry (PRIME and G3-PLC) according to their open specification.

- Perform a theoretical and simulation study of the performance of current narrowband power line communication technologies for transmitting information in the low voltage networks under different scenarios.

- Propose a mechanism for improving the performance of NB-PLC transmissions in environment where impulsive noise is dominant, while not decreasing its data bit rate.

- Implement a simulation framework that replicates the behaviour of a NB-PLC standard from a network's perspective taking into account physical (i.e. attenuations,

reflections and noise sources) and telematic (i.e. connection establishment processes, channel access, packet fragmentation, etc.) effects. This framework shall become very helpful when designing and dimensioning future AMI deployments.

- Obtain estimated values of the needed time to read all meters in a low voltage narrowband power line network using the developed simulation framework.

1.3 Thesis Outline

This thesis can be divided in three main parts. The first one (Chapters 2 and 3) provides a qualitative description of the PLC environment. Chapter 2 details the transceiver's implementations of the main narrowband power line communications solutions proposed in the last five years. In addition to this, Chapter 3 describes the most popular models to emulate the channel's transfer function and the different noise sources present in the PLC medium. This two chapters are aimed to introduce to the reader the matter of the thesis and help him in understanding the main parameters and factors that will be analysed in the rest of the document.

Alternatively, the second part (Chapters 4 to 6) focuses on the study of the physical layer of the communications for a PRIME and G3-PLC's transceiver. Its performance is assessed in terms of Bit Error Rate (BER) as a function of the Signal to Noise Ratio (SNR) for different types of PLC environments. As shown in Chapter 4, PRIME is specially vulnerable in environments with impulsive noise. This poor performance in such common scenarios in PLC networks motivates the other two chapters. Chapter 5 provides a survey of the most common techniques to improve the communication's performance of OFDM-based systems in impulsive noise channels. Additionally, Chapter 6 studies how compressed sensing techniques are used for estimating the impulsive component of the noise based on the unused subcarriers. This estimation is used at the receiver to improve the BER figure. Moreover, a new reorganization of the subcarriers used for data transmission is proposed to considerably enhance the communication's performance. This proposed modification is tested in one of the NB-PLC technologies that showed a higher sensitivity to impulsive noise interferences: PRIME.

Finally, the last part (Chapter 7) deals the question of the communication's performance but from a network's perspective. To address such an analysis, a network simulation framework has been developed based on OMNeT++ network simulator. This framework counts with implementations of PRIME's transceivers according to the standard and a replica of a typical low voltage distribution network. Simulations carried out analyse the performance in different noise scenarios. To do this, results from previous chapter are used to emulate the physical layer of communications whereas the data link

and application layers are directly implemented with OMNeT++. The metric used in these simulations is the amount of devices that can be polled in a given period of time. This is a key parameter that will allow utility companies to know how often consumption's data can be gathered and, therefore, how accurately they can obtain the state of the network.

The document is structured in eight chapters and five appendixes. The following paragraphs briefly described the content that is addressed in each one of them.

Chapter 2 reviews the most up-to-date technologies developed to transmit information through the power lines using a narrowband spectrum. It focuses on two designs developed by the energy industry (PRIME and G3-PLC) and two recommendations endorsed by standardisation organisms (IEEE P1901.2 and G.hnem). A detailed description of the transceiver's architecture for each design is done through the chapters' subsections and a qualitative comparison is done afterwards.

Chapter 3 describes the main physical effects that occur in the power line communication channel. Additionally, it also includes how these effects are taken into account by mathematical models that emulate the channel's transfer function and the different noise sources that are considered. They are well-known models typically used in the literature.

Chapter 4 focuses on the physical layer's performance for two of the previously described narrowband PLC standards: PRIME and G3-PLC. Their performance is assessed in three different scenarios: under additive white Gaussian, measured background and impulsive noise. Both the background and impulsive interferences are computed with the model described in Chapter 3 using measured data reported in the literature. The performance is computed in terms of bit error rates for different signal to noise ratios using a Matlab's simulation framework. Simulation results are compared with theoretical values for validation purposes. The main conclusion extracted from this chapter is the poor performance experienced when transmissions are impaired by impulsive noise, especially in PRIME's case. This result motivates the survey carried out in the next chapter.

Chapter 5 provides a review of the most recently proposed mechanisms to improve the performance of OFDM-based systems in impulsive noise environments. This state of the art is divided in three subsections: one of them deals with techniques that are applied in the time domain (i.e. before the OFDM demodulation is performed) whereas the second one describes methods used in the frequency domain (i.e. after the OFDM demodulation). A third subsection introduces the last proposals for impulsive noise cancellation, which make use of compressed sensing techniques.

Chapter 6 describes in detail one of the latest proposed techniques to improve the performance of OFDM-based systems in impulsive noise environments: compressed sensing. Additionally, it also explains one of the main contributions of this thesis: how an

accurate estimation of the impulsive noise component can be achieved by exploiting some characteristics of the compressed sensing approach and doing a concrete reconfiguration in the frequencies used for the data subcarriers. This estimation is used by the receiver device to cancel it from the incoming signal. As a result, the communication's performance is greatly improved. Simulations asses the behaviour of this technique when applied to the NB-PLC solution that showed a poorer performance in impulsive noise environments: PRIME.

Chapter 7 addresses the other main line of work that this thesis focuses on: how previous physical effects influence the overall PLC system from a network's perspective. This chapter details the development of a simulator able to estimate the behaviour of a PRIME's PLC network. Results from previous chapters are re-used in order to model the effects of the PLC channel. The chapter includes simulation results corresponding to the expected number of meters that can be polled in a given period of time. These results show that when the channel is impaired by impulsive noise, a longer time is needed to perform this action. A comparison is also made in the case of using the difference set-based compressed sensing technique described in Chapter 6.

Chapter 8 summarizes all the contributions given by this thesis, draws some general conclusions and lists a number of open issues that are left as future lines of work. In addition, the chapter also includes a list of all published papers generated from this thesis.

The document also include a number of appendixes in order to provide extra information to the interested reader. They are described, together with their relation with the thesis' chapters, in the following paragraphs:

Appendix A details the implementation of the Orthogonal Matching Pursuit and Block Orthogonal Matching Pursuit used in the difference set-based compressed sensing proposed in Chapter 6.

Appendix B provides some complexity analysis of the Compressed Sensing technique that is applied in this thesis.

Appendix C lists all the null and data frequencies that should be used in order to implement the compressed sensing algorithm detailed in Chapter 6.

Appendix D details all the data that is transmitted within the PRIME's frames.

Finally, **Appendix E** describes the concrete MAC procedure for registration and promotion of service nodes.

The whole structure of the thesis together with the relationships between chapters and appendixes is schemed in Figure 1.2.

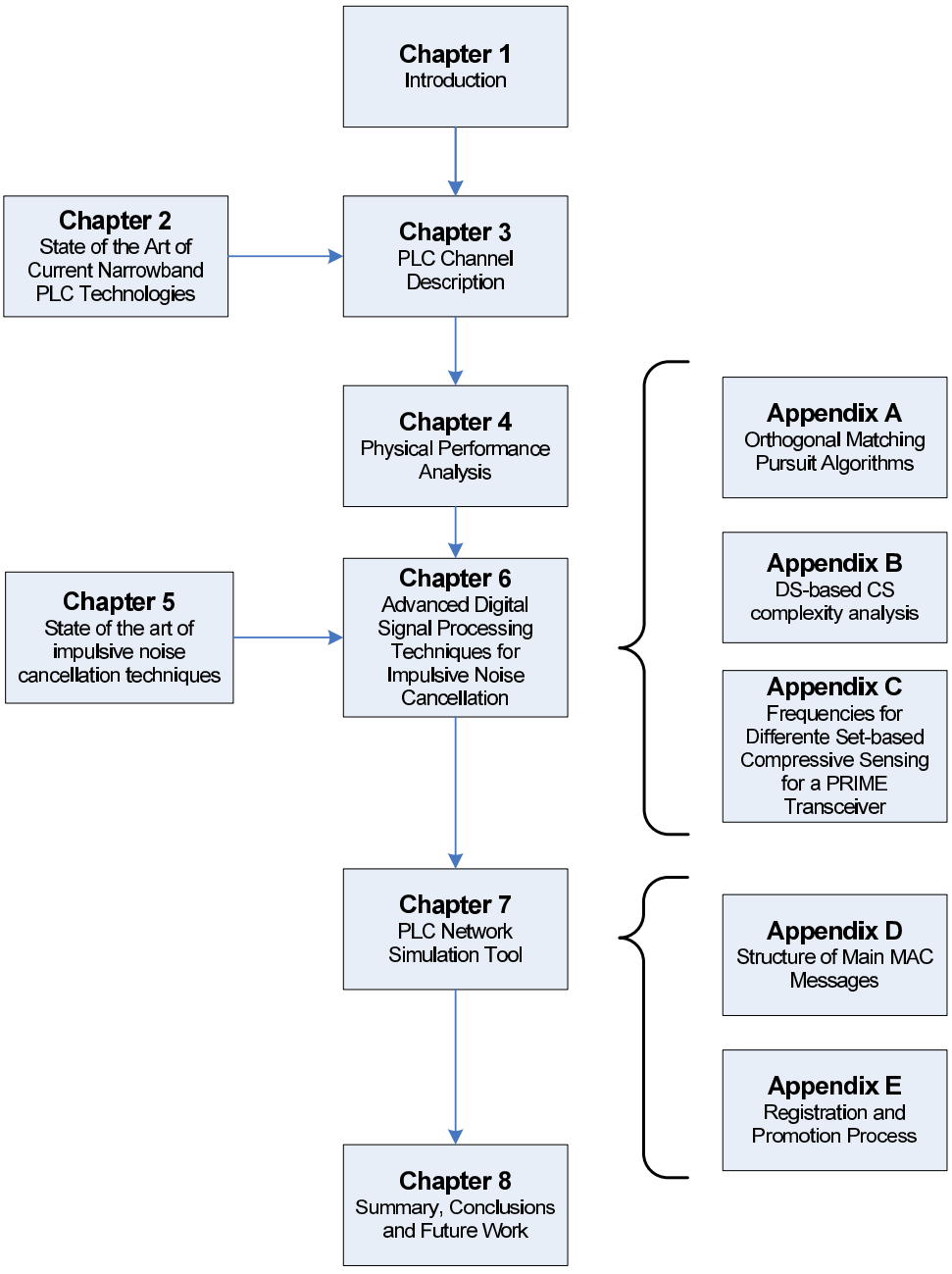

Figure 1.2: *Structure of the chapters and their relations with the appendixes.*

Chapter 2

State of the art of current narrowband PLC technologies

2.1 Introduction

The first carrier signal was introduced in the medium and low voltage distribution networks in 1930. This effort continued in the following decades in the pursuit of a new bi-directional communication mode suitable for several applications such as control and measurement of devices. As an example, the Tokyo Electro Company carried out several experiments during the 70s reporting successful communications with several hundreds of devices [24].

Due to the recent interest of the energy companies on the smart grid paradigm, the possibility of communicating using the power lines has attracted the attention of the industry once more due to the suitability of this transmission medium [9,25]. As a result, specifications for new transceiver's designs have been standardized in order to enable the creation of coexistent and compatible narrowband PLC networks.

The transmission of narrowband signals over the power supply network is limited to specific frequencies. The European standard CENELEC EN 50065 [26] specifies the transmission of PLC signals between frequencies 9kHz to 148.5kHz. This band is more extensive in the case of the Japanese and US regulation, where the available frequencies go up to 500kHz and are regularized by the FCC entity [27] (See Figure 2.1).

This chapter describes four of the most recent and popular solutions for Narrowband Powerline Communications (NB-PLC): PRIME, G3-PLC, IEEE P1901.2 and G.hnem. In the following sections, a detailed description of each one is provided making special emphasis in the main features. Additionally, a qualitative comparison is done afterwards, stressing their strengths and weaknesses of each one of them.

2.2 PRIME description

In 2009, a group of vendors formed the PoweRline Intelligent Metering Evolution (PRIME) alliance, mainly led by the Spanish utility Iberdrola. The idea was to provide an open specification for a power line transceiver using the CENELEC-A band that could target the need for communications in the last mile of the power networks. Currently, PRIME' solution is being rolled-out mainly in Spain, Portugal and the United Kingdom [4].

A PRIME's frame (Figure 2.2) is composed of a preamble signal, followed by some physical layer's information placed in the header, and the payload encapsulating data from the MAC layer. This preamble consists of a linear chirp and is used for synchronization and channel estimation's purposes. Equation 2.1 mathematically describes the chirp signal. It sweeps all frequencies where OFDM data subcarriers will be placed (starting at $f_0 = 41992$Hz and finishing at $f_f = 88867$Hz) during $T = 2048\mu s$).

$$s(t) = \cos\left(2\pi t\left(f_0 + t\frac{f_f - f_0}{2T}\right)\right), \quad 0 < t < T \tag{2.1}$$

An scheme for a PRIME transmitter is shown in Figure 2.4. The transceiver makes use of the spectrum between 42 and 89 kHz to insert OFDM symbols (same frequency band as the sweep done by the chirp signal). Each one of these symbols consists of 97 sub-carriers placed in the mentioned bandwidth (See Figure 2.3). In the payload, one of these carriers is a pilot with the mission of giving a phase reference for the receiver. In the case of the header the number of pilots is increased to 13 and are meant to estimate the sampling frequency offset and phase reference for the data subcarriers. Additionally, subcarriers present in negative and positive frequencies are conjugated of each other so that the output of the Inverse Discrete Fourier Transform (IDFT) block is a pure real signal. To build up such an spectrum, a clock frequency of 250kHz and a 512-length IDFT are used, giving a subcarrier spacing of $\Delta f = 250\text{kHz}/512 = 488.28125$Hz. Before the parallel to serial conversion (Figure 2.4), a cyclic prefix extension of 48 samples ($192\mu s$) is performed to avoid Inter Symbol Interference (ISI) [28]. The whole transmission' scheme is represented in Figure 2.4.

Additionally, prior to entering the OFDM block (Figure 2.4), data is modulated with a Differential Phase Shift Keying (DPSK) modulation. The payload might be modulated with a DBPSK, DQPSK or D8PSK (Differential Binary/Quadrature/8 Phase Shift Keying respectively) constellation. Moreover, redundancy may be added to the message to allow the implementation of Forward Error Correction (FEC) techniques at the receiver. The choice of one specific constellation with or without FEC depends on how noisy the channel is. In addition, the header is always DBPSK modulated with the use of FEC. The reason for this more robust mode is that the information encapsulated in the header

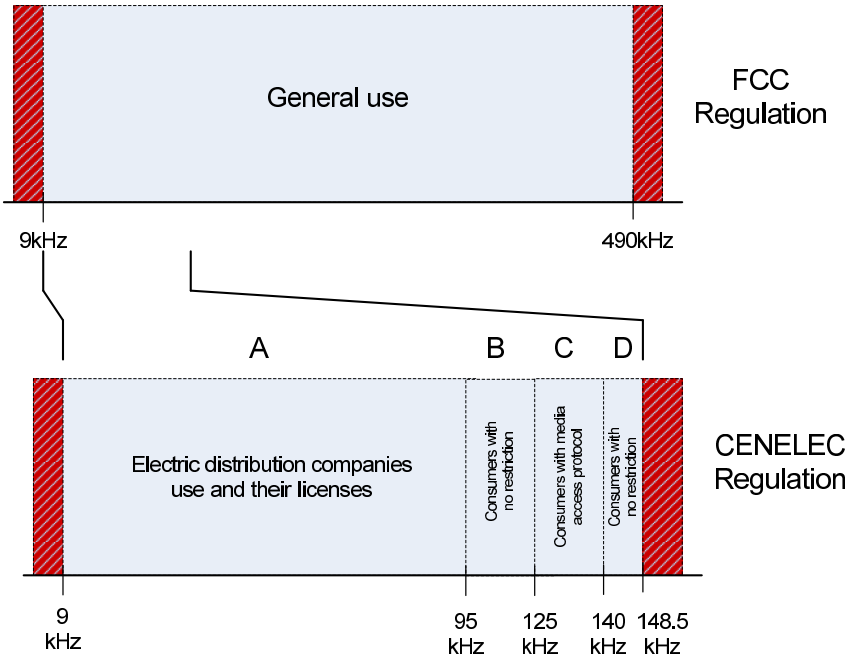

Figure 2.1: *Frequency regulation for narrowband PLC.*

PREAMBLE	HEADER	PAYLOAD
2048 µs	4480 µs	M x 2240 µs
	2 OFDM Symbols	M OFDM Symbols

Figure 2.2: *PRIME's frame.*

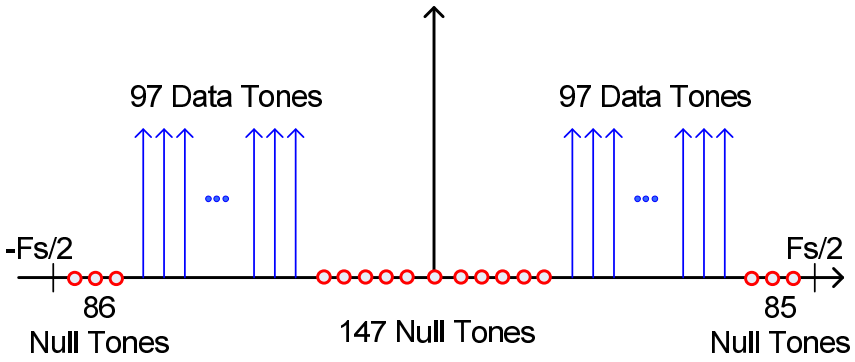

Figure 2.3: *PRIME spectrum. Frequencies are approximated.*

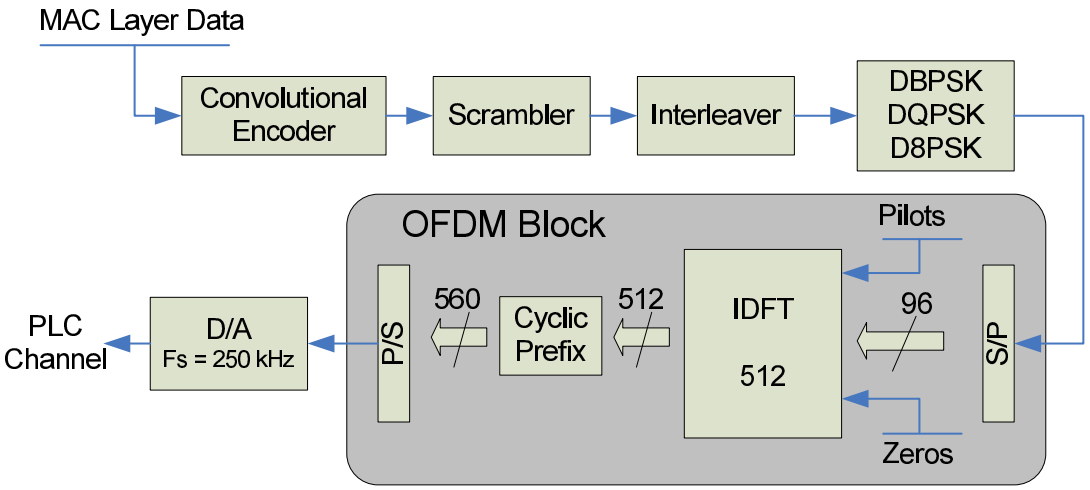

Figure 2.4: *PRIME's transmitter scheme.*

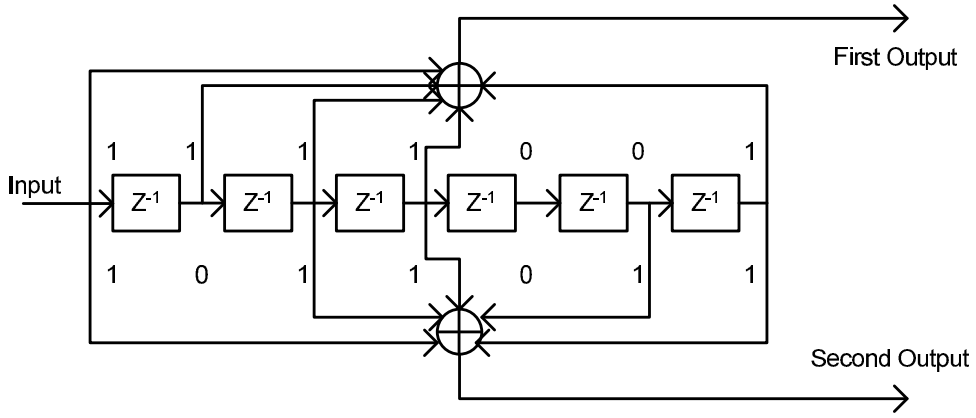

Figure 2.5: *Scheme of PRIME's convolutional encoder.*

is vital for decoding the rest of the frame. This information includes, for instance, the type of constellation used for the payload.

The FEC's mechanism in PRIME consists of a convolutional encoder working together with an interleaver. The convolutional encoder is a 1/2 rate encoder with a binary generator polynomial $g_{encoder} = [001111001, 001011011]$. A schematic representation of the convolutional encoder used by PRIME is shown in Figure 2.5. The interleaver's function is to shuffle the input bits. The features of the encoder are generally enhanced by the use of the interleaver, which provides protection against burst errors that might corrupt several consecutive symbols. In case of PRIME, the shuffling is done over an entire OFDM symbol (i.e. 96, 192 or 288 bits depending on the digital modulation).

Finally, the scrambler block is used to randomize the incoming data from the encoder. This guarantees that the Power Spectrum Density (PSD) of the signal does not depend on the transmitted information.

2.3 G3-PLC description

In 2011, the G3-PLC Alliance organization sponsored by ERDF was formed in order to support, promote and implement G3-PLC in smart grid applications. Its members come from the key stakeholders in the smart grid ecosystem, including utility companies, equipment and semiconductor manufacturers, system integrators and IT vendors. In Europe, it is mainly present in countries such as Ireland, France and Holland [4].

As well as PRIME, G3-PLC uses an OFDM-based modulation. In this case, 36 subcarriers are modulated between 34 and $90kHz$. In contrast with PRIME's transceiver, only positive frequencies are used (Figure 2.6). Once the spectrum has been transformed to time domain, only the real part is transmitted.

A G3-PLC's frame (Figure 2.7) starts with a preamble, used for channel estimation's purposes; is followed by a header, which encapsulates data regarding the PHY layer; and ends with the payload, which carries the data for the higher layer. In this case, the preamble is composed of 8 P symbols and 1 M symbol. P symbols are 36 tones whose phase follows a pseudo-random sequence. These tones are mapped in the same frequencies that will be used by the data subcarriers later on in order to be used for equalisation at the receiver. M symbols are a copy of P but each of the carriers has a phase change of π radians. The payload is formed by groups of 4 OFDM symbols and its length is set in one of the header's fields.

The overall block diagram is shown in Figure 2.8. The OFDM modulation is computed with a sampling frequency of 400kHz and an IDFT of 256 samples. In this case, the frequency separation to achieve orthogonality is $\Delta f = 400kHz/256 = 1562.5$Hz. The first subcarrier is mapped to the position 23 (35.938kHz) in the IDFT and the last one to the position 58 (90.625kHz) (See Figure 2.6).

Moreover, prior to entering the OFDM modulation block, all bits are digitally modulated following either a DBPSK, DQPSK or D8PSK constellation. This results in different transmission rates as is shown in Table 2.1.

The FEC in G3-PLC consists of a nested structure of a Reed-Solomon and a convolutional encoder together with an interleaver. These three elements are used in the *normal* operation mode, whereas for the *robust* mode, an extra block inserts 3 redundant bits for each input data bit (block *Repetition Code* in Figure 2.8).

The structure of the convolutional encoder is identical to the one used in PRIME. For the Reed-Solomon, two possible configurations are used: RS($N = 255$, $K = 239$,

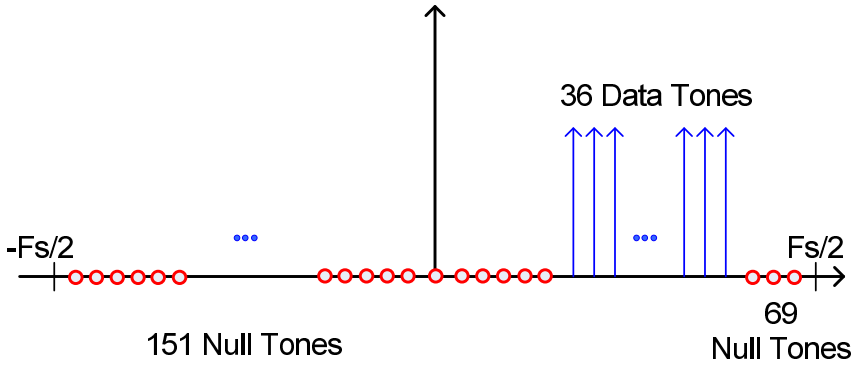

Figure 2.6: *G3-PLC spectrum. Frequencies are approximated.*

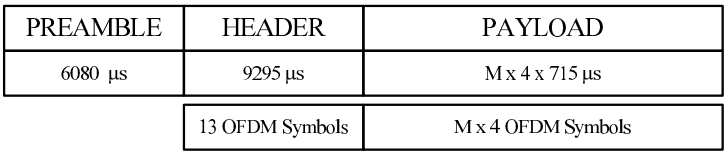

Figure 2.7: *G3-PLC frame*

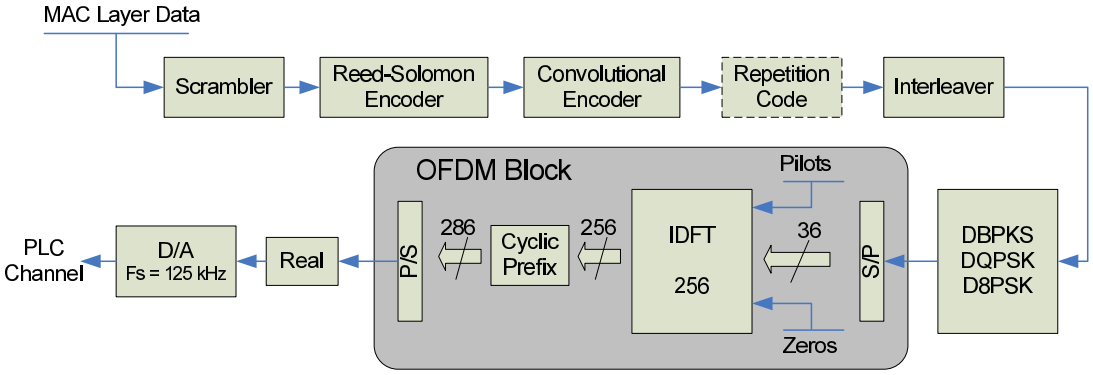

Figure 2.8: *G3-PLC Transmitter scheme.*

Table 2.1: *Transmission data bit rates in kbps for the analysed transceivers.*

	PRIME		G3-PLC		P1901.2		G.hnem	
Comm. Mode	FEC-ON	FEC-OFF	Robust	Normal	ROBO	Normal	Robust	Normal
BPSK	21.4	42.9	3.2	15.8	4	24.7	1.5	24
QPSK	42.9	85.7	-	34	49.6	49.6	3	47.9
8PSK	64.3	128.6	-	54.6	74.5	74.5	4.5	76.7
16-QAM	-	-	-	-	16.4	99.3	6	102.3

Table 2.2: *Transceiver's parameters for all NB-PLC solutions analysed. Listed values are for the CENELEC-A bandplan.*

OFDM System Parameter	PRIME Values	G3-PLC Values	P1901.2 Values	G.hnem Values
Clock Frequency (F_s)	250kHz	400kHz	400kHz	200kHz
Sub-carrier Spacing (Δf)	488.28125Hz	1562.5Hz	1562.5Hz	1562.5Hz
Number of Data Subcarriers (payload)	96	36	36	33 (maximum)
Number of Pilot Subcarriers (payload)	1	0	0	3
FFT Size	512 (2048μs)	256 (640μs)	256 (640μs)	128 (640μs)
Cyclic Prefix Samples	48 (192μs)	30 (75μs)	30 (75μs)	32 (160μs)
Windows Samples	0	8	8	8
Effective Cyclic Prefix Samples	48 (192μs)	22 (55μs)	22 (55μs)	24 (120μs)
OFDM Symbol Duration	2240μs (2048μs + 192μs)	695μs (640μs + 55μs)	695μs (640s + 55μs)	760μs (640μs + 120μs)
Preamble Duration	2048μs	6080μs	6080μs	5800μs

$R = 16$) and RS($N = 255$, $K = 247$, $R = 8$), where N is the total number of symbols per codeword and K and R are the number of data and parity symbols per codeword, respectively. Given this, the number of correctable symbols is $R/2$. Each one of the symbols has a fixed size of 8 bits.

As mentioned, an interleaver is used to avoid burst errors which may corrupt several constellation symbols in a row. However, in contrast to PRIME, the interleaver block used in G3-PLC applies a two-dimensional shuffle of data and, additionally, it does this shuffling between several OFDM symbols. The first step is to arrange the whole frame in a matrix with as many columns as the number of subcarriers and as many rows as the number of OFDM symbols to be transmitted in the frame. Then, all columns are circularly shifted a number of times that depends on the size of the matrix. Next, all rows are circularly shifted as well. This interleaver design requires a more complex transceiver. However, as it will be seen in the following chapter, the extra complexity trades off in terms of a higher robustness.

2.4 IEEE P1901.2 description

The IEEE P1902.2 is the recent proposal made by the Institute of Electrical and Electronics Engineers (IEEE) in order to design a narrowband power line transceiver. Due to its later appearance, some parts are based on both PRIME and G3-PLC's designs. In addition, it provides mechanisms for the coexistance with this two solutions by dynamically changing the frequencies that will be used as data subcarriers.

The IEEE P1901.2 specification contains the physical and data link layer description for a narrowband power line communication solution for the transmission of information

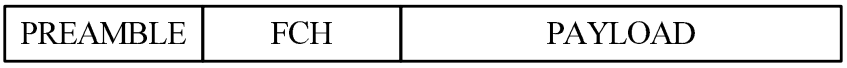

Figure 2.9: *IEEE P1901.2 frame structure.*

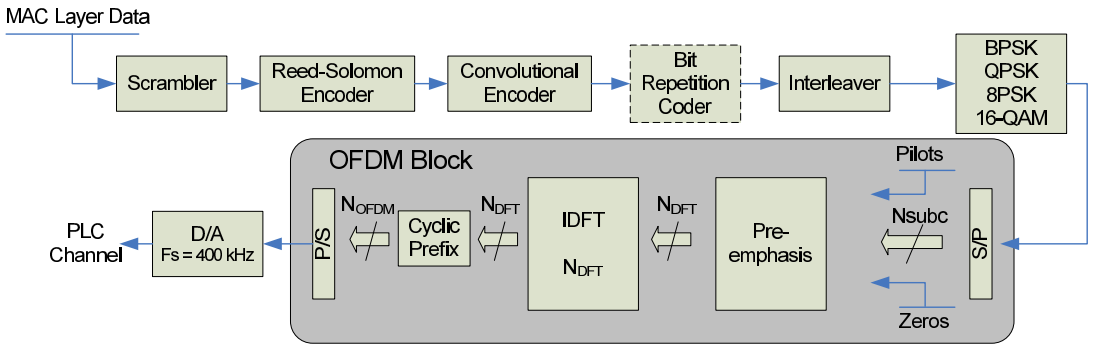

Figure 2.10: *IEEE P1901.2 transmitter scheme.*

using the 10-490kHz bandwidth. With respect to the physical layer, the transceiver is configured with different parameters in order to adequate the transmitted signal to the corresponding bandplan to be used (i.e. CENELEC or FCC).

The structure of an IEEE P1901.2's frame (Figure 2.9) is very similar to the one used by G3-PLC (Figure 2.7). It consist of a preamble, that helps the receiver in the equalization and synchronization process; a Frame Control Header (FCH), that contains the information of the encapsulated data; and a payload with the information of upper layers.

The transmitter is based on an OFDM modulator that inserts a number of carriers on the corresponding transmission bandwidth. The transmitter' scheme is shown in Figure 2.10 [29]. Variables N_{subc}, N_{DFT} and N_{OFDM} correspond to the number of data subcarriers, number of points for the IDFT and number of points for the OFDM symbol (including the cyclic extension) respectively. IEEE P1901.2 defines different values depending on the bandplan in use. The concrete values for the CENELEC-A bandpland are shown in Table 2.2.

Each one of the subcarriers can be modulated with several digital modulators: DBPSK, DQPSK, D8PSK and 16-QAM. As it can be seen, a new digital modulator with a higher number of symbols has been included for the IEEE P1901.2 with respect to PRIME and G3-PLC. This faster constellation is intended to be used in situations where the channel presents good enough conditions. Additionally, coherent modulators (i.e. BPSK, QPSK and 8PSK) can optionally be used by the transceivers. Moreover, transmitters can use the feedback information from the other end to pre-emphasise the output signal with the intention of overcoming a highly attenuated frequency band.

All bits entering the digital modulators are previously processed by a two-stage coding

architecture. As in G3-PLC, an inner Reed-Solomon and outer convolutional coder add redundant information to the message to help the receiver in correcting some of the errors that occurred in the transmission. Additionally, there exists an interleaver that enhances the properties of the decoders by scattering long bursts of errors. This block does a two-dimensional interleaving taking into account bits corresponding to several number of OFDM symbols.

The Bit Repetition Coder block is used in transmissions with more robust configurations. This block replicates the input bit R times at its output. Different values of R are used depending on the communication's modes. R may be set to 1, 4 and 6 for the normal, ROBO and Super-ROBO mode respectively.

2.5 G.hnem description

The G.hnem specification is detailed in the ITU-T G.9902 recommendation for narrowband power line communications below 500kHz, which was approved in October 2012. This recommendation is thought to be used in either indoor or outdoor environments to implement the communications' infrastructures for Smart Grid's applications such as AMI, home automation and electric vehicles management [30]. Due to its time of creation, it also gathers some of the main characteristics of the previously described PLC solutions.

The G.hnem standard [30] contains the physical and data link layer specifications needed for a transceiver's implementation. Figure 2.11 shows the structure of a G.hnem's frame. It starts with a preamble sequence, designed to help the receiver in the detecting process; followed by the PHY Frame Header (PFH), which includes information needed when decoding the rest of the frame; it also includes Channel Estimation Symbols (CES), meant to be used in the equalization of the received signal; and finally, the information is encapsulated in the payload.

The PHY transceiver's design counts with several configurations to be used depending on the available bandplan for communication (i.e. CENELEC A/B/C/D or FCC). In any case, all configurations use an OFDM-based modulation with different numbers of carriers and pilots.

Figure 2.12 shows the scheme of the G.hnem transceiver according to [30]. As in the case of IEEE P1901.2, variables N_{subc}, N_{FFT} and N_{OFDM} correspond to the number of data subcarriers, number of points for the IDFT and number of points for the OFDM symbol (including the cyclic extension). G.hnem defines different values depending on the bandplan in use (i.e. CENELEC-A/B/C/D or FCC). The concrete values for the CENELEC-A bandpland are shown in Table 2.2. All data subcarriers are modulated

Figure 2.11: *G.hnem's frame structure.*

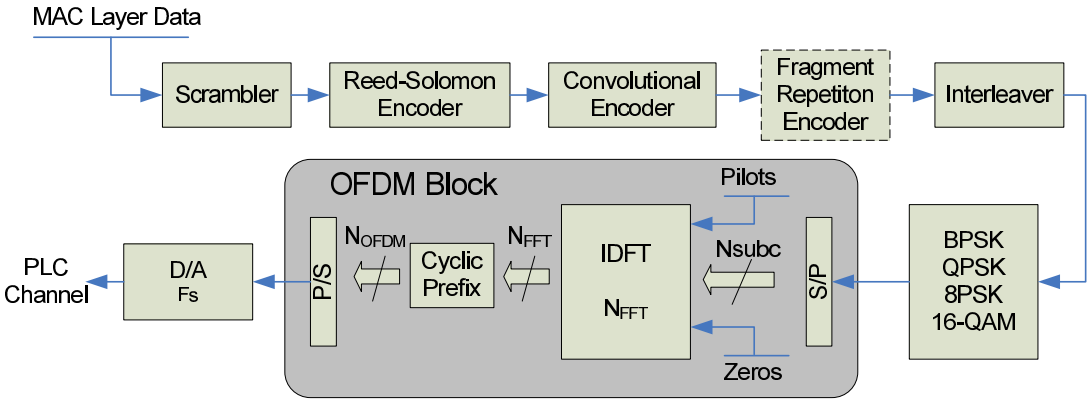

Figure 2.12: *G.hnem Transmitter Scheme.*

using one of the available coherent digital modulations: BPSK, QPSK, 8PSK and 16-QAM.

As in G3-PLC, G.hnem includes FEC techniques in its normal communication mode. They consist of an inner and outer blocks that implement a convolutional and Reed-Solomon encoder respectively. With this respect, the redundancy added by the Reed-Solomon encoder depends on the length of the transmitted message. More redundancy is added for longer streams of information. In contrast, the coding rate for the convolutional encoder does not depend on the message and can be set to either 1/2 or 2/3. The properties of the encoder are enhanced by the used of an interleaver, as it could be seen in previous schemes. However, in contrast with previous standards, G.hnem allows for two configuration of the interleaver. One of them interleaves the bits within an AC-cycle (either 60 or 50 Hz) whereas the other one performs what is called fragment interleave, which consists of interleaving over blocks of bits with variable lengths (longer than one OFDM symbol in all cases).

In addition, the Fragment Repetition Encoder (FRE) block is an optional block that is only used in the robust communication mode for G.hnem. The FRE provides repetitions of fragments with the repetition rate of R. Each fragment is copied R times. The FRE supports the values $R = \{1, 2, 4, 6, 12\}$ (value of $R = 1$ corresponds to the normal mode of operation).

2.6 Standards discussion

After the previous description of the main features of the four main standards for narrowband power line communication solutions, a qualitative comparison is made in the

following paragraphs. A summary of the principal parameters for the physical layer is given in Table 2.2. Additionally, Table 2.1 lists the transmission data bit rates for some communication's modes.

One of the things that is worth mentioning about the standards is their different assumption about the transmission channel. Whereas PRIME uses a cyclic extension of $192\mu s$, G3-PLC, G.hnem and IEEE P1901.2 choose a shorter one ($75 - 160\mu s$). This extension should be set accordingly to the delay profile of the channel so there are no overlaps due to the reflected contributions. Additionally, it can be observed that different sizes are chosen for the IDFT/DFT transformation. PRIME uses the highest DFT/IDFT size, which allows for a higher number of available subcarriers. This is translated into a higher transmission rates. Nevertheless this requires a more complex transceiver.

Another interesting difference is the decision on the digital modulators. Earlier designs (PRIME and G3-PLC) use a non-coherent (i.e. DPSK) scheme whereas coherent (i.e. PSK) modulators are used in IEEE P1901.2 and G.hnem. In general, the choice between coherent and non-coherent modulation represents the trade-off between complexity and performance. Non-coherent demodulators do not need carrier frequency offset correction. In contrast, the SNR gain of PSK over DPSK is around 3dB in additive white Gaussian noise channels when assuming perfect channel knowledge [31]. In non-Gaussian noise environments, the SNR loss in DPSK systems is increased when the noise becomes more impulsive. The reason for this is that high powerful pulses can corrupt the phase reference which results in error propagation [32].

All considered standards implement some kind of error correction functions. Unlike PRIME, which use FEC only in their robust mode, the rest of the standards include this features by default. G3-PLC, G.hnem and IEEE P1901.2 use an outer-inner codification by means of a Reed-Solomon and a convolutional coder combination.

It is well know that the correction capabilities of decoders are enhanced by the use of an interleaver block. Burst errors produced by impulses are scattered by the interleaver so the decoder *sees* them with a more isolated pattern. Nevertheless, the interleaving structure can be designed in several ways. With respect to the NB-PLC solutions studied, PRIME uses an OFDM symbol interleaver (i.e. interleaving is done over all bits corresponding to the same OFDM symbol). In contrast with this, the rest of the standards have bet for a longer interleaver design. G3-PLC and IEEE P1901.2 perform this operation over all the bits in the packet and G.hnem can chose between two kind of interleaving: over fragments (i.e. groups of OFDM symbols) and over an AC-cycle.

The election of a longer or shorter interleaver has consequences on the quality of communications. On one hand, a shorter interleaver has the advantage that can be implemented with a simpler hardware. On the other hand, a longer interleaver scatters

errors over a larger number of bits, as a result, they are more isolated and corrections are more likely. However, having a long interleaver also increases the latency at the receiver, since the whole interleaved frame needs to be present before starting the deinterleaving process. This might be an important issue depending on the application.

2.7 Conclusions

Recent years have seen a growing interest of both the industry and the scientific community in using the power line networks as an alternative communication medium. Part of the reasons of this new popularity is due to the plausible use as information exchange mechanism in the Smart Grid paradigm. As a result, both the industry and standardisation organisations are making efforts in order to define robust and useful solutions.

This chapter has focused on the description of four of the most popular narrowband power line communications solutions; two of them developed by the industry (PRIME by the Spanish utility Iberdola and G3-PLC by the French EDF) and two designed by standardisation organisations (IEEE P1901.2 by the IEEE and G.hnem by the ITU-T).

The described standards count with a similar structure: they are OFDM-based transceiver mostly using a phase shift keying modulation and applying some kind of forward error correction techniques to increase robustness in the communication. Nevertheless, there are subtle differences among all of them. As stated by Dr. Galli [11], these differences are the result of a lack of agreement on the channel model, which leads to different assumptions on its effects over the transmitted signal (as an example, the cyclic extension should be determined by the power delay profile of the channel).

Pilot projects are being deployed (an example can be found in [12]) to provide empirical performances of some of this solutions. Results from this field test would give an idea of how appropriate these technologies are for Smart Grid's applications.

Some of the details described in this chapter will become helpful when analysing the communication's performance and when introducing the improvements that this thesis proposes in the forthcoming chapters.

Chapter 3

PLC channel description

3.1 Introduction

Simon Haykin wrote in the introduction for the chapter dedicated to noise and propagation in his book *Modern Wireless Communication* [33]:

> *"The study of propagation also provides clues to receiver techniques for compensating the impairments introduced through wireless transmission."*

This gives an idea of how important it is to study the modifications introduced by the channel since they are the source of most problems and limitations.

Although this idea is expressed in a wireless environment, as stated by Stefano Galli [34], both PLC and wireless environments share a number of characteristics. Most of them are due to the fact that both channels were not "designed" for carrying communication signals.

PLC channels suffer from different types of problems:

- Frequency-dependent attenuation of the channel.
- Channel's transfer function depends on location, network topology and connected loads.
- Non-Gaussian noise sources.

As it will be seen in the forthcoming chapters, these physical effects will have consequences in the transmitted signals. The channel's transfer function attenuates the transmitted signal differently depending on the frequency. As a result, the shape of the received spectrum is not equal to the one that was transmitted. Nevertheless, this kind of effects are typically undone with the use of equalizers at the receiver.

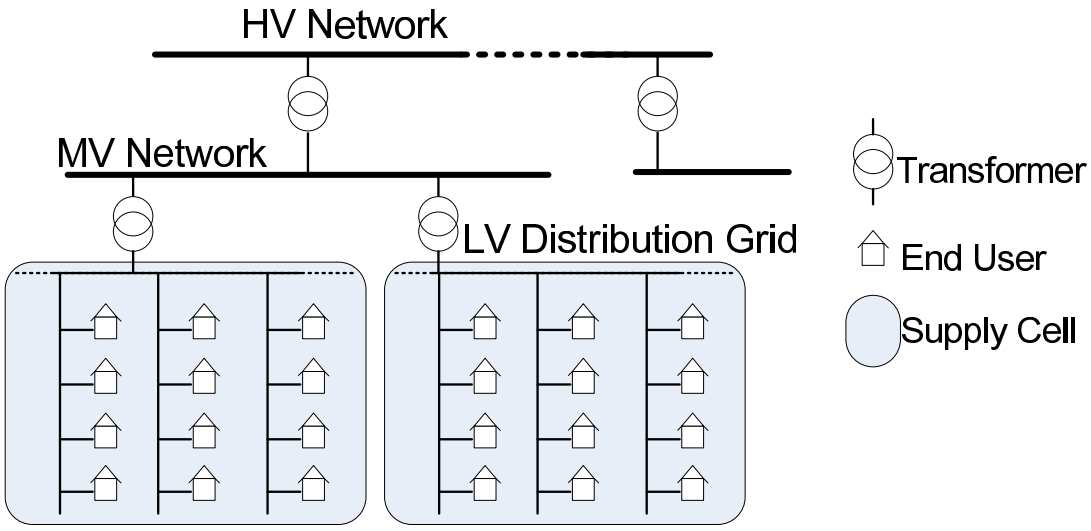

Figure 3.1: *Generic European power supply network structure. Adapted from [6].*

Alternatively, the presence of different noise sources influences the transmitted signal by adding an undetermined amount of power to it. Noise sources with an impulsive behaviour are specially harmful for the transmission techniques that are currently being used in PLC environments.

The following sections describe how all these effects are modelled in this thesis. First of all, Section 3.2 describes the generic structure of the distribution energy network making special focus on the low voltage grid, as it will be the main scenario for the rest of this work. Then, Section 3.3 describes the most common methods to model the power line's transfer function and details the specific process followed in order to take into account the multipath effect and attenuations. After this, Section 3.4 describes the main noise sources present in the the PLC networks and details in more depth the models used to emulate background and impulsive noise interferences, as they are the effects most commonly considered in the literature. And finally, some conclusions are drawn in Section 3.5.

3.2 Low-voltage network topology

The typical structure of the European 50 Hz power distribution grid, according to [6], is shown in Figure 3.1. The long-distance supply is provided on a 110 to 380 kV on the high voltage (HV) network. It is then transformed down to 10 to 30 kV for the medium voltage (MV) section. The used voltage depends on the travelled distances, which may be up to 10 km in the rural environments. Finally, the third section consists of the low voltage (LV) network, also referred to as *last mile*, where voltages are in the range of 230 to 400 V.

The present work focuses on the low voltage distribution grid. This network consists of a three-phase network that physically corresponds to the part of the network between the transformer stations and the end users' connections. As seen in Figure 3.1, end users are grouped in what is called *supply cells* and, depending on the load, more than one transformer might serve the whole cell. Additionally, according to [6], supply cells consist of up to 10 branches with maximum of 30 users per branch; which means that each cell serves up to 300 users.

Moreover, a low impedance is found at the point where the distribution line enters the house. A typical indoor power line exhibits a characteristic impedance in the range of $40-80\ \Omega$. According to [35], the input house impedances follow a uniform distribution in the range of $[0,5]+j[-5,-5]\ \Omega$, i.e. very close to a short circuit. This fact is also the responsible for the high attenuation of the power line channel.

3.3 Channel transfer function

The PLC network has a tree-wise topology. There exists a main distribution line and a number of secondary ones that are connected to it as branches. These secondary lines have different termination loads. As in wireless environmental, multipath effects occur caused by reflections and impedance mismatches which disturbs the transmitted signals.

One popular model used to compute the transfer function of the PLC channel is the one described by Phillips [36] and by Zimmerman and Dostert [7]. This model estimates the time delay due to each transmission path and its corresponding attenuation given the cable length. All these contributions are then summed up, as the following expression shows:

$$H(f) = \sum_{i=1}^{N} \underbrace{g_i}_{\text{weight}} \cdot \underbrace{e^{-(\alpha_0+\alpha_1 \cdot f^k)\cdot d_i}}_{\text{attenuation}} \cdot \underbrace{e^{-j2\pi f\cdot(d_i/v_p)}}_{\text{delay}} \tag{3.1}$$

where N stands for the number of considered paths; g_i is the associated weight for each path; α_0, α_1 and k are parameters based on the cable model and geometric dimensions; d_i is the path length; and the factor d_i/v_p stands for the delay of each path. Both attenuation and delay are dependent on the frequency f. This empirical method, based on parameters adjusted by measurements, is commonly known as **Top-Down Approach**.

A few years later, Banwell and Galli proposed a channel model based on Multiconductor Transmission Lines (MTL) theory [37]. Following this model, the PLC network is represented with its discrete element model which takes into account all kind of delays, attenuations and reflections. This method has as a major advantage: it is possible to compute the transfer function of any PLC link before it is deployed and in a deterministic

way. However, a complete detailed knowledge of the topology is needed, which, in some cases, is not available. This method is commonly referred to as **Bottom-Up Approach** and, due to the analytical approach of this thesis, it is the method that will be used to model the PLC channel. A number of previous studies (such as the ones in [38–41]) have also used this kind of approach when addressing the modelling of the PLC channel's transfer function.

In the following, a detailed description of the steps followed in the computations are given.

3.3.1 Modelling of the channel's transfer function following a bottom-up approach

The major attenuation of the signal in a PLC network is due to losses in the transmission media (wires) and its terminations (loads). A cable can be modelled very accurately using its per-unit-length parameters. Theses are the resistance, capacitance, inductance and admittance per unit of length (R, C, L and G, respectively). They are used to compute cable's characteristic impedance (Z_c) and propagation constant (γ):

$$Z_c = \sqrt{\frac{R + j\omega L}{G + j\omega C}} \tag{3.2}$$

$$\gamma = \alpha + j\beta = \sqrt{(R + j\omega L) \cdot (G + j\omega C)} \tag{3.3}$$

where ω is the angular frequency (i.e. $\omega = 2\pi \cdot f$).

These parameters are also known as the distributed line parameters [42]. In Equation 3.3 both α and β stand for the attenuation and phase shift per unit of length respectively and are measured in Np/m and rad/m.

Alternatively, the Transmission Matrix of a two-port network describes the relationship between their voltage and current values at both ports. Figure 3.2 shows a two-port network defined by its ABCD parameters [42]. Equation 3.4 defines the relationship between the pairs (U_1, I_1) and (U_2, I_2) using a transmission matrix when considering the current directions and voltages as depicted in Figure 3.2.

$$\begin{bmatrix} U_1 \\ I_1 \end{bmatrix} = [T] \begin{bmatrix} U_2 \\ I_2 \end{bmatrix} = \begin{bmatrix} A & B \\ C & D \end{bmatrix} \begin{bmatrix} U_2 \\ I_2 \end{bmatrix} \tag{3.4}$$

All ABCD parameters can be computed based on the distributed line parameters (Z_c and γ) and cable's lengths (l). As seen in Equation 3.4, they can be used to relate the input and output voltages (i.e. build a transfer function).

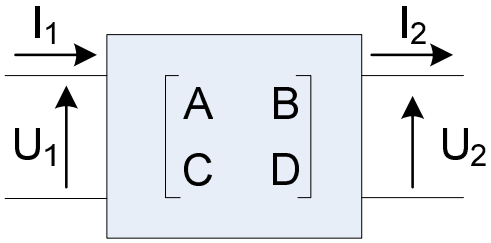

Figure 3.2: *Transmission Matrix description of a two-port network.*

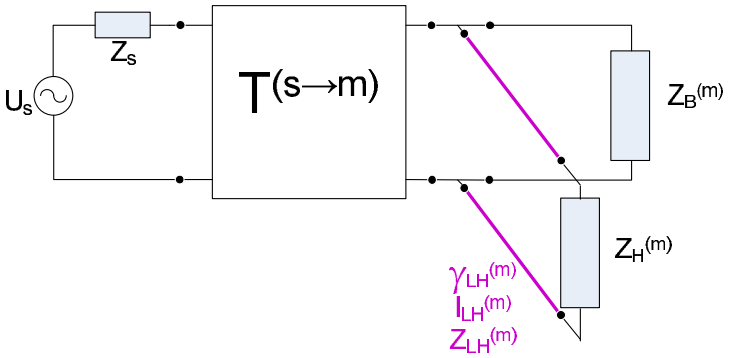

Figure 3.3: *Generic scheme of the circuits that interconnects the MV/LV transformer to the m^{th} end-customer.*

Given the definition of the previous transmission matrix model, the generic circuit that interconnects the MV/LV transformer to any given user (m) is schemed in Figure 3.3. In this figure, distribution cables between the transformer and the m^{th} user are modelled by the transmission matrix $T^{s\to m}$ whereas the rest of the network is seen as a parallel impedance $Z_B^{(m)}$. Additionally, the user's input impedance $(Z_H^{(m)})$ is not directly connected to the main distribution line, so the local loop cable (referred by subindex LH) also needs to be taken into account. The process to be followed in order to compute the overall transfer's function (i.e. $H^{(s\to m)}(f)$) is given in the following paragraphs.

First of all, let's begin with the impedance $Z_B^{(m)}$, which is due to the rest of the elements that are placed downstream the node of interest. In order to compute its value, an iterative process is followed starting from the impedance placed at the farthest position from the transformer (let's assume this node is placed at position N). Figure 3.4 shows a generic scheme of the main distribution line and the local loops for each user.

Starting from node placed at position N, the impedance seen at the input of its local loop can be computed with the equation that computes the input impedance of a loaded transmission line:

$$Z_{LL}^{(N)} = Z_{LH}^{(N)} \cdot \frac{Z_H^{(N)} + Z_{LH}^{(N)} \cdot \tanh(\phi_{LH}^{(N)})}{Z_{LH}^{(N)} + Z_H^{(N)} \cdot \tanh(\phi_{LH}^{(N)})} \tag{3.5}$$

where $Z_{LH}^{(N)}$ stands for the characteristic impedance of the transmission line for the

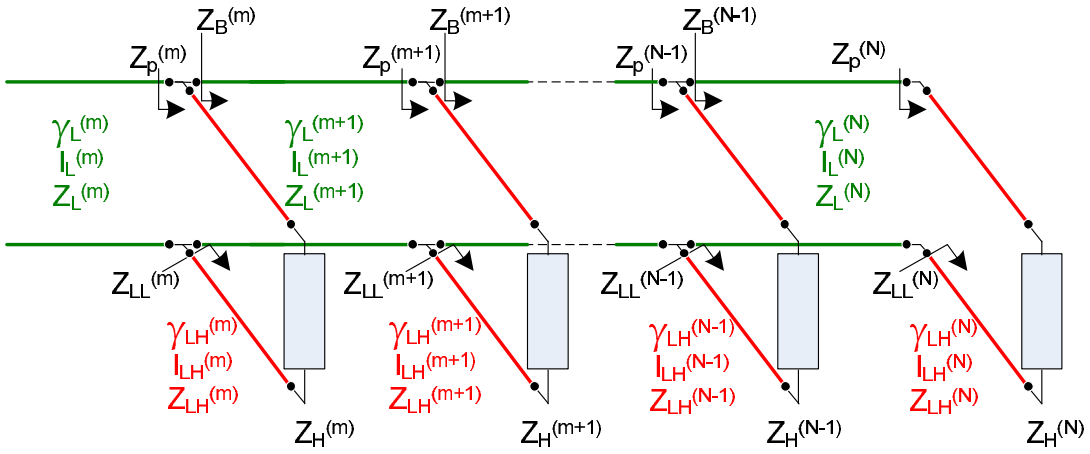

Figure 3.4: *Generic network segment as an example of the computation of* $Z_B^{(m)}$.

local loop; $Z_H^{(N)}$ is, as mentioned, the user's input impedance; and $\phi_{LH}^{(N)} = \gamma_{LH}^{(N)} \cdot l_{LH}^{(N)}$ represents the propagation through the local loop.

When moving in the upstream direction, the same computation can be done for node $N-1$. However, at this point, the impedance at the input of its local loop is placed in parallel with the impedance seen to the downstream direction ($Z_B^{(N-1)}$). Analogously to Equation 3.5, it can be computed with:

$$Z_B^{(N-1)} = Z_L^{(N)} \cdot \frac{Z_{LL}^{(N)} + Z_L^{(N)} \cdot \tanh(\phi_L^{(N)})}{Z_L^{(N)} + Z_{LL}^{(N)} \cdot \tanh(\phi_L^{(N)})} \tag{3.6}$$

As Figure 3.4 shows, both $Z_B^{(N-1)}$ and $Z_{LL}^{(N-1)}$ are placed in parallel, so their combined value (expressed by $Z_p^{(N-1)}$) is computed with:

$$Z_p^{(N-1)} = \frac{Z_B^{(N-1)} \cdot Z_{LL}^{(N-1)}}{Z_B^{(N-1)} + Z_{LL}^{(N-1)}} \tag{3.7}$$

For any generic node placed at position m, previous equations can be redefined as:

$$Z_B^{(m)} = Z_L^{(m+1)} \cdot \frac{Z_p^{(m+1)} + Z_L^{(m+1)} \cdot \tanh(\phi_L^{(m+1)})}{Z_L^{(m+1)} + Z_p^{(m+1)} \cdot \tanh(\phi_L^{(m+1)})} \tag{3.8}$$

$$Z_{LL}^{(m)} = Z_{LH}^{(m)} \cdot \frac{Z_H^{(m)} + Z_{LH}^{(m)} \cdot \tanh(\phi_{LH}^{(m)})}{Z_{LH}^{(m)} + Z_H^{(m)} \cdot \tanh(\phi_{LH}^{(m)})} \tag{3.9}$$

$$Z_p^{(m)} = \frac{Z_B^{(m)} \cdot Z_{LL}^{(m)}}{Z_B^{(m)} + Z_{LL}^{(m)}} \tag{3.10}$$

Once $Z_B^{(m)}$ is computed, it is the moment to compute the transmission matrix from the transformer to the m^{th} user (i.e. $T^{(s \to m)}$). This time, the computation is started

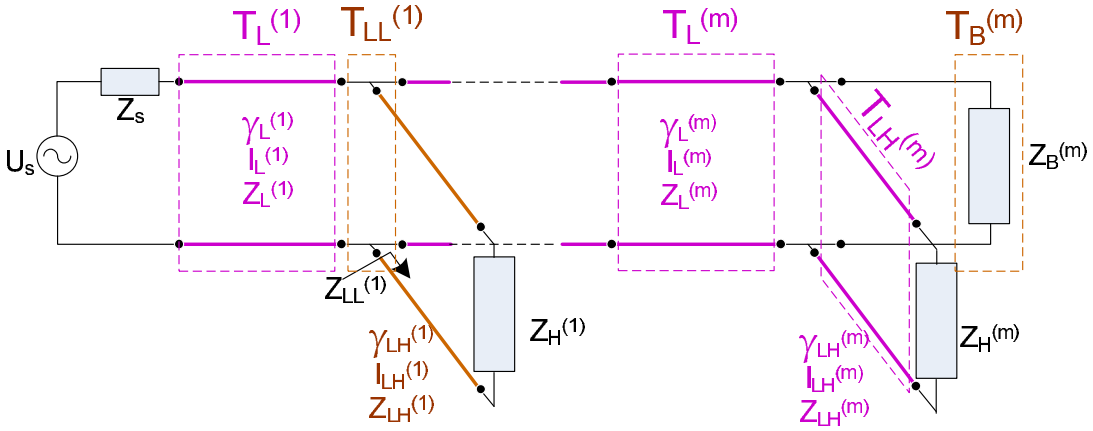

Figure 3.5: *Generic network segment as an example of the computation of $T_{s\to m}$.*

from the nodes placed at the nearest positions to the transformer. Figure 3.5 shows a schematic of the circuit that exists from the MV/LV transformer to a generic end user placed at position m.

As it can be seen, the different segments can be modelled by their respective transmission line matrices. The first segment is the distribution line from the transformer to the first local loop. This transmission matrix can be computed with [42]:

$$[T_L^{(1)}] = \begin{bmatrix} \cosh(\phi_L^{(1)}) & Z_L^{(1)} \cdot \sinh(\phi_L^{(1)}) \\ \frac{1}{Z_L^{(1)}} \cdot \sinh(\phi_L^{(1)}) & \cosh(\phi_L^{(1)}) \end{bmatrix} \tag{3.11}$$

The next segment is the one corresponding of a local loop which belongs to an end-user different to m. In this case, the transmission matrix is the one which models an impedance placed in parallel [42]:

$$[T_{LL}^{(1)}] = \begin{bmatrix} 1 & 0 \\ \frac{1}{Z_{LL}^{(1)}} & 1 \end{bmatrix} \tag{3.12}$$

where $Z_{LL}^{(1)}$ can be computed as the input impedance of a loaded transmission line (Equation 3.9). This same process is continued iteratively in a downstream direction until the m^{th} derivation is reached.

Once $Z_B^{(m)}$ and $T_{s\to m}$ are computed, the scheme shown in Figure 3.3 is completed. Now, in order to reach the $Z_H^{(m)}$ load, the transmission matrix of the parallel impedance ($T_B^{(m)}$ in Figure 3.5; computed using an analogous expression as the one in Equation 3.12) and the transmission matrix for the local loop line ($T_{LH}^{(m)}$ in Figure 3.5; computed using an analogous expression as the one in Equation 3.11) need to be included in the computation.

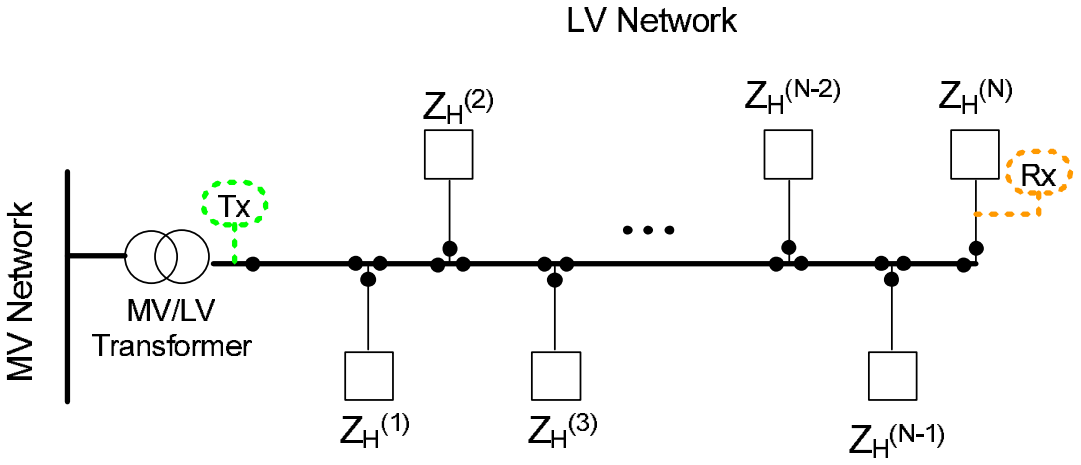

Figure 3.6: *Generic simplified transmission scenario, as used in [43].*

The overall transmission matrix can be computed as the multiplication of each one of the transmission matrices which modelled each segment of the network. In the case of the m^{th} node, this leads to:

$$T^{(s\to m)} = T_L^{(1)} \cdot T_{LL}^{(1)} \cdot T_L^{(2)} \cdot T_{LL}^{(2)} \cdot \cdots \cdot T_L^{(m-1)} \cdot T_{LL}^{(m-1)} \cdot T_L^{(m)} \cdot T_B^{(m)} \cdot T_{LH}^{(m)} = \begin{bmatrix} A^{(m)} & B^{(m)} \\ C^{(m)} & D^{(m)} \end{bmatrix} \quad (3.13)$$

In order to obtain the pursued transfer function from the source to the m^{th} user, the following computation can be made taking into account the definition stated in Equation 3.4:

$$H^{(s\to m)}(f) = \frac{U_m(f)}{U_s(f)} = \frac{Z_H^{(m)}(f)}{A^{(m)}(f) Z_H^{(m)}(f) + B^{(m)}(f)} \quad (3.14)$$

3.3.2 Numerical example

All the formalism described in previous subsection is now implemented in a test case to see the kind of effects that are produced by the power line channel. The scenario under study is shown in Figure 3.6 and it is taken from the paper published by L. Lampe et al. [43]. It consists of a transmitter and a receiver placed in a main distribution line with several branches due to all the end-users connected to the network.

For this numerical example, models NAYY150SE and NAYY50SE are used for the main supply cables and the local loop cables respectively, as suggested in [43, 44]. The per-unit-length parameters can be computed using cables' physical properties with:

$$\begin{aligned} R &= \sqrt{\rho \cdot \pi \cdot f \cdot \mu_0 / r^2}, \qquad G = 2\pi \cdot f \cdot C \cdot tan(\delta_c) \\ L &= \mu_0 \cdot \vartheta / (2r), \qquad C = 2 \cdot \epsilon_0 \cdot \epsilon_r \cdot r / \vartheta \end{aligned} \quad (3.15)$$

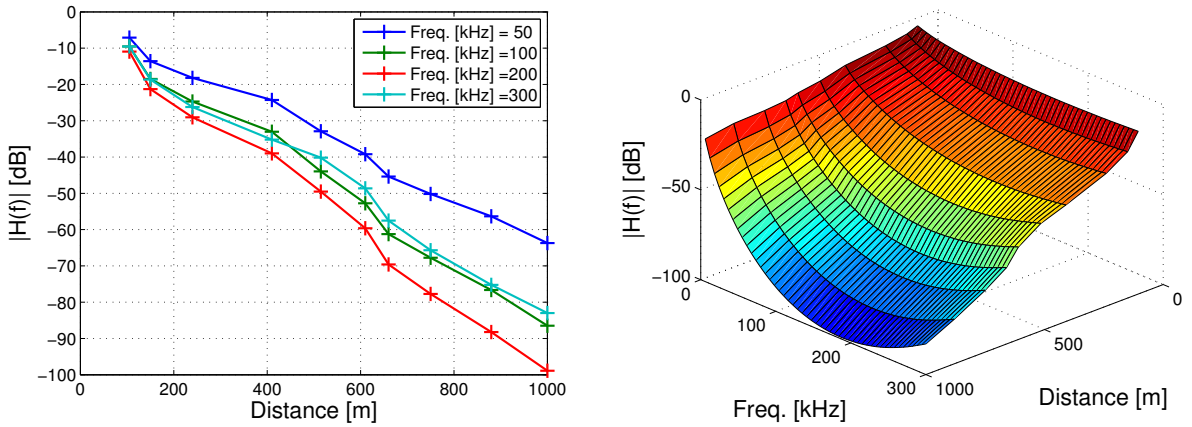

(a) (b)

Figure 3.7: *Channel transfer function for several locations of the receiver. (a) Transfer function for some frequencies; (b) transfer function depending on the distance and frequency.*

where μ_0 is the vacuum permeability, ϵ_0 is the vacuum permittivity, ϵ_r stands for the relative permittivity, $tan(\delta_c)$ is the dielectric's loss tangent, and ρ is the conductor' specific resistance. Additionally, r and ϑ denote the radius of the cable and the thickness of the insulation (see [6]). The numerical values for the NAYY150SE are $r = 15.6$ mm and $\vartheta = 3.6$ mm; whereas for the and NAYY50SE, they are $r = 9.4$ mm and $\vartheta = 2.8$ mm. The rest of the parameters are $\epsilon_r = 4$, $\rho = 2.8 \cdot 10^{-8}$ Ω·m and $\tan(\delta_c) = 0.01$ for both cases.

Additionally, the MV/LV transformer is modelled as a resistor in series with a capacitor and both in parallel with an inductance. Values are set to $R_T = 8\ \Omega$, $L_T = 25\ \mu$H and $C_T = 48$ nF for the resistance, inductance and capacitance, respectively, according to [45].

Inspired in the experiment analysed in [43], Figure 3.7a shows the magnitude transfer function that exists from the Tx to the Rx node in Figure 3.6 when transmitting in a network with 10 nodes (i.e. $H^{(s\to 10)}(f)$ in Equation 3.14). This transfer function is computed for frequencies $f = \{50, 100, 200, 300\}$ kHz and for different locations of the receiver node. Input impedances for the end users ($Z_H^{(m)}$) are generated randomly according to a uniform distribution of $[0, 5]+j[-5, 5]\ \Omega$ as stated in [43].

As seen in Figure 3.7, attenuation increases rapidly with the distance for all frequencies. Represented results, which were computed using the transmission lines theory detailed in the previous section, are in good agreement with the ones shown in the publication by Lampe et al. [43]. Additionally, Figure 3.7b shows the transfer function for the different locations of the receiver with a higher frequency resolution.

3.4 Channel noise sources

As it has already been mentioned, the power line channel is a very hostile and harsh communication medium. Regarding noise disturbances present in the PLC channel, the following sources are typically considered [8, 46]:

- *Coloured background noise.* It has a relatively low power spectral density which varies with frequency. This type of noise is due to the contribution of several low power noise sources. Its envelope stays constant for long period of time.
- *Narrow-band noise.* It is due to broadcasters in long and short wave range and it is also affected by some radio receivers like amateur radio. Its intensity and frequency varies over time and place.
- *Periodic impulsive noise synchronous to the mains frequency.* Its duration is very short (around microseconds) and are mainly caused by the switching of rectifier diodes. It occurs in a repetition rate of 50 or 100 Hz (in Europe).
- *Periodic impulsive noise asynchronous to the main frequency.* It is mainly caused by switching power supplies. Frequencies of occurrence are between 50 kHz and 2 MHz. They usually occur in a short period of time and with a relatively low amplitude.
- *Asynchronous impulsive noise.* Caused by switching transients in the network. The impulses have a duration which varies from micro to milliseconds. Its power spectrum density may raise 50 dB over the background noise.

As in many other studies [43, 47–50], the analysis carried out in this thesis will take into account two main disturbance sources: the **background** and the **asynchronous impulsive** noise. Therefore, the total discrete-time noise will be seen as:

$$\text{total\_noise}[n] = z[n] + i[n] \tag{3.16}$$

where the terms $z[n]$ and $i[n]$ stand for background and impulsive noise respectively and n represents the discrete time index. A detailed description of the computation for each noise source will be given in the following sections.

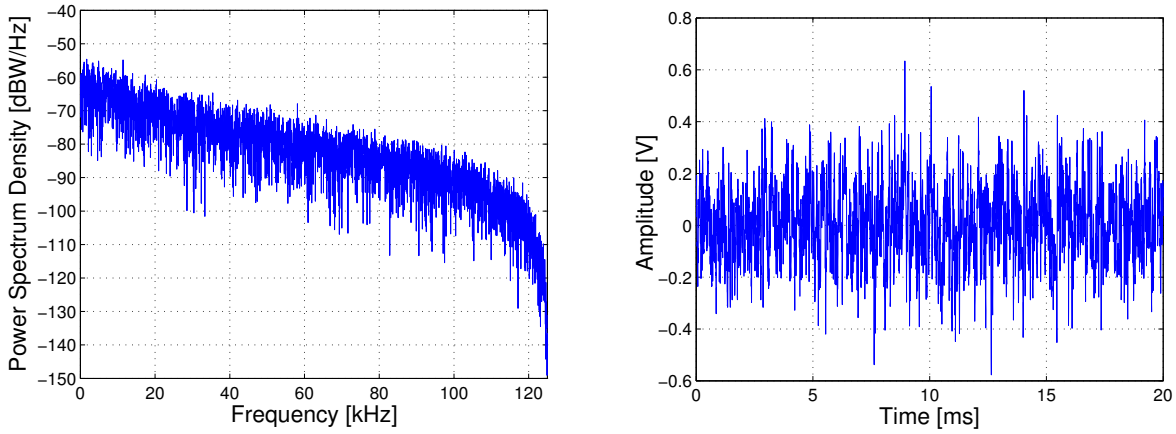

(a) (b)

Figure 3.8: *Hooijen's background noise model. (a) Spectral realisation. (b) Time realisation.*

3.4.1 Background noise in narrowband PLC channels

A series of measurements carried out in the city of Amsterdam [51] are typically used to characterize the background noise present in the PLC network. Using a spectrum analyser controlled by a PC, a number of noise samples were automatically acquired during a period of four weeks at four different locations. The work carried out by O. G. Hooijen in [51] studies the whole CENELEC-A band with a frequency resolution of 1 kHz.

As reported in Hooijen's study, the Power Spectrum Density (PSD) of the noise was found to follow a decreasing function with frequency which, on average, is approximated with the following expression:

$$N(f) = 10^{K-3.95\cdot10^{-5}\cdot f} \qquad [W/Hz] \tag{3.17}$$

where K follows a normal distribution with mean $\mu = -5.64$ and a standard deviation of $\sigma = 0.5$, and f is the frequency in Hertz.

As mentioned in [51], the value of K in Equation 3.17 does change with time and transmitter-receiver locations. This change occurs more often during the day than during the night, although it is not very significant in both cases.

A realization for background noise can be synthesized by filtering a white noise source, as it was proposed in [52]. The idea is to transform the power spectrum density using a linear filter. This is done in Figure 3.8, where the generated PSD and a time realisation of Hooijen's background noise is shown.

3.4.2 Impulsive noise in narrowband PLC channels

Middleton's model is one of the most popular models of impulsive noise. D. Middletone developed statistical-physical models for electromagnetic interference in a series of papers [53–55].

As stated in [55], Middleton's work is based on developing statistical-physical models for man-made and natural electromagnetic interferences.

Middleton's Noise Model classifies the noise in three general cases: *Class A*, *Class B* and *Class C*. *Class A* is typically used for modelling PLC channels [56–58].

The Probability Density Function (PDF) of the impulsive noise, $p_A(i)$, according to Middletone's Class-A noise can be written as:

$$p_A(i) = \sum_{m=0}^{M-1} e^{-A} \frac{A^m}{m!} \frac{1}{\sqrt{2\pi\sigma_m^2}} e^{-\frac{i^2}{2\sigma_m^2}} \tag{3.18}$$

where

$$\sigma_m^2 = \sigma_Z^2 \frac{m/A + \Gamma}{1 + \Gamma} = \sigma_I^2 \frac{m}{A} + \sigma_Z^2 \tag{3.19}$$

M is the number of considered sources, i stands for the impulsive random variable, A is known as the *impulsive index*, σ_m^2 is the variance of the m^{th} noise source and $\Gamma = \sigma_Z^2/\sigma_I^2$ is the mean power ratio between background and impulsive noise, sometimes referred to as *Gaussian-to-Impulsive variance Ratio* (GIR).

Note how Equation 3.18 is a weighted sum of Gaussian distributions, each one of them with a variance that increases with m.

Thanks to some derivations detailed in [59], the PDF given in Equation 3.18 can be expressed in terms of decibels with:

$$p_A(i_{dB}) = \sum_{m=0}^{\infty} e^{-A} \frac{A^m}{m!} \cdot L_m \cdot D \cdot \exp(D \cdot i - L_m \cdot e^{D \cdot i}) \tag{3.20}$$

with $L_m = (m \cdot \sigma_I^2/A + \sigma_Z^2)^{-1}$ and $D = (\log_e(10))/10 \approx 0.23$.

An example of the probability distribution function of Equation 3.20 is shown in Figure 3.9a using $A = 0.5$, $\Gamma = 0.001$ and $\sigma_Z^2 = 1\text{mW}$. Thin lines show the different contributions for 4 different noise sources ($M = 4$) without taking into account the $A^m/m!$ factor. It can be seen how, due to the different variance values, the curves are placed in different position in the abscissas axis.

The factor $A^m/m!$ makes the terms decrease very quickly as m increases. Figure 3.9b shows the evolution of this term as a function of m. The thick line in Figure 3.9a represents the weighted sum of all contributions (as in Equation 3.20). This curve shows

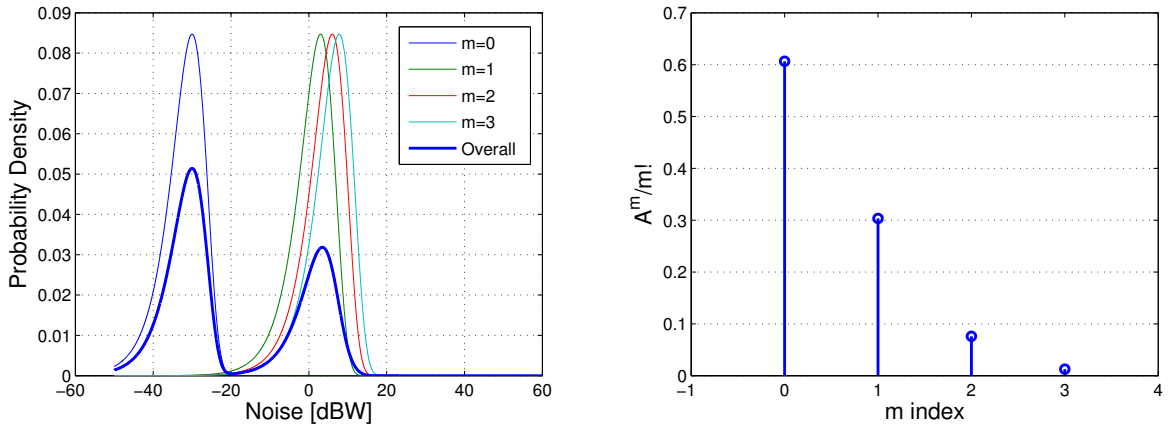

(a) (b)

Figure 3.9: *Probability density function of Middleton's impulsive noise model. (a) Individual terms and total PDF of the Class-A noise transformed in dBW (Equation 3.20). Parameters are:* $A = 0.5$, $\Gamma = 0.001$ *and* $\sigma_Z^2 = 1mW$. *(b) Decrement of* $A^m/m!$ *factor as* m *increases. It makes the first noise sources more dominant.*

very explicitly the behaviour of the modelled noise: the highest peak represents a low-power noise contribution which is very present in the channel (its probability is high) whereas the lowest peak represents the impulsive samples, that have a lower occurrence but a higher power.

A complementary representation of Equation 3.18 is the exceedance probability ($P(x \geq X)$). Its relationship with the PDF can be seen in Figure 3.10. The PDF for the noise in dBW is shown at the top of the figure, whereas the exceedance is represented in the bottom plot. The value of the exceedance at a given point x_0 is the area under the PDF to the right of x_0.

Even though the exceedance probability includes all the information about the statistical values of a signal, a few calculations are needed to obtain a concrete realisation of an impulsive noise source. For this purpose, the Monte Carlo Inverse Transform Method ([60], page 54) can be used in order to generate noise samples following a given Middelton distribution. This method makes use of the exceedance probability to create the noise samples. First of all, an uniform distribution in the interval [0,1] is created using N samples. Using an exceedance plot, such as the one shown in Figure 3.10, these uniformly distributed values are mapped into power values, which are then translated into N amplitudes that follow the required PDF.

Figure 3.11 shows a time realization of a Middleton's Class-A noise with $A = 0.5$, $\Gamma = 0.001$ and $\sigma_Z^2 = 1$ mW. There, it can be seen the background and impulsive components of the noise. Moreover, an histogram of those noise values is presented in Figure 3.11b. It shows a complete agreement with the PDF shape in Figure 3.9a, as it could be expected.

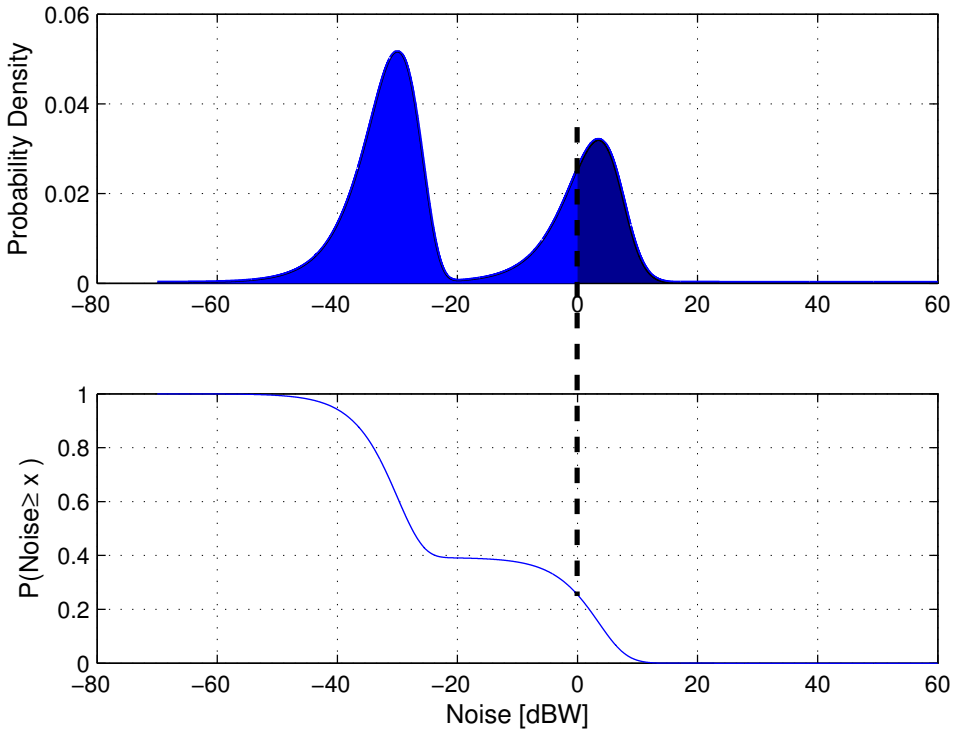

Figure 3.10: *Relation between the exceedance and probability density function of Class-A noise. The exceedance value for x=0 is the area under the PDF curve from x=0 to the right.*

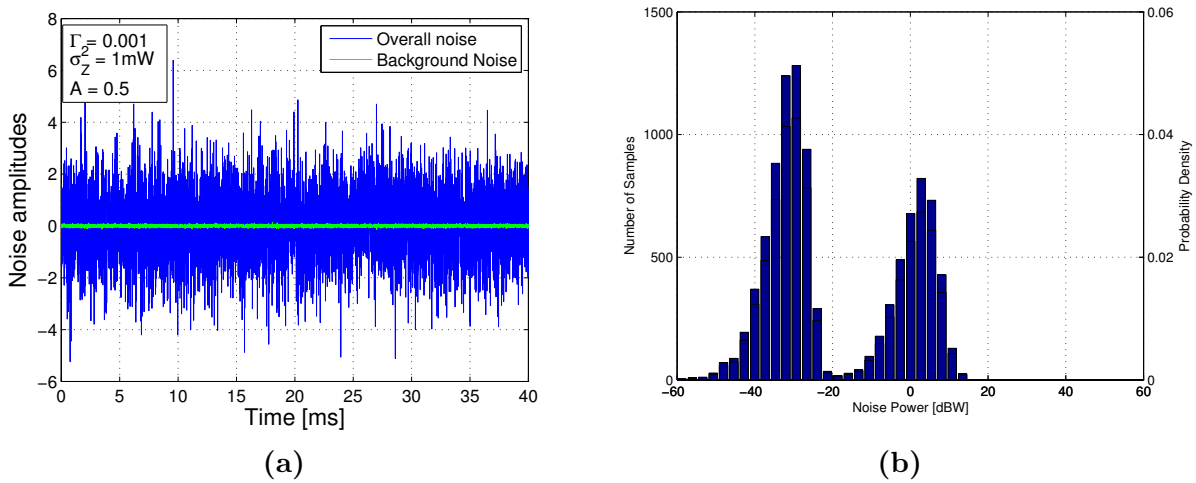

(a) **(b)**

Figure 3.11: *Impulsive noise realization. (a) Middleton's noise realization using Monte Carlo's Inverse Method. (b) Histogram of the samples. It resembles the PDF shape in Figure 3.9a.*

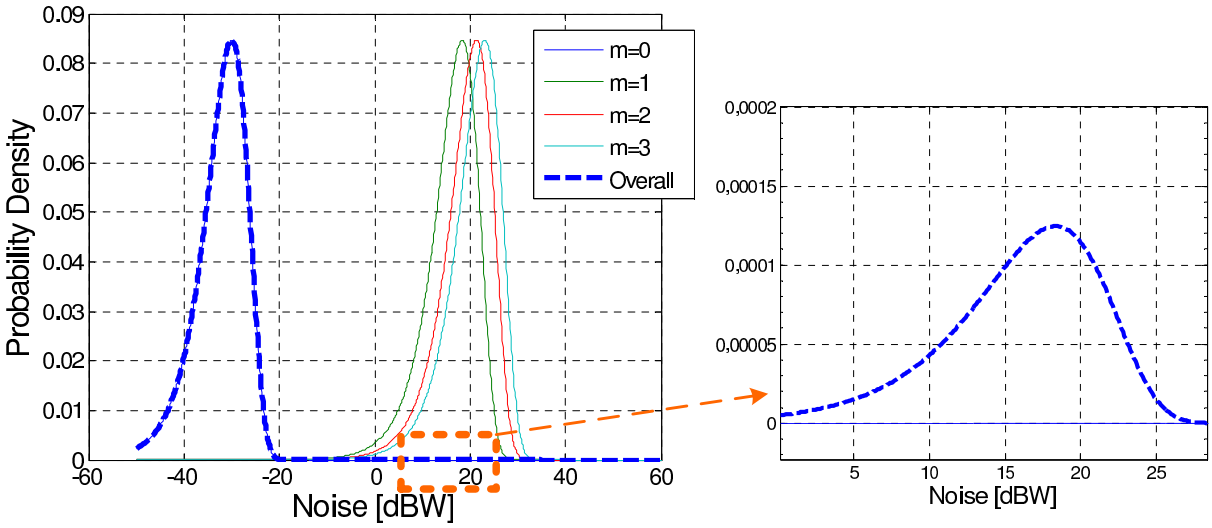

Figure 3.12: *Impulsive noise realisation with parameters* $A = 1.47 \cdot 10^{-4}$, $\Gamma = 0.1$ *and* $\sigma_z^2 = 1mW$, *taken from [61].*

Previous values for Middleton's impulsive noise model were used just for explicative purposes. In the rest of this thesis, in order to reproduce a scenario as realistic as possible, values obtained from narrowband power line communications measurements are used. Impulsive noise parameters, reported in [61] are set to $A = 1.47 \cdot 10^{-4}$ and $\Gamma = 0.1$. Figure 3.12 depicts the probability density function of this type of noise. Due the low probability of the impulses, a zoomed version of the image is also provided. For this set of parameter, a time realisation of the noise is given in Figure 3.13.

3.5 Conclusions

This chapter describes the main problems that have to be considered when transmitting information through the power lines. As it is done in a number of studies in the literature, the analysis is focused on two channel effects: channel's transfer function and channel's noise sources.

With respect to the channel's transfer function, a multiconductor transmission line model is used to emulate the propagation effects of the signal in the power lines. This approach models accurately attenuations and reflections that occur in the channel using physical cable's parameters and the topology of the network. This kind of approach has previously been used in several publications to analytically determine the behaviour of a given distribution grid.

Regarding the noise sources in the PLC channel, both background and impulsive noise sources are considered in this thesis. Whereas the background model is obtained from real field measurement, Middleton's Class-A statistical model is used to emulate impulsive

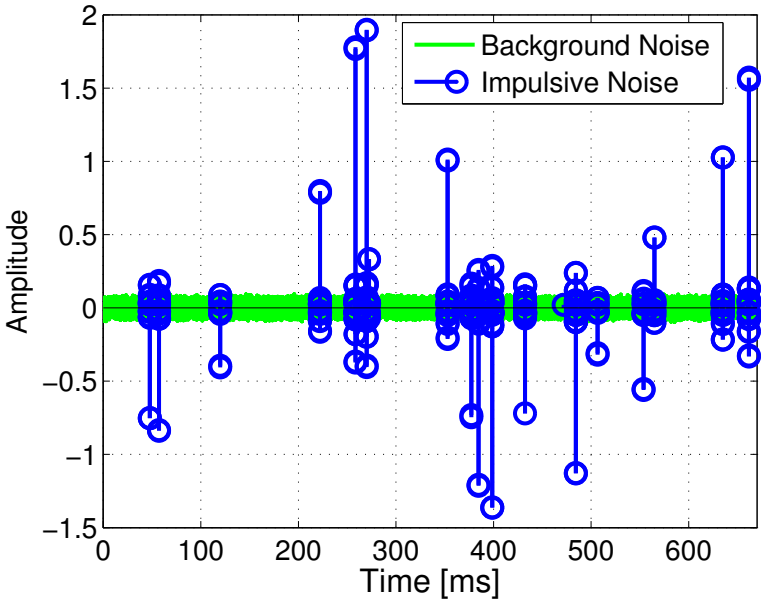

Figure 3.13: *Time realisation of the impulsive noise with parameters taken from [61].*

noise sources. As it will be seen in Chapter 4, the presence of impulsive noise in the power line channel produces severe disturbances in the communication's performance.

Finally, all channel effects described in this section will be taken into account in the forthcoming chapters to assess the different transmission techniques proposed in this dissertation.

Chapter 4

Physical performance analysis

4.1 Introduction

The present chapter focuses on the performance evaluation of two of the most popular, and previously presented, solutions for narrow band power line communications endorsed by the industry: PRIME and G3-PLC. This evaluation takes into account the physical layer of the communication' stack. The metric used in the analysis is the bit error rate (BER) as a function of the signal-to-noise ratio (SNR). This feature is typically used when evaluating the physical layer of communication' systems

The analysis takes into account the different channel noise sources described in Chapter 3 in order to evaluate the differences in performance for each PLC solution. Results show how G3-PLC behaves significantly better than PRIME when the channel is impaired by impulsive noise. As it will be seen, these differences are due to the different transceiver configurations used in PRIME and G3-PLC.

The chapter is divided in several sections and each one of them is focused on evaluating the performance of both PLC standards under different noisy environments. Section 4.2 studies the performance in a typical scenario such as an additive white Gaussian noise environment. Section 4.3 modifies the transmission channel to include the background noise described in Section 3.4.1. Finally, asynchronous impulsive noise is included in Section 4.4, where theoretical and simulated performances are discussed.

4.2 Performance evaluation in additive white gaussian noise channel

A common way to study the performance of a communication system is analysing its behaviour in an Additive White Gaussian Noise (AWGN) channel. The reason for this is that it is a very well known channel model that has two major advantages: first of all, it models accurately a number of the transmission mediums and, second of all, theoretical

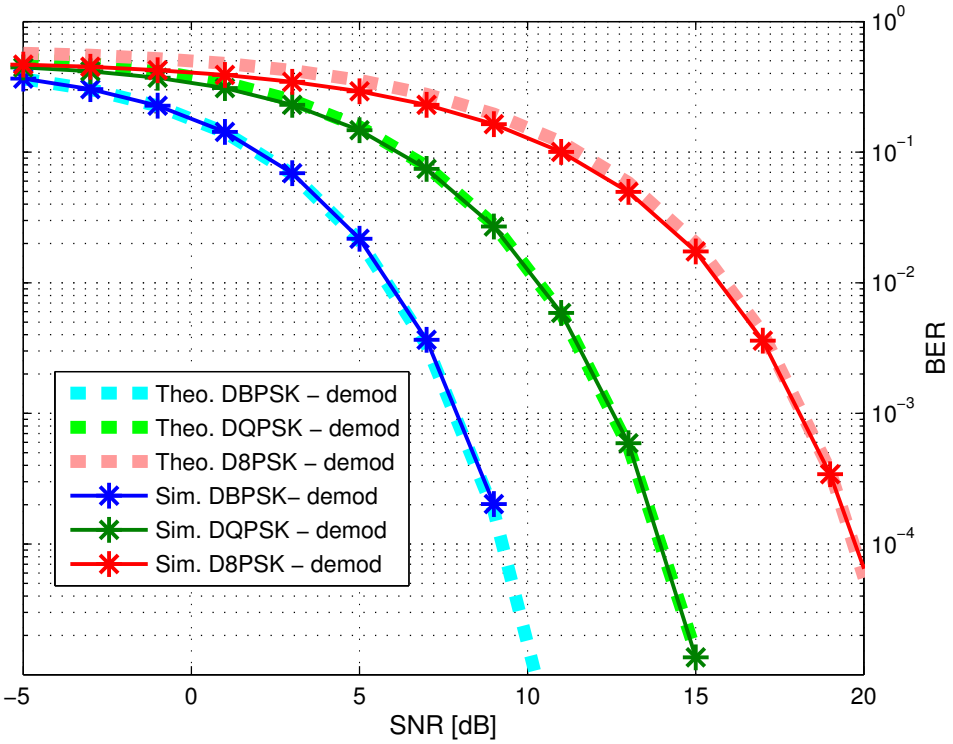

(a)

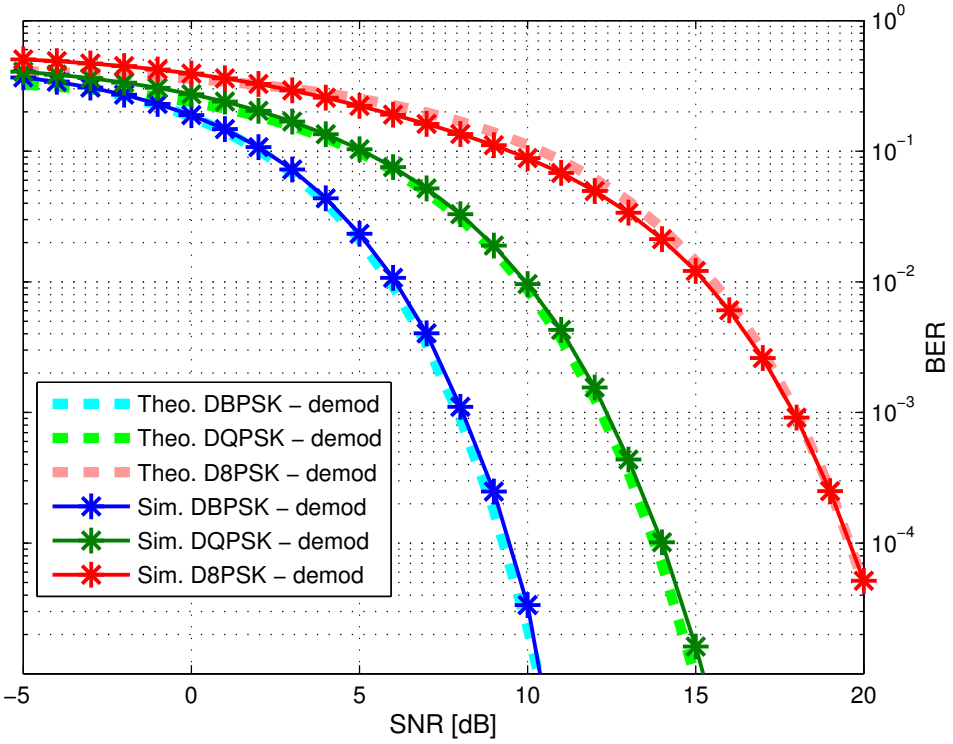

(b)

Figure 4.1: *Performances for additive white Gaussian noise (AWGN) at the demodulator. Theoretical and simulated values. (a) PRIME's performance. (b) G3-PLC's performance.*

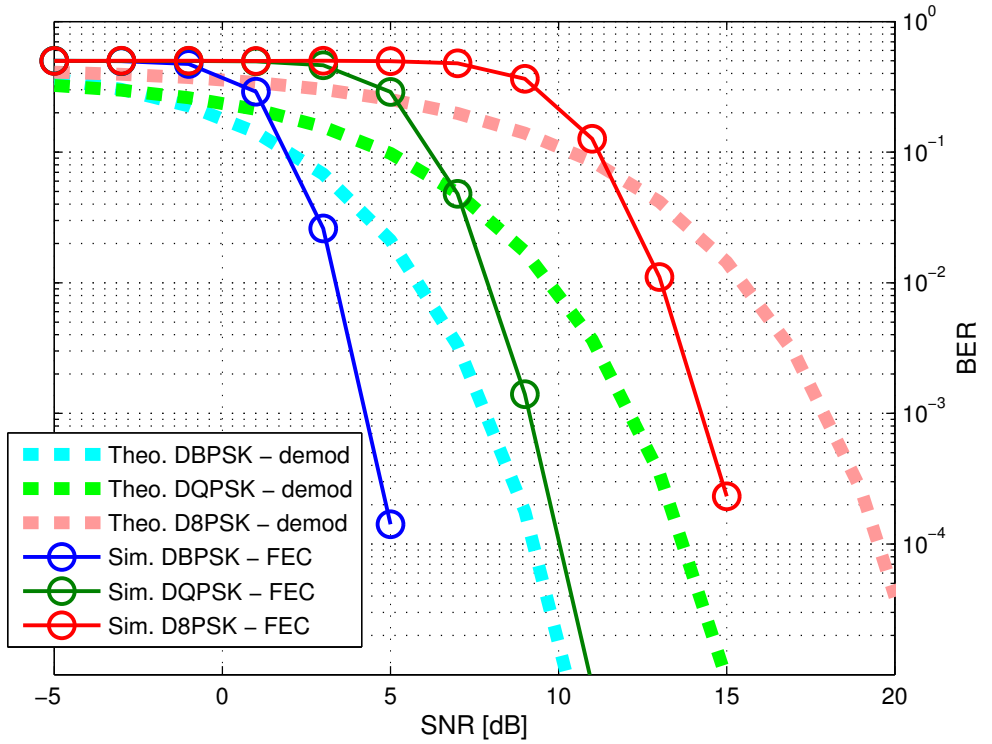

(a)

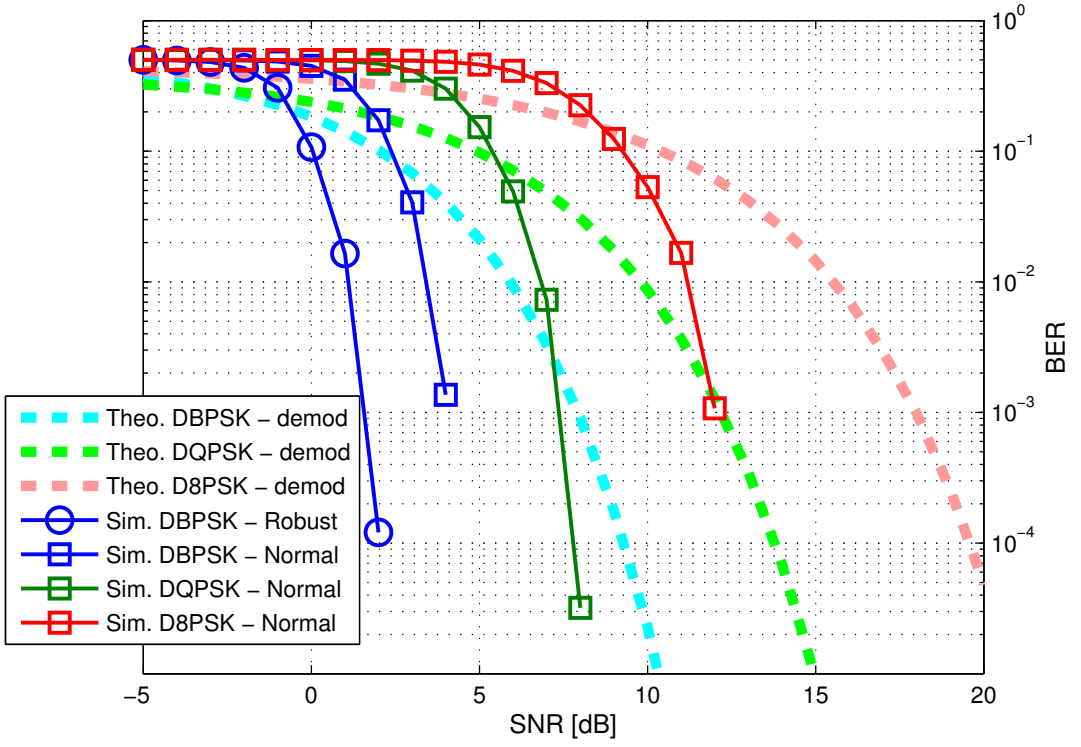

(b)

Figure 4.2: *Performances for additive white Gaussian noise (AWGN) when using FEC. (a) PRIME's performance. (b) G3-PLC's performance*

performances can easily be computed thanks to the statistical properties of such a noise source.

Performances in case of dealing with an additive white Gaussian noise channel can be seen in Figure 4.1. Graphs represent the bit error rate at the output of the digital demodulators at the receiver side (see Figures 2.4 and 2.8 for PRIME and G3-PLC's transceivers respectively). This performance corresponds to the communication mode where FEC is disabled. The different color lines stand for the different available constellations described in Sections 2.2 and 2.3. Additionally, the dashed thick lines represent the theoretical performances for DBPSK, DQPSK and D8PSK under an AWGN channel, which computation is detailed in the following paragraphs.

The theoretical performance for a Differential-BPSK as a function of the SNR can be computed with [62] (Page 324):

$$P_e^{(DBPSK)} = \frac{1}{2}e^{-SNR/2} \tag{4.1}$$

Additionally, the performance for DQPSK and D8PSK can be computed with Equations 4.2 and 4.3 respectively [63].

$$P_e^{(DQPSK)} = \frac{sin(\pi/4)}{4\pi}\int_{-\pi/2}^{\pi/2}\frac{e^{[-SNR\cdot(1-cos(\pi/4)\cdot cos(\theta))]}}{1-cos(\pi/4)\cdot cos(\theta)}\mathrm{d}\theta \tag{4.2}$$

$$P_e^{(D8PSK)} = \frac{sin(\pi/8)}{4\pi}\int_{-\pi/2}^{\pi/2}\frac{e^{[-SNR\cdot(1-cos(\pi/8)\cdot cos(\theta))]}}{1-cos(\pi/8)\cdot cos(\theta)}\mathrm{d}\theta \tag{4.3}$$

As it can be seen in Figure 4.1, simulations results are in good agreement with theory.

Moreover, Figure 4.2 represents the performance achieved when using redundancy in the transmitted message. As described in Sections 2.2 and 2.3, PRIME defines a FEC mode to increase its robustness whereas G3-PLC has a Normal mode which includes some redundancy and a Robust mode with higher communication guarantees. PRIME's FEC mode is represented in Figure 4.2a in circles and G3-PLC's Normal and Robust modes are represented in Figure 4.2b in squares and circles respectively.

The extra redundancy introduced by G3-PLC is translated into a more robust communication when compared to PRIME. However, this extra redundancy is also the responsible for G3-PLC's lower transmission rates, as seen in Table 2.1.

4.3 Performance evaluation in PLC background noise channel

Performances in the previous section showed the behaviour of both PRIME and G3-PLC in a channel impaired by Additive White Gaussian Noise. However, as argued in Section

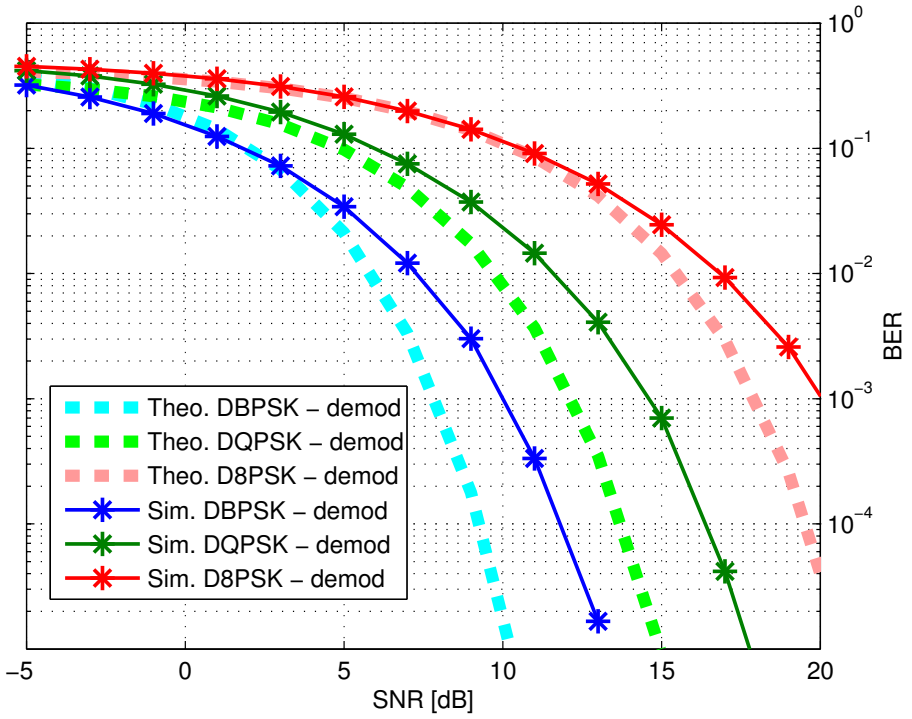

(a)

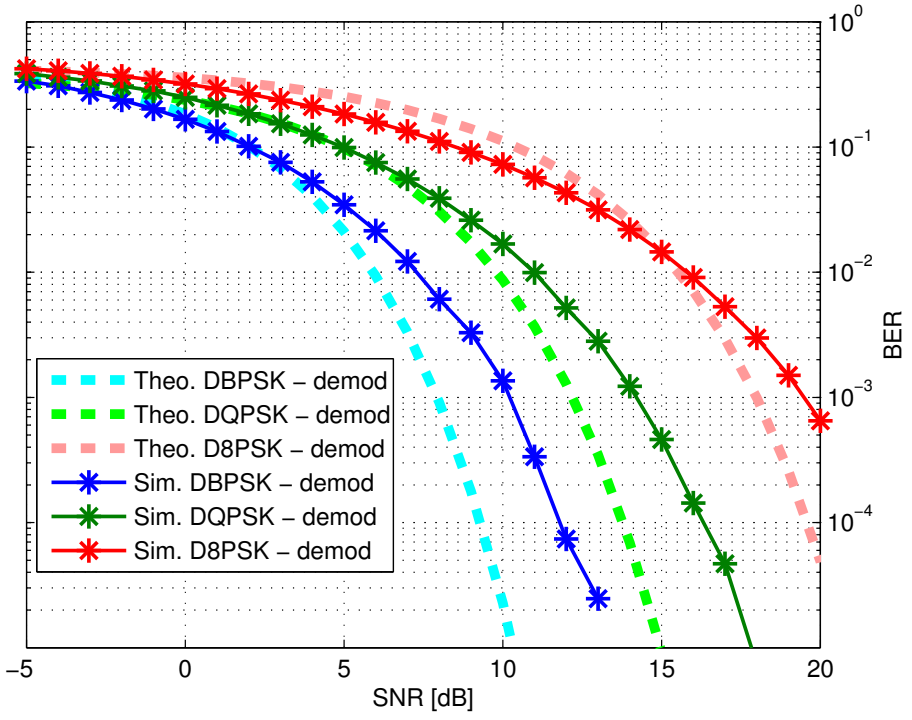

(b)

Figure 4.3: *Performances at the demodulator for PLC channel with Hooijen's background noise model. (a) PRIME's performance. (b) G3-PLC's performance*

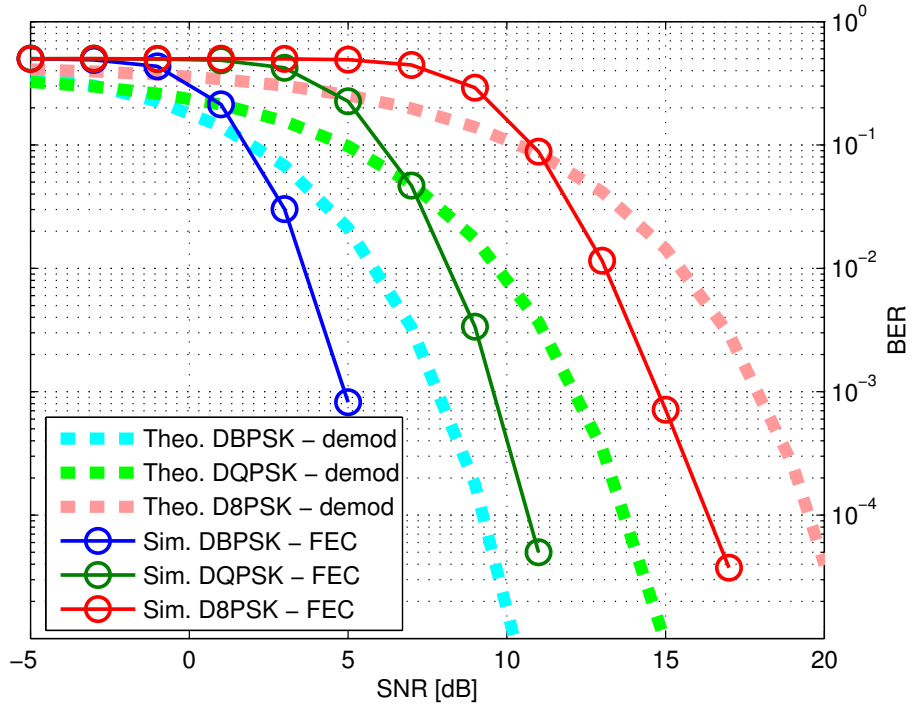

(a)

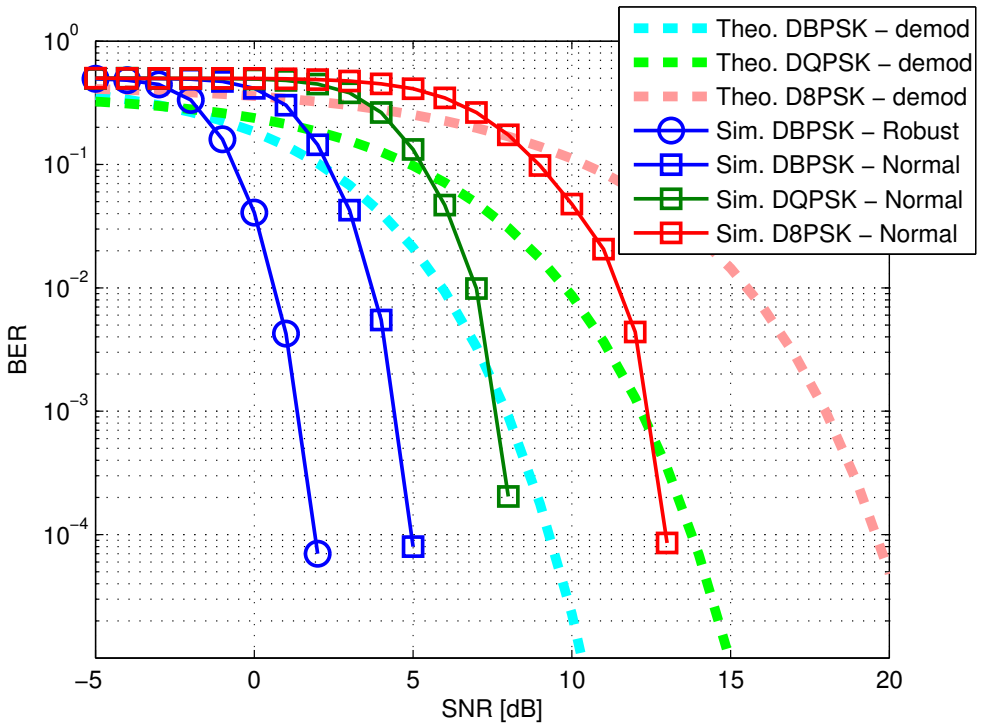

(b)

Figure 4.4: *Performances when using redundancy for PLC channel with Hooijen's background noise model. (a) PRIME's performance. (b) G3-PLC's performance*

3.4.1, measurements carried out in low voltage networks have shown that the background noise present in PLC channels does not follow a white Gaussian trend.

The noise source model for the PLC channel is modified in this section to implement the background noise defined by Hooijen in [64] (previously defined in Equation 3.17).

Analogously as in the previous section, Figures 4.3 and 4.4 detail the performance using and without using the error correction techniques available in PRIME and G3-PLC. Different colors and markers (stars, circles and squares) represent the different communication modes.

As it can be seen, the performance is slightly worse, but the curves follow a similar trend as when the channel is modelled with a white Gaussian noise source.

4.4 Performance evaluation in impulsive noise channel

As mentioned in Chapter 3, one of the most damaging effects in PLC networks is the impulsive noise interference. This section focuses on the performance achieved when this kind of disturbance is present in the communication's channel.

In order to emulate a real-life scenario, Middleton's parameters for the impulsive noise model described in Section 3.4.2 were set to $A = 1.47 \cdot 10^{-4}$ and $\Gamma = 0.1$ according to measurements reported in [61]. This produces an impulsive noise source 48 dB more powerful than the background noise. In some cases this relationship may be up to 50 dB [38, 58, 65].

To help in understanding how powerful noise pulses affect OFDM-based communications, its mathematical formulation is briefly reviewed in the following paragraphs.

Let's consider the vector of digitally modulated symbols $x[m]$ with $m = 0, 1, \cdots, K-1$. In order to transform this vector to time domain using a N-length IDFT, $x[m]$ is extended with $N - K$ zeros to form the new vector $S[k]$ with $k = 0, 1, \cdots, N-1$ (i.e. frequency-domain indexes). The discrete time domain signal, $s[n]$, generated from vector $S[k]$ is:

$$s[n] = \frac{1}{\sqrt{N}} \sum_{k=0}^{N-1} S[k] \cdot e^{-j\frac{2\pi}{N}n \cdot k} \tag{4.4}$$

where $n = 0, 1, \cdots, N-1$ stands for time-domain indexes. At the receiver side, the transmitted signal arrives corrupted by both additive background and impulsive noise. For simplicity, in this derivation the channel's transfer function is assumed to be transparent. The discrete received signal in time domain ($r[n]$) can be expressed as:

$$r[n] = s[n] + z[n] + i[n]; \qquad n = 0, 1, \cdots, N-1 \tag{4.5}$$

where $z[n]$ denotes the effects of the background noise and $i[n]$ is due to the impulsive noise sources. The additive impulsive noise usually has larger amplitude values than both the background noise and the received signal, however, it only occurs at specific time instants. The received samples ($r[n]$) are processed by a DFT to extract the information present in the subcarriers. The demodulated data symbol received on the k^{th} subcarrier, $R[k]$, can be expressed by:

$$\begin{aligned} R[k] &= \frac{1}{\sqrt{N}} \sum_{n=0}^{N-1} r[n] \cdot e^{-j\frac{2\pi}{N}n\cdot k} \\ &= \frac{1}{\sqrt{N}} \sum_{n=0}^{N-1} (s[n] + z[n] + i[n]) \cdot e^{-j\frac{2\pi}{N}n\cdot k} \\ &= S[k] + Z[k] + \frac{1}{\sqrt{N}} \sum_{n=0}^{N-1} i[n] \cdot e^{-j\frac{2\pi}{N}n\cdot k} \end{aligned} \tag{4.6}$$

where $S[k]$ is the transmitted symbol placed at the k^{th} subcarrier and the second and third terms of the equation are due respectively to the background and impulsive noise.

A simplified model for the impulsive noise can be created assuming that it consists of random samples occurring only at certain time instants. Mathematically, it can be described using a rectangular function:

$$i[n] = \Pi\left(\frac{n - (T_{noise}/2)}{T_{noise}}\right) \cdot B[n] \cdot e^{j\theta[n]} \tag{4.7}$$

where $\Pi\left(\frac{n-(T_{noise}/2)}{T_{noise}}\right)$ defines a pulse of width equals to T_{noise}, and both $B[n]$ and $\theta[n]$ follow some random process that models the amplitude and phase variation of the impulsive samples respectively.

Given this definition, the interference due to the impulsive pulses can be expressed as:

$$I[k] = \frac{1}{\sqrt{N}} \sum_{n=0}^{N-1} \Pi\left(\frac{n - (T_{noise}/2)}{T_{noise}}\right) \cdot B[n] \cdot e^{j\theta[n]} \cdot e^{-j\frac{2\pi}{N}n\cdot k} \tag{4.8}$$

As it can be deduced from previous equation, the influence of an impulse is spread over all the spectrum frequencies due to the DFT mechanism (i.e. every k component of $I[k]$ is computed based on every n component of $i[n]$). The key consequence is that no matter how short those impulses are, they will affect all subcarriers in the received spectrum. Figure 4.5 shows the effect previously described by displaying an OFDM modulated (blue) and a noise signal (red) in time and frequency domain. Looking at the

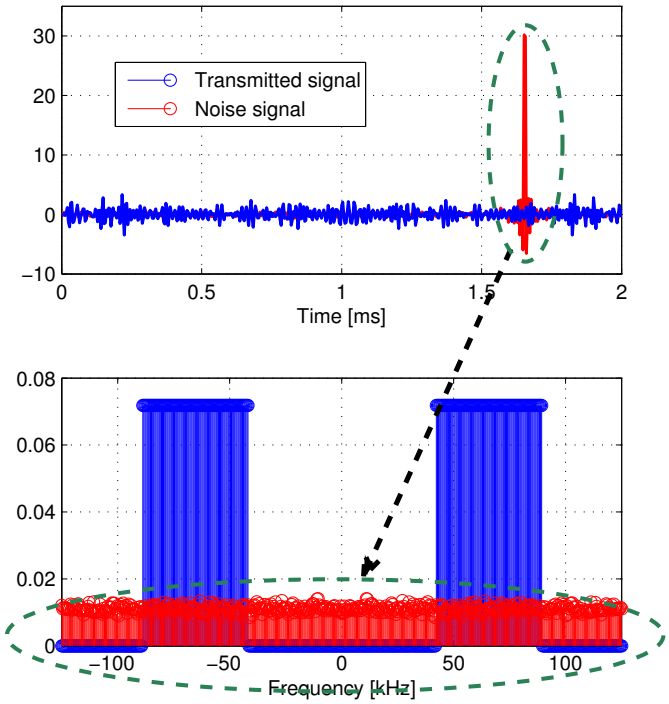

Figure 4.5: *Effect of the noise impulse in time and frequency domain.*

frequency components of both signals, it can be seen how the impulsive noise's power spreads over all frequencies in the spectrum.

To understand how this affects the performance in terms of BER, the theoretical performance when transmitting both a single-carrier and an OFDM signal through an impulsive noise channel are derived in the following paragraphs.

If the channel noise has a white Gaussian behaviour, the performance when using single carrier DBPSK modulation is described in Equation 4.1.

However, in case of dealing with one impulsive noise source, the theoretical performance can be written as a weighted average of the performance for an AWGN and an impulsive channel (adapted from [6]):

$$\begin{aligned} P_e^{(DBPSK)} &= (1-A)\cdot\frac{1}{2}\cdot e^{-\frac{P_S}{\sigma_Z^2}} + A\cdot\frac{1}{2}\cdot e^{-\frac{P_S}{\sigma_1^2}} \\ &= (1-A)\cdot\frac{1}{2}\cdot e^{-\frac{P_S}{\sigma_Z^2}} + A\cdot\frac{1}{2}\cdot e^{-\frac{P_S}{\sigma_Z^2}\cdot\frac{1}{\left(1+\frac{1}{\Gamma\cdot A}\right)}} \end{aligned} \tag{4.9}$$

where P_S is the signal power; σ_Z^2 and σ_1^2 are the background and impulsive variance of the channel noise, respectively; and A and Γ are the impulsive noise parameters as described in Chapter 3. Note that impulsive noise parameters A and Γ influence the

performance achieved by multiplying the SNR (i.e. P_S/σ_Z^2). As a consequence, the signal's power is virtually decreased (since A and Γ typically have values lower than 1). Figure 4.6a shows the theoretical performance of DBPSK in a white Gaussian (i.e. first term in Equation 4.9) and in an only-impulsive (i.e. second term in Equation 4.9) channel in blue and purple respectively. Black circles represent the overall contribution (i.e. $P_e^{(DBPSK)}$ in Equation 4.9). It can be seen in the figure that, for small values of the SNR, the first term is dominant. The middle area has a flat performance around $A/2$ until the received signal has enough power to overcome the impulses' amplitude. For higher SNR values, the decreasing behaviour of the second term is dominant. According to [6], the difference in the performance corresponds to $-10\log_{10}(A\Gamma) \approx 48.3$ dB, as marked in the figure.

As argued before, one consequence of using an OFDM-based system is that the power of noise impulses is spread over all subcarriers. This produces that the power of the impulsive noise is virtually reduced. Therefore, when using an OFDM modulation, the expected performance can be expressed as:

$$\begin{aligned} P_e^{(OFDM)} &= (1-A)\cdot\frac{1}{2}\cdot e^{-\frac{P_S}{\sigma_Z^2}} + A\cdot N_{DFT}\cdot\frac{1}{2}\cdot e^{-\frac{P_S}{\sigma_I^2/N_{DFT}}} \\ &= (1-A)\cdot\frac{1}{2}\cdot e^{-\frac{P_S}{\sigma_Z^2}} + A\cdot N_{DFT}\cdot\frac{1}{2}\cdot e^{-\frac{P_S}{\sigma_Z^2}\cdot\frac{N_{DFT}}{\left(1+\frac{1}{\Gamma\cdot A}\right)}} \end{aligned} \tag{4.10}$$

with the same parameters as in Equation 4.9 and N_{DFT} is the DFT length.

In case of being affected by an impulse, the SNR in Equation 4.10 is increased by a factor equal to the DFT length. Additionally, in case a pulse affects any sample within the OFDM symbol, it will affect all subcarriers due to the noise spread effect. As a consequence, the second term in P_e^{OFDM} is also increased by N_{DFT}.

Figure 4.6b shows the theoretical performance when transmitting an OFDM signal through a channel with impulsive noise. As in Figure 4.6a, blue and purple circles represent the first and second term in Equation 4.10 respectively. The figure is coherent with the results previously explained: the flat part of the curve occurs at a higher BER value (due to the higher chance of being affected by an impulse) and zero BER is achieved at a lower SNR (as a consequence of the spread effect in OFDM).

Figure 4.7 shows the simulated performance when both PRIME and G3-PLC's transmissions are corrupted by impulsive noise. In the case of PRIME, circles stand for the use of FEC blocks whereas for G3-PLC, squares and circles represent the performance for the Normal and Robust mode respectively. Additionally, the blue and purple thick lines represent the theoretical performance as shown in Figure 4.6b. As it can be seen,

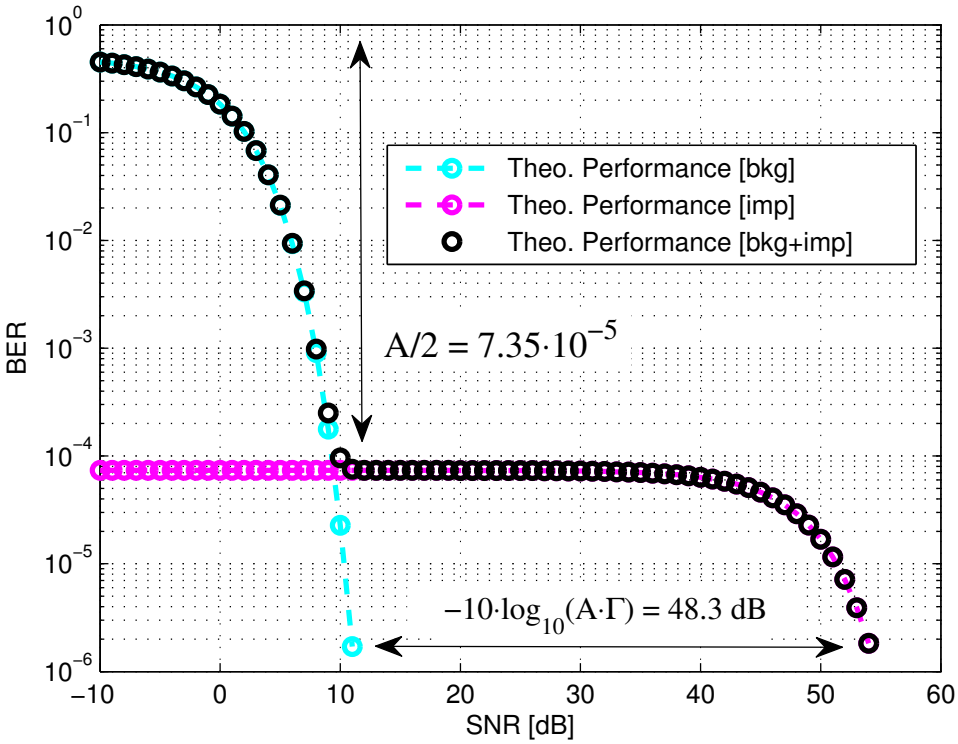

(a)

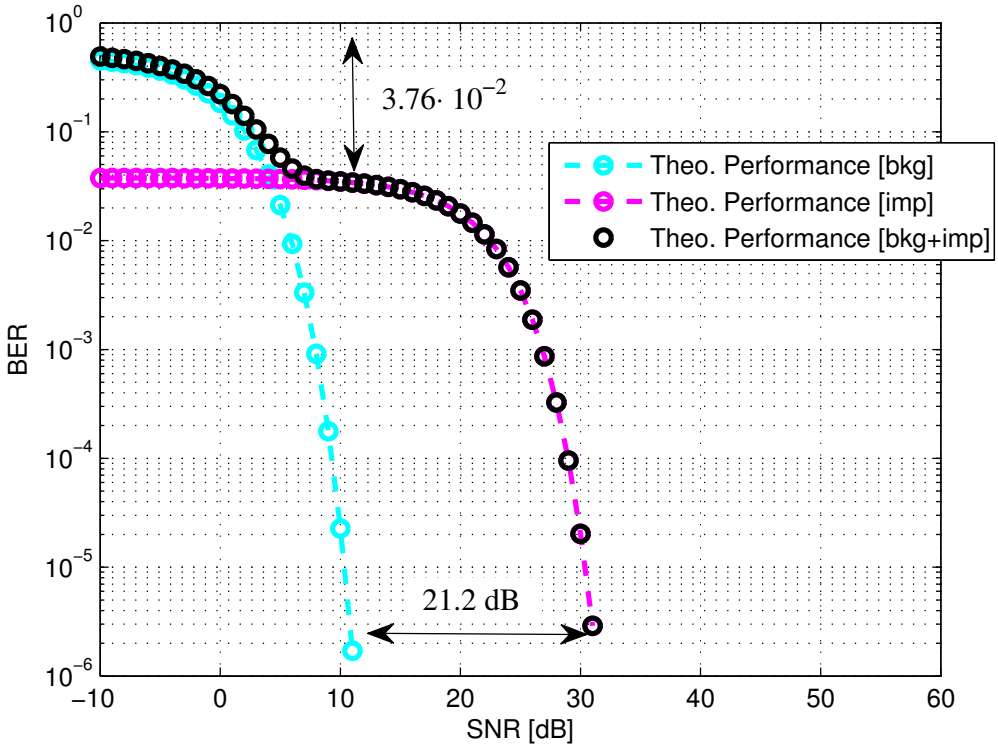

(b)

Figure 4.6: *Theoretical performance in Impulsive Noise channel. (a) DBPSK transmission. (b) OFDM transmission (N_{DFT} is set to 512).*

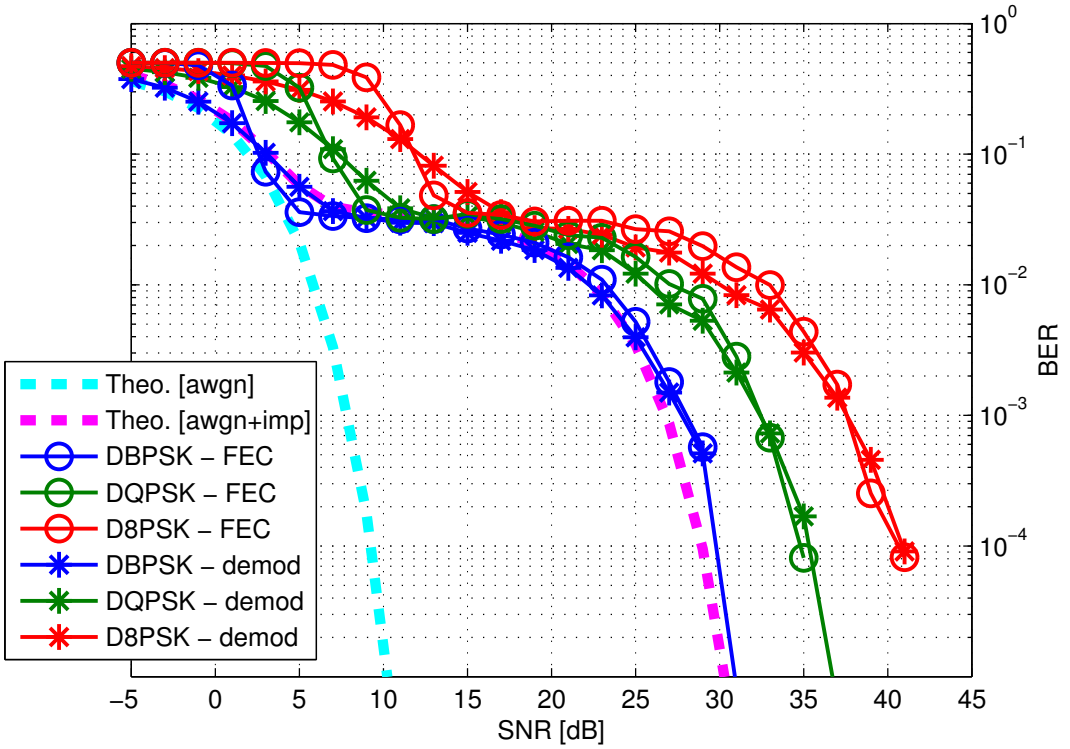

(a)

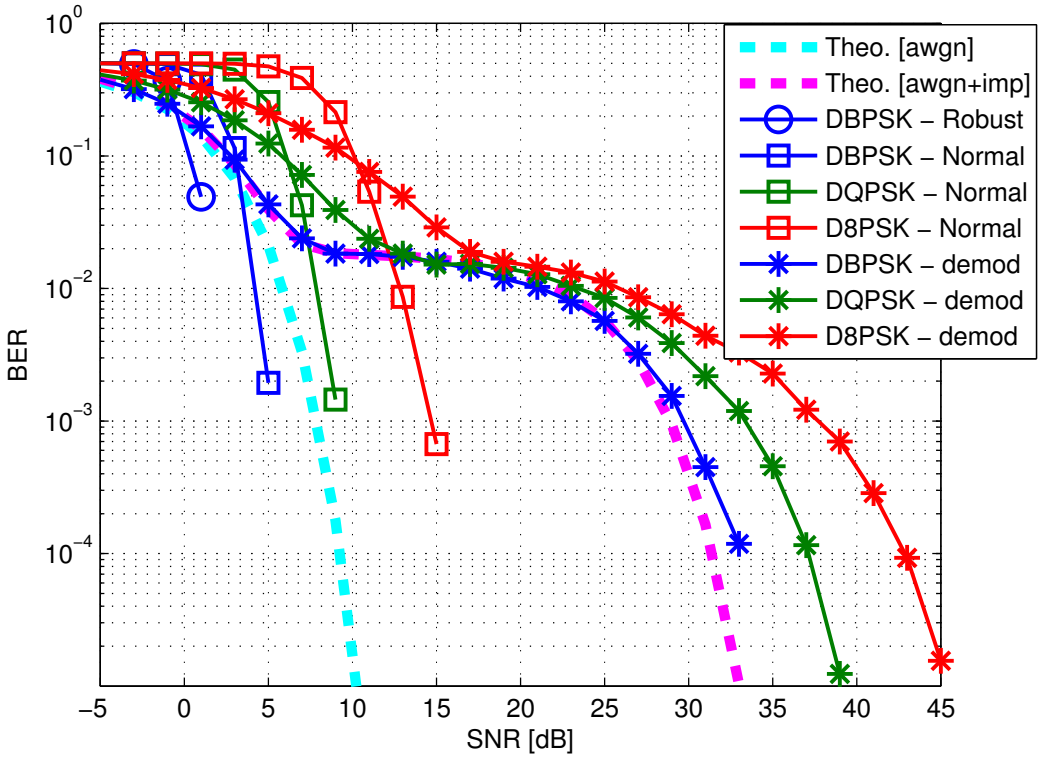

(b)

Figure 4.7: *Performances in Impulsive Noise Channel. Theoretical values represent performance at the demodulator (a) PRIME's performance. (b) G3-PLC's performance.*

the curves corresponding to the performance at the demodulator follow the same trend for PRIME and G3-PLC and show a good agreement with the theoretical values.

The big difference appears when looking at the performance achieved when using the FEC and Normal/Robust mode for PRIME and G3-PLC respectively. Figure 4.7b shows how Normal and Robust modes in G3-PLC are able to undo the interference produced by the high noise pulses. However, by looking at Figure 4.7a, it can be seen that, both stared and circled lines follow the same trend for each color. A conclusion that can be drawn from this is that FEC techniques in PRIME do not work significantly well in impulsive noise environments, since there is no effective gain by using or not using them.

The reason for this lack of improvement in the performance when using the FEC mode resides in how PRIME's FEC deals with the highly powerful noise pulses. As mentioned, the energy of these short pulses is spread over the whole OFDM spectrum due to the DFT. In the case that an OFDM symbol is hit by an impulse, most of the subcarriers will be corrupted. Moreover, since the interleaving is done within the same OFDM symbol, errors are not scattered enough for the Viterbi decoder to correct them. This results in a performance similar to the one obtained at the demodulator as Figure 4.7b shows.

4.5 Conclusions

This section focuses on the study of the physical performance of two of the main narrow band PLC solutions developed by the industry: PRIME and G3-PLC. As it is commonly done in the communication field, this performance is analysed in terms of bit error rate as a function of the signal to noise ratio.

The different sections in the chapter provide detailed figures with the achieved performance of both PRIME and G3-PLC in several communication scenarios: under a white Gaussian noise channel, when including the background noise model developed by O. Hooijen and when the channel includes impulsive noise sources. A special attention is paid to the case when impulsive noise is present in the channel. As results have shown, this kind of noise is very damaging to OFDM-based communication systems.

Section 4.4 provides theoretical derivations and explanations of the effects that occur when transmitting through an impulsive noise channel. Additionally, it has been shown how these theoretical results are in good agreement with the output produced by the simulations.

When comparing the performance achieved by PRIME and G3-PLC, it could be seen how G3-PLC is able handle the high power impulses. In contrast, in that environment, the performance achieved by PRIME is seriously deteriorated.

To conclude, this chapter has shown how impulsive noise severely affects communications when using a PRIME's PLC transceiver. This poor performance motivates the two following chapters, where several techniques are studied to mitigate the effects of this type of noise. Modifications are proposed for the current transceiver's design in order to increase its robustness to such kind of interferences.

Chapter 5

State of the art of impulsive noise cancellation techniques

5.1 Introduction

Previous chapter showed that impulsive noise has a very damaging effect in PLC systems. Even though the transceiver's design for G3-PLC is able to cope with this high powerful pulses, the price to pay is a more complex hardware and a lower transmission rates than what be could expected from a system with such bandwidth. In contrast, the simpler design and higher transmission rates in PRIME make transmissions very vulnerable to impulsive noise sources, as it could be seen in Figure 4.7.

The performance improvement in impulsive noise environments has gather the attention of the research community and many efforts are done in the direction of finding relatively simple solutions to this problem. During this chapter, a review of the most up-to-date approaches in OFDM-based systems is carried out.

This state of the art is structured in two different groups depending on where each technique is applied. According to this, Section 5.2 deals with signal processing techniques applied in the time domain (i.e. before the DFT is performed at the receiver), whereas Section 5.3 focuses on modification to the signal in the frequency domain (i.e. after the DFT is performed at the receiver). Additionally, Section 5.4 introduces a new trend for impulsive noise cancellation, which make use of compressed sensing techniques.

5.2 Time-domain techniques

Time domain techniques are applied right before the OFDM demodulation takes place at the receiver, as seen in Figure 5.1.

This kind of techniques are widely applied in impulsive noise environments both PLC [38, 66] and any other channel which suffers these effects (such as wireless [67, 68]). The

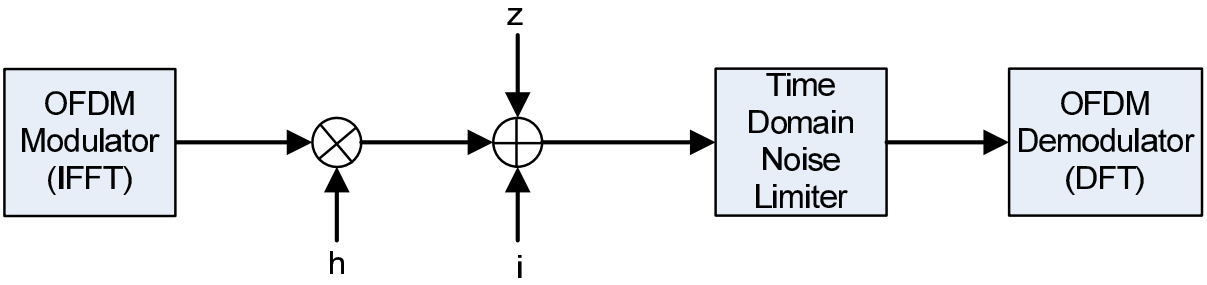

Figure 5.1: *Scheme for non linear limiters used to combat impulsive noise.*

main reason of their popularity lies in their simplicity and efficiency. The most common techniques are *clipping* and *blanking*; and the main reason for their popularity lies in their simplicity and efficiency. Equations 5.1 and 5.2 show their mathematical description.

$$r[n]^{(clipping)} = \begin{cases} r[n]^{(rx)} & \text{, if } |r[n]| < A_{th}^{clip} \\ A_{th}^{clip} e^{j \cdot \angle(r[n])} & \text{otherwise} \end{cases} \tag{5.1}$$

$$r[n]^{(blanking)} = \begin{cases} r[n]^{(rx)} & \text{, if } |r[n]| < A_{th}^{blank} \\ 0 & \text{otherwise} \end{cases} \tag{5.2}$$

In both equations n runs from 0 to $N-1$, where N is the DFT length. A_{th} is the limiting threshold, $r[n]$ is the received signal and $r[n]^{(clipping)}$ and $r[n]^{(blanking)}$ are the processed signals using clipping and blanking technique respectively. The main idea is to reduce the effect of large amplitude values at the input of the demodulator. In some cases, like when using blanking, the sample value affected by the impulsive noise is lost. However, this sacrifice avoids the noise energy to corrupt all sub-carriers in the spectrum.

S. V. Zhidkov carries out a wide analysis of these two techniques extended with a derivation of closed-form expressions for the signal to noise ratio (SNR)for wireless environments [69, 70]. In those studies, the author provides a theoretical analysis on the performance characterization of receivers using clipping, blanking and combined blanking-clipping limiters. Simulations results provided in the papers report an optimal threshold for clipping and blanking limiters. As a result, blanking technique is shown to offer a better performance in highly impulsive environments. However, this analysis is not applied to a concrete PLC technology but to a general OFDM-based system. Additionally, there are no details on how the optimal threshold can be computed a priori.

The works carried out by K.S. Al-Mawali et al. [71, 72] apply the same procedure to a specific PLC scenario. In concrete, [71] shows the performance for a pre-computed threshold and [72] uses an adaptive threshold which slightly improves the results (although no details are provided on the computation of the adaptive behaviour).

G. Ndo et al. describe an algorithm based on the Bussgang's theorem [73] on their works [74] and [75]. Results show that the computed threshold is closed to the optimal

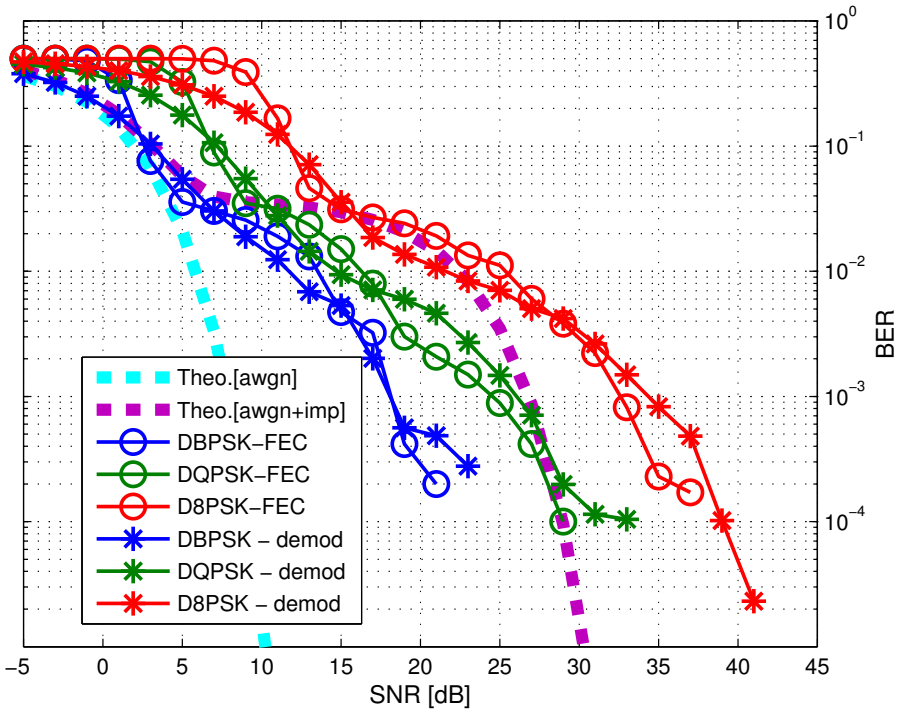

Figure 5.2: *Performance when clipping the input signal at the receiver. Clipping value is set to 2.2 times the variance of the signal. Dashed lines stand for the theoretical performance of an OFDM-DBPSK modulation.*

one. Improvements of 2.5 dB and 3 dB are reported for highly and weakly impulsive noise scenarios.

More recently, the computation of the optimal threshold is also addressed in [76], there it is applied to the IEEE P1901.2 standard for PLC. This computation is based on the signal's variance and the obtained results are close to the optimal threshold.

To have an idea of the effects of this technique, simulations carried out in the previous chapter have been modified to include a clipping block at the input of a PRIME's receiver. Figure 5.2 shows the performance achieved for different SNR values when setting the threshold to $2.2\sigma_s$, as recommended in [58]. A significant improvement can be seen when using DBPSK (blue line with stars) compared with the theoretical performance (dashed purple line).

One of the latest proposals with respect to the clipping/blanking approach is the one done in [77]. The V.N Papilaya and A. J. H. Vinck propose an additional threshold to this mechanism. This new threshold, named *replacement*, is located between the clipping and blanking threshold. In case a sample falls inside this area, the output value is computed as the average of all samples within the OFDM symbol. Performances are improved, although not significantly.

A different direction is followed in [78], where a mask function is computed based on the monitoring of the guard frequency bands of a DVB-T transmission. A position estimator block creates a negative window that masks the samples that contains impulsive noise in order to avoid its entrance into the receiver.

Alternatively, while previous studies focuses on the detection of the noisy pulses, the works presented by J. Radic and N. Rozic [79,80] turn their attention to the reconstruction of the samples hit by the noise pulses. Instead of directly discarding these samples so that the noise does no enter the receiver, they are reconstructed using a minimum square error optimisation criteria. However, those papers assume the perfect knowledge of the position and parameters of the noise interference, which is not a realistic situation.

Finally, one of the latest works for impulsive nose removal in time domain is the one done by P. Torio and M. G. Sanchez in [81]. Similarly to what was proposed in [78], they use null carriers in the OFDM spectrum to create an estimation of the position and amplitudes of the impulsive noise signal. Results obtained with this technique improve the performance achieved by other limiting techniques (like clipping/blanking). However, no details are included in the paper on how the positions and amplitude estimations are done.

5.3 Frequency-domain techniques

Several authors have also worked on how to reduce the impulsive effects by processing the received signal in the frequency domain, i.e. after the OFDM demodulation has been performed.

One typical scheme it to use an iterative loop to estimate and cancel the impulses based on the received information. Figure 5.3 shows a general scheme of the process carried out. In reference [48], a feedback loop with iterative detection uses two estimator (one in time and one in frequency domain) that exchange information between themselves. Both estimators use the information to detect and reconstruct the impulsive noise samples. The procedure has several steps: an FFT is applied to the input signal. Then, the transmitted information is interpreted. Thanks to this, the impulsive noise is reconstructed and subtracted from the received signal. The same process is repeated iteratively. This scheme is proposed for general OFDM system and it is not particularised for narrow band PLC technologies.

One concrete proposal for this approach is the one followed by the study presented by J. Haring in [82] and H. Matsuo [83]. These initial works describe an iterative process for cancellation of the impulsive noise signal. The block diagram of the receiver described in [82] is shown in Figure 5.4. A maximum likehood (ML) detection is applied to the

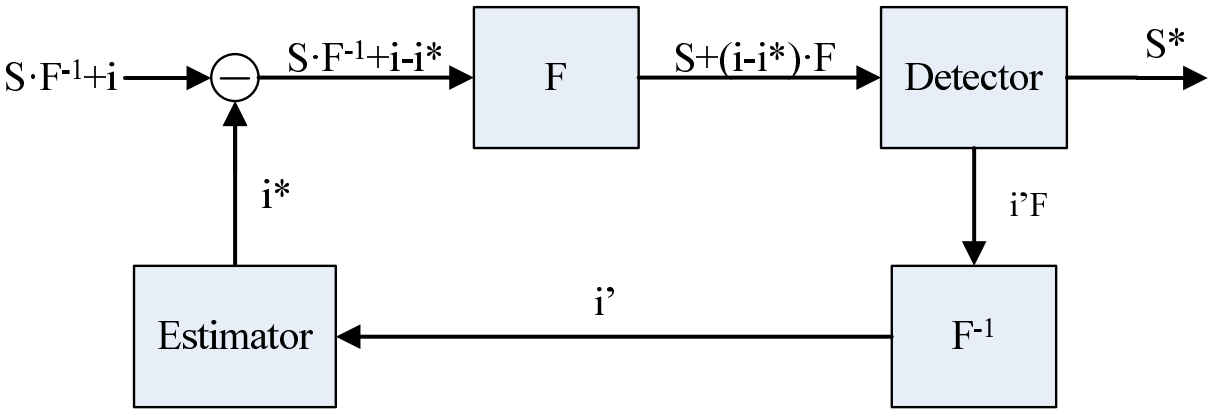

Figure 5.3: *General scheme to overcome the impulsive noise in frequency domain. Adapted from [6] (Page 216).*

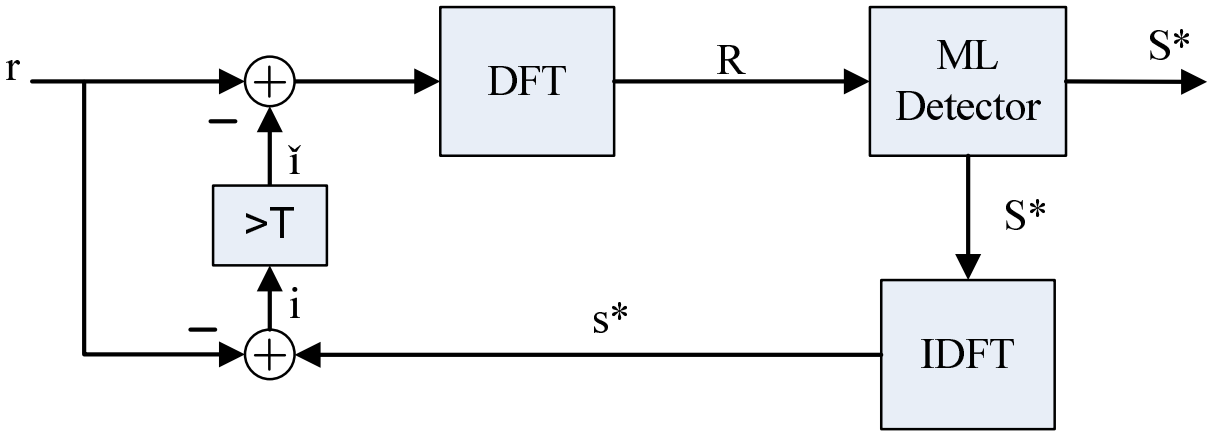

Figure 5.4: *General scheme to overcome the impulsive noise in frequency domain, as proposed in [82].*

received signal r after it has passed a DFT. The detector extracts the K data sub-carriers to form the $S^{(m)}$ vector with the constellation symbols. The estimated vector $S^{(m)*}$ represent the m^{th} iteration of the process. $S^{(m)*}$ is then converted back into the time domain and subtracted from the received vector r. The resulting signal ($i^{(m)} = r - s^{(m)*}$) is passed through a thresholding block to identify whether an impulsive noise corrupted the transmission. In this case, the $\breve{i}$ signal is subtracted from the received one and the iteration process continues. The algorithm stops when $S^{(m+1)} \approx S^{(m)*}$.

An alternative scheme is proposed by S. V. Zhidkov in [84]. The main idea of the algorithm is to estimate the impulsive noise term $\hat{U}$ (see Figure 5.5) so it can be subtracted from the input signal. In order to do so, a first estimation of the transmitted symbols is performed in the 'Demapping & Pilot Insertion' block. By subtracting this first estimation with the incoming signal, an approximation of the total noise is obtained: $\hat{D}$. $\hat{D}$ is translated to time domain to detect where noisy peaks occur. The final processed signal R^{comp} is obtained by removing the estimated impulsive noise.

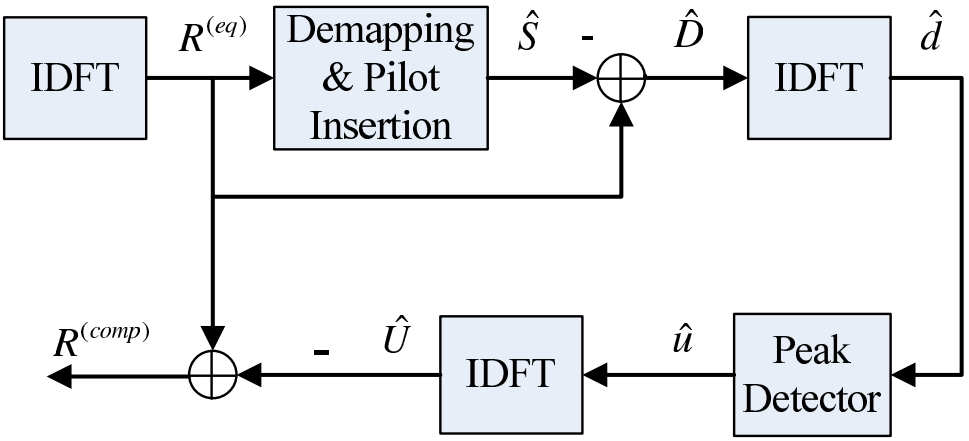

Figure 5.5: *Block diagram of the method proposed in [84]. The original scheme includes channel equalization that has been omitted here for clarity.*

According to simulations reported in [84], gains of around 2 dB are achieved when implemented this method at the receiver.

Almost the same year, J. Armstrong and H. A. Suraweera report the same scheme but including an optional clipping/blanking block at the input [67] . The main difference with the work presented by Zhidkov resides in the non linearity applied by the de-mapping block.

Although these two methods were proposed for Digital Video Broadcast Terrestrial (DVB-T), the same idea could be extrapolated to a narrower-band environment. As a matter of fact, more recently, in [50], a similar scheme is used to detect and correct errors in a narrowband PLC environment.

More recently, studies by A. Mengi and H. Vinck [57, 58] have revisited the iterative idea and combined with clipping and blanking techniques leading to a performance improvement when compared with a process without iterations.

Other recent studies have focused on the design of the interleaver used inside the transceiver. As an example, [85] proposes the use of an interleaver longer than one OFDM symbol. As explained in Section 4.4 the use of a longer interleaver would spread the burst errors produced by impulsive noise over several OFDM symbols, enhancing the capabilities of the decoder, since errors are more scattered. The study proposes a 10 ms interleaver in order to increase the performance of PRIME and, at the same time, reduce the complexity of a G3-PLC transceiver (as seen in Chapter 2, G3-PLC uses an interleaver of up to 256 OFDM symbols, whereas 10 ms would correspond to approximately 14 symbols). As an example, Figure 5.6a shows the performance achieved by PRIME when extending the interleaver to 5 OFDM symbols (which corresponds to the 10 ms proposed). The improvement is barely noticeable when compared with results shown in Section 4.4. However, Figure 5.6b shows the result when the interleaver is

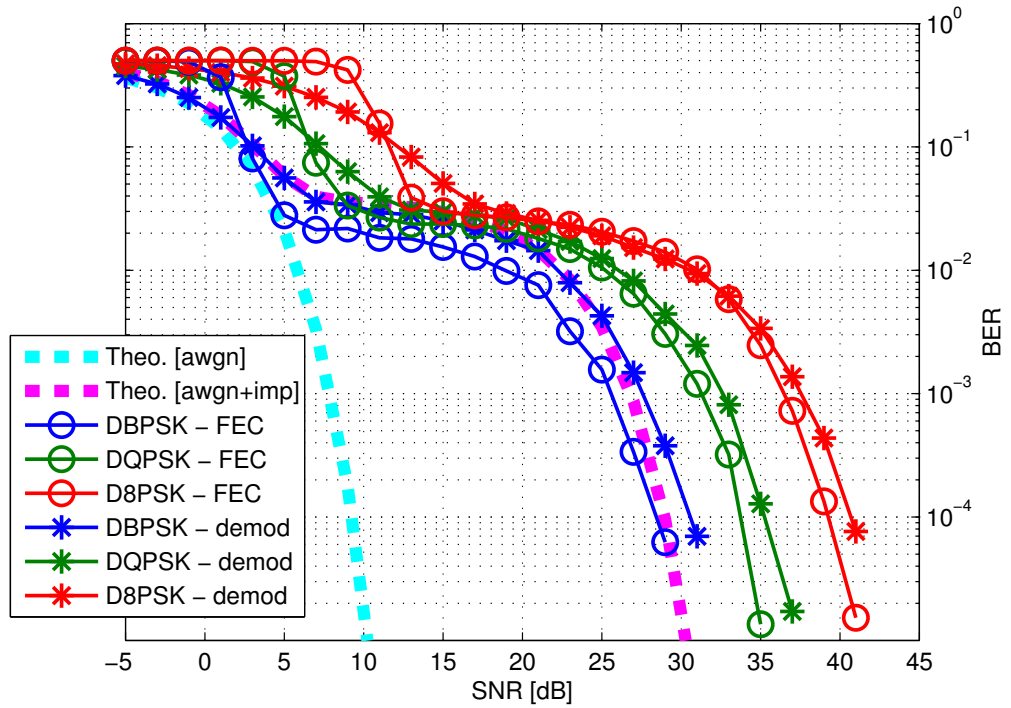

(a)

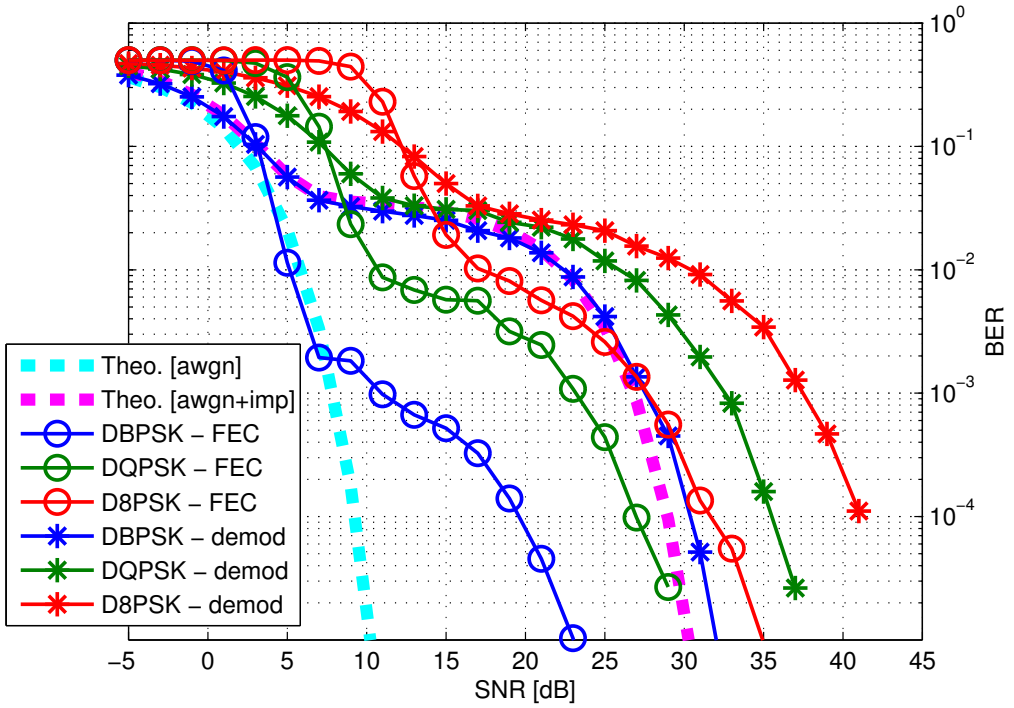

(b)

Figure 5.6: *PRIME performance when using different interleaver sizes. (a) 5-symbol interleaver. (b) 50-symbol interleaver. Dashed lines stand for the theoretical performance of an OFDM-DBPSK modulation.*

extended to the 50 OFDM symbols (still lower than the interleaver used by G3-PLC). The performance of the second waterfall is considerable enhanced. Nevertheless, the price to pay for this better behaviour is a more complex transceiver and a longer transmission latency.

Finally, the research presented in [86] proposes a the use of a Time Domain Interleaver (TDI), which is further extended in [87] by a Time Domain Interleaver with additional Orthogonal Transform (TDI-OT) system. The main idea is to shift the interlaver closer to the channel (i.e. after the IDFT at the transmitter and before the DFT at the receiver). The motivation for this proposal is that each OFDM symbol be only affected by one impulsive noise sample instead of a whole burst. In this way, the amount of noise energy that enters the receiver chain per OFDM symbol is decreased and, thus, the performance is improved. Results reported in the studies show an enhancement in the performance. However, as stated in [86] and [87], this configuration is only valid in moderate impulsive noise scenarios (5 impulses per second).

5.4 Compressed sensing for impulsive noise cancellation

Apart from previous techniques described in this chapter, there is an additional mechanism that has recently been proposed to avoid impulsive noise effects in OFDM-based systems: Compressed Sensing (CS). The basic idea is to exploit null carriers present in the transmitted spectrum to estimate the noise existing in the channel. Using this estimation, the impulsive noise vector can be reconstructed based on the assumption that it has a sparse representation. This approach has also been suggested for BB-PLC and Digital Line Subscribers (DLS) systems by Lampe [35] and Al-Naffouri et al. [88] respectively.

One advantage when compared with the previous frequency-based techniques is that it is not based on demodulating the incoming symbols in order to compute the noise approximation. This means that, even though next versions of the transceiver change or include new digital modulations, this techniques will keep on working since it does not rely on the constellation that is being used. In addition, it does not include redundancy in the transmitted message, therefore, there is no reduction in the data bit rates.

The proposed technique to improve PRIME's behaviour in impulsive noise environment is based on the compressed sensing. For this reason, a more detailed description on how this method exploits the null subcarriers and how its performance can be enhanced is developed in the following chapter.

5.5 Conclusions

A conclusion that can be drawn from this section is that there have existed some efforts in developing techniques for impulsive noise removal in OFDM-based systems. A very common approach is to include in the transmitted message some redundancy that can be used by the receiver to correct as many errors as possible. As a matter of fact, this has been the technique implemented in all the studied narrowband PLC standard. One direct disadvantage of these approaches is the reduction of effective bit rate.

Most of the techniques discussed in this chapter try to deal with the effect of impulsive noise before the transforming symbols into bits. However, there is not a clear winning choice that outperforms the rest.

The author sees room for improvement in this field. Specially focusing on a recent flow of research that is based on compressed sensing techniques. These concepts have never been applied to a narrowband power line communication standard, as far as the author's knowledge. The following chapter describes how these recent ideas can be applied for the cancellation of the impulsive noise.

Chapter 6

Advanced digital signal processing techniques for impulsive noise cancellation

6.1 Introduction

Thanks to the development of microelectronics, electronic has experienced a revolution going from a predominant analogue world (on its early stages) to an every day more presence of digital circuits. However, all digital designs could not be done without two important analogue parts: the Analogue to Digital Converter (ADC) and the Digital to Analogue Converter (DAC). In order to obtain a reliable digital version of the analogue signal, the sampling process has to be fast enough. This lower bound is known as the Nyquist theorem [89]:

Theorem 1. *If a function $x(t)$ contains no frequencies higher than B Hertz, it is completely determined by giving its ordinates at a series of points spaced $1/(2B)$ seconds apart.*

Nowadays, as technology develops, the use for faster ADCs is more and more demanded. However, in many occasions, due to the need to reduce memory allocation, the acquired information is automatically compressed (even using lossy compressed algorithms). The question that Donoho raises in [90] is:

> *"Why go to so much effort to acquire all the data when most of what we get will be thrown away? Can we not just directly measure the part that will not end up being thrown away?"*

Compressed sensing, also known as compressed sensing or CS, is a technique that tries to answer those questions by performing data acquisition at lower rate than the

one stated by the Nyquist's theorem. In order to do this, CS is based on two principles: sparsity and incoherence.

According to [91], the sparsity property is referred to the signal of interest (the analogue signal that is been measured). It refers to the idea that the information contained by this signal is not directly related to its bandwidth. CS exploits the fact that certain signals may have a compressed (or more sparse) representation when expressed in the proper mathematical basis.

In contrast, the incoherence refers to the measurement (or sensing) mechanism. It expresses the idea that a spread signal may have a more dense representation when expressed in the appropriate basis. A clear example is the time-frequency duality of a signal. Whereas a sine waveform has wide representation in time, it can be represented in frequency domain in a more compressed manner. The opposite occurs when the waveform has the shape of a Dirac's delta.

The key aspect is that efficient sampling mechanisms can be designed to acquire only essential information so it can be compressed in a small amount of data. Alternatively, there exist numerical optimization strategies to reconstruct the full-length signal based on the under-sampled measured version.

The transceiver's design proposed in this chapter makes use of improvements in the reconstruction capabilities of CS. As pointed out in [92], the goodness of the reconstruction depends directly on the measurement method. As reported [93], the CS properties can be improved by using a Partial Fourier Matrix indexed by a subset based on Difference Sets (DS). To the best of authors' knowledge, no results have been published regarding the use of Difference Set-based Compressed Sensing for impulsive noise cancellation in OFDM systems.

In contrast with other recent proposed techniques [38, 57, 58, 75, 77], simulations show that the impulsive noise effects are almost completely cancelled when using DS-based CS. Additionally, when compared with other techniques that provide a good performance (such as [58]), compressed sensing counts with the advantage that it does not depend on the type of digital modulation being used. This allows for an easier backwards compatibility in the future.

This chapter is structured as follows: after this introduction, compressed sensing general ideas are concreted mathematically in Section 6.2. Section 6.3 details the process follows in order to apply the Compressed Sensing formulation to impulsive noise cancellation in OFDM systems. The performance achieved when removing the impulsive noise components are shown in Section 6.3.1. This performance is improved in Sections 6.3.2 and 6.4 by assuming a block-sparsity structure of the noise and by selecting certain null carriers for noise sensing respectively. Finally, Section 6.5 shows the concrete performance

achieved when using all mentioned configurations in a PLC transmission in terms of bit error rate as a function of the signal to noise ratio.

To help the reader through the mathematical derivation, the notation followed in this chapter is briefly defined in the following paragraph:

Bold lower-case letters ($\boldsymbol{a}$) denote vector, whereas bold upper-cases ($\boldsymbol{A}$) represent matrices; $\boldsymbol{A_i}$ represents the i^{th} column in matrix $\boldsymbol{A}$; $\boldsymbol{A^T}$, $\boldsymbol{A^H}$ and $\boldsymbol{A^\dagger}$ represent transpose, Hermitian transpose and inverse of $\boldsymbol{A}$ respectively; and $\rho(\boldsymbol{A}) = \sqrt{\lambda_{max}(\boldsymbol{A})}$ where $\lambda_{max}(\boldsymbol{A})$ stands for the largest eigenvalue of $\boldsymbol{A}$.

6.2 Compressed sensing basics

The main goal in compressed sensing is to recover a signal, $\boldsymbol{x} \in \mathbb{C}^N$, which is a k-sparse vector in an original basis (time, for instance) based on an observed or measured vector, $\boldsymbol{y} \in \mathbb{C}^M$, in an observation domain (such as frequency). A k-sparse vector means a vector that has at most k non-zeros components; mathematically expressed as $||\boldsymbol{x}||_0 \leq k$. Both $\boldsymbol{x}$ and $\boldsymbol{y}$ are related through the following expression:

$$\boldsymbol{y} = \boldsymbol{\Phi} \cdot \boldsymbol{x} \tag{6.1}$$

where $\boldsymbol{\Phi} \in \mathbb{C}^{M\text{x}N}$ is commonly referred as *measurement* or *sensing matrix*.

One could think that $\boldsymbol{x}$ can be recovered by pre-multiplying both sides in Equation 6.1 by $\boldsymbol{\Phi^{-1}}$. However, in order to force $\boldsymbol{y}$ to be a compressed version of $\boldsymbol{x}$, the condition of $M < N$ is imposed. This produces an infinite number of vectors $\boldsymbol{x}$ that satisfy $\boldsymbol{y} = \boldsymbol{\Phi} \cdot \boldsymbol{x}$, since the system is under-determined.

Nevertheless, as stated by Candes in [91], if there are enough observations and $\boldsymbol{\Phi}$ matrix obeys certain properties (later detailed), the $\boldsymbol{x}$ vector can be recovered with the following optimization program:

$$\begin{aligned} \underset{x \in \mathbb{C}^N}{\text{minimize}} \quad & ||\boldsymbol{x}||_{l1} \\ \text{subject to} \quad & \boldsymbol{y} = \boldsymbol{\Phi} \cdot \boldsymbol{x} \end{aligned} \tag{6.2}$$

Even though reconstruction can be achieved using previous algorithm, for CS to be really a powerful tool, it should also be able to deal with sparse signal mixed with noise. In any real application, measured data will inevitably be corrupted by at least a small amount of noise (for instance the noise introduced by measurement devices). In case of $\boldsymbol{x}$ being a transmitted signal, most of the times it will be corrupted by some time of noise present in the channel.

Taken this into account, the problem in Equation 6.1 can be reformulated to:

$$\boldsymbol{y} = \boldsymbol{\Phi} \cdot \boldsymbol{x} + \boldsymbol{z} \tag{6.3}$$

where $\boldsymbol{\Phi}$, $\boldsymbol{x}$ and $\boldsymbol{y}$ are as in Equation 6.1 and $\boldsymbol{z}$ is an unknown random term with dimensions Mx1.

Following [91], the new minimisation problem can be re-written as:

$$\begin{aligned} \underset{x \in \mathbb{C}^N}{\text{minimize}} \quad & ||\boldsymbol{x}||_{l1} \\ \text{subject to} \quad & ||\boldsymbol{y} - \boldsymbol{\Phi} \cdot \boldsymbol{x}||_{l2} \leq \epsilon \end{aligned} \tag{6.4}$$

where ϵ is related to the variance of $\boldsymbol{z}$ [90, 94, 95].

The Restricted Isometry Property (RIP) details the sufficient condition for a measurement matrix $\boldsymbol{\Phi}$ to recover sparse signals corrupted by noise. It is defined as [96]:

Definition 1. *For each integer $P = 1, 2, \cdots$, define the isometry constant δ_P of a matrix $\boldsymbol{\Phi}$ as the smallest number such that*

$$(1 - \delta_P)||\boldsymbol{x}||_{l2}^2 \leq ||\boldsymbol{\Phi}\boldsymbol{x}||_{l2}^2 \leq (1 + \delta_P)||\boldsymbol{x}||_{l2}^2 \tag{6.5}$$

hold for all P-sparse vectors $\boldsymbol{x}$.

As stated in [91], a matrix $\boldsymbol{\Phi}$ obeys the RIP of order P if δ_P is not too close to one. In that case, the recovery algorithm described in Equation 6.4 can handle noise gracefully.

Regarding the reconstruction algorithms, they can be grouped into three major lines [97]: Basis Pursuit (BP), the Matching Pursuit / Orthogonal Matching Pursuit (MP/OMP) and the Bayesian Compressed Sensing (BCS). A more detailed description of these algorithms together with its sub-groups is available in [98].

As mentioned in [98], BP-based CS algorithms, although very robust, are more complex than MP/OMP and BCS. This makes them infeasible for many practical situations.

Alternatively, publications like [99, 100] propose the use of Sparse Bayesian Learning (SBL) algorithm to deal with impulsive noise with satisfactory results. However, according to the literature, an Orthogonal Matching Pursuit approach can be performed with a lower number of operations. As stated in [99], the proposed SBL algorithm has a complexity that goes from $\mathcal{O}(N^2 \cdot M)$ to $\mathcal{O}(N^3)$. However, in case of using an OMP process, the complexity is reduced to $\mathcal{O}(N \cdot M)$; which, for hight values of M and N, represents a considerable difference [101]. Appendix B provides some details about the computation of this complexity inspired by the work of J. Wang et al. [101].

Motivated by this performance numbers, following sections focus on the Orthogonal Matching Pursuit approach to study how compressed sensing can be used for impulsive noise removal in PLC systems.

6.3 Application to impulsive noise removal

This section explicitly details the CS procedure for impulsive noise cancellation. In order to set notation, OFDM is briefly reviewed. In contrast with the theoretical derivation done in Chapter 4, now a vector/matrix approach is followed for the sake of clarity.

Let $\boldsymbol{x} \in \mathbb{C}^K$ denote the vector of PSK constellation points to be transmitted in an OFDM symbol. Prior entering the Fourier transformation (see scheme in Figure 2.4), this vector is expanded to the N-dimensional vector $\boldsymbol{S}$ by introducing $N - K$ zeros. The transmitted time-domain OFDM symbol is given by $\boldsymbol{s} = \boldsymbol{F}^{\dagger} \cdot \boldsymbol{S}$, where † represents Hermitian transpose operation and $\boldsymbol{F}$ is DFT matrix detailed in the following equation:

$$\boldsymbol{F} = \begin{bmatrix} \alpha^0 & \alpha^0 & \alpha^0 & \cdots & \alpha^0 \\ \alpha^0 & \alpha^1 & \alpha^2 & \cdots & \alpha^{(N-1)} \\ \vdots & \vdots & \vdots & \ddots & \vdots \\ \alpha^0 & \alpha^{(N-1)} & \alpha^{2\cdot(N-1)} & \cdots & \alpha^{(N-1)\cdot(N-1)} \end{bmatrix} \tag{6.6}$$

where $\alpha = e^{-\frac{2\pi j}{N}}/\sqrt{N}$.

The time-domain OFDM symbol ($\boldsymbol{s}$) is transmitted after appending a cyclic prefix with a given length ($\boldsymbol{s_c}$).

The time-domain signal at the receiver side can be seen as:

$$\boldsymbol{r} = \boldsymbol{h} * \boldsymbol{s_c} + \boldsymbol{z} + \boldsymbol{i} = \boldsymbol{H} \cdot \left(\boldsymbol{F}^{\dagger} \cdot \boldsymbol{s} + \text{cyc}\right) + \boldsymbol{z} + \boldsymbol{i} \tag{6.7}$$

where $\boldsymbol{h}$ models the channel's impulsive response, $*$ represents the convolution operation, $\boldsymbol{z}$ stands for the white Gaussian noise and $\boldsymbol{i}$ represents the impulsive noise sources.

Let now $\Omega \subset \mathbb{Z}_N$ be the frequency's indexes that are used to send data subcarriers (i.e. data tones) and $\hat{\Omega} \subset \mathbb{Z}_N$ denote those not used for data subcarriers (i.e. null tones). Given this, let $\boldsymbol{F^{(1)}}$ and $\boldsymbol{F^{(2)}}$ be matrices formed by the rows of $\boldsymbol{F}$ (Equation 6.6) indexed by $p \in \Omega$ and $p' \in \hat{\Omega}$ respectively.

Thanks to the distributive property of the Fourier transform, the frequency-domain received OFDM symbol can be decomposed in:

$$\begin{aligned} \boldsymbol{y} &= \boldsymbol{F} \cdot \boldsymbol{r} = \boldsymbol{F} \cdot (\boldsymbol{h} * \boldsymbol{s_c} + \boldsymbol{z} + \boldsymbol{i}) \\ \boldsymbol{v} &= \boldsymbol{F^{(1)}} \cdot \boldsymbol{r} = \boldsymbol{F^{(1)}} \cdot (\boldsymbol{h} * \boldsymbol{s_c} + \boldsymbol{z} + \boldsymbol{i}) \\ \boldsymbol{w} &= \boldsymbol{F^{(2)}} \cdot \boldsymbol{r} = \boldsymbol{F^{(2)}} \cdot (\boldsymbol{z} + \boldsymbol{i}) \end{aligned} \tag{6.8}$$

Notice that the term $\boldsymbol{w}$ is only composed of the noise variables ($\boldsymbol{z}$ and $\boldsymbol{i}$) since the subcarriers indexed by $\boldsymbol{F^{(2)}}$ do not carry information (i.e. $\boldsymbol{s_c}(f = p') = \boldsymbol{0}$). The expressions show how $\boldsymbol{v}$, data tones (i.e multiplied by $\boldsymbol{F^{(1)}}$), are decoupled from $\boldsymbol{w}$, null tones (i.e. multiplied by $\boldsymbol{F^{(2)}}$), which is a desired effect. In fact, the existence of this feature

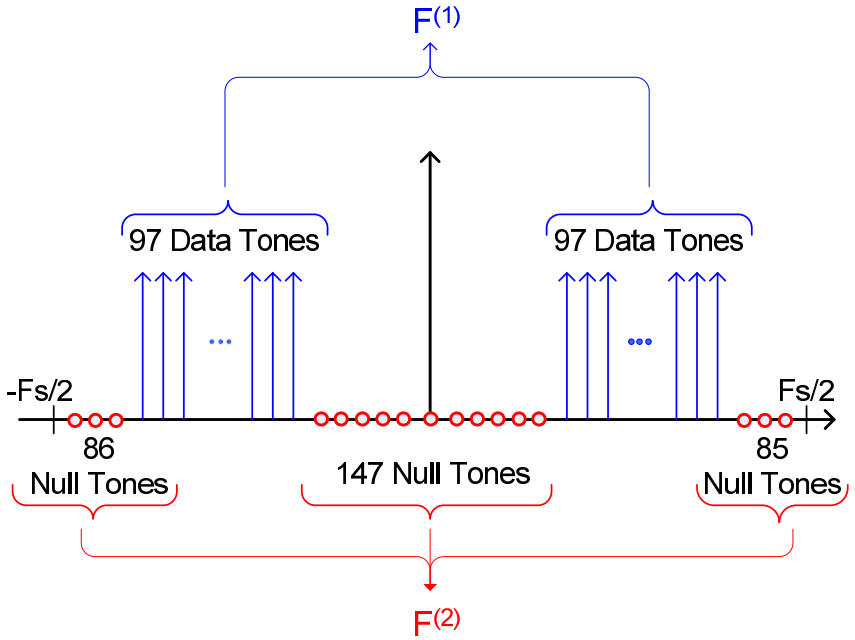

Figure 6.1: *Spectrum decomposition of a PRIME' symbol for Compressed Sensing (See Section 2.2).*

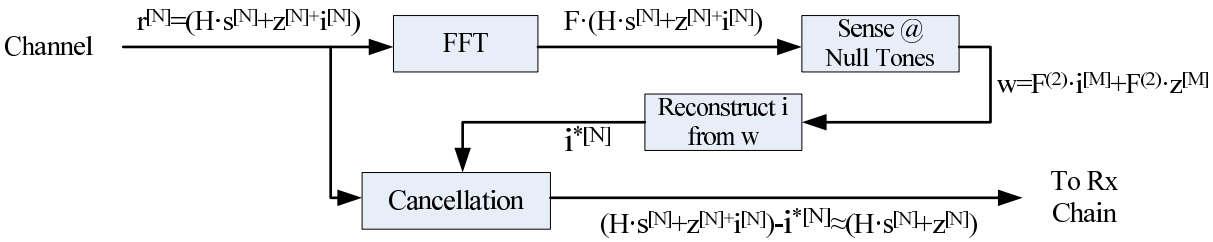

Figure 6.2: *Impulsive noise reconstruction via Compressed Sensing.*

will force the use of some kind of Fourier matrices as measurement transformation for compressed sensing, as it will be discussed in a few sections. This decoupling process is graphically shown in Figure 6.1.

From Equation 6.8, the term that contains only noise samples is:

$$\boldsymbol{w} = \boldsymbol{F^{(2)}} \cdot \boldsymbol{i} + \tilde{\boldsymbol{z}} \tag{6.9}$$

where $\boldsymbol{i}$ is assumed to be a sparse signal and $\tilde{\boldsymbol{z}} = \boldsymbol{F^{(2)}} \cdot \boldsymbol{z}$ some stochastic random process (white noise). This makes Equation 6.9 analogous to Equation 6.3. Thanks to this analogy, CS can be used to reconstruct the impulsive noise component ($\boldsymbol{i^*}$) based on some measurements ($\boldsymbol{w}$) corrupted by noise ($\tilde{\boldsymbol{z}}$).

Once the reconstructed impulsive noise vector ($\boldsymbol{i^*}$) is obtained, it is subtracted from a buffered version of the received signal ($\boldsymbol{r}$). The overall process, together with the dimensions of all signals, is shown in Figure 6.2.

6.3.1 General recovery conditions

As mentioned before, the restricted isometry property can be used to compute the reconstruction capabilities of a measurement matrix. However, since computing the RIP constant is in general a NP-hard problem, measurement matrices are usually characterized by its coherence, . Moreover, as stated in [102, 103] certain conditions on the coherence guarantee a stable reconstruction of a sparse vector using BP, OMP or BCS.

The *matrix coherence* parameter was introduced in [104] to heuristically characterize the performance of an MP algorithm. Later on, it was shown in [105] that the coherence plays a fundamental role when determining the recovery guarantees for OMP algorithms. Given a measurement matrix $\mathbf{\Phi}$, its coherence is defined as [92]:

Definition 2. *The coherence, $\mu(\mathbf{\Phi})$, of an MxN matrix $\mathbf{\Phi}$ is the largest absolute inner product between any two columns of $\mathbf{\Phi}$:*

$$\mu\left(\Phi\right) = \max_{1 \leq p \neq q \leq N} \frac{|\langle \boldsymbol{\phi_p}, \boldsymbol{\phi_q} \rangle|}{||\phi_p||_2 \cdot ||\phi_q||_2} \tag{6.10}$$

$\mu\left(\Phi\right)$ is in the range $\left[\sqrt{\frac{N-M}{M \cdot (N-1)}}, 1\right]$, where the lower bound is known as the Welch's bound [106].

This coherence is used in [107] to enunciate the following theorem

Theorem 2. *If*

$$k < \frac{1}{2}\left(1 + \frac{1}{\mu(\Phi)}\right) \tag{6.11}$$

then, for each vector $\boldsymbol{y} \in \mathbb{R}^M$, there exists at most one k-sparse signal such that $\boldsymbol{y} = \mathbf{\Phi} \cdot \boldsymbol{x}$.

Theorem 2 guarantees that, if the condition is hold, any k-sparse vector can be recovered from $\boldsymbol{y} = \mathbf{\Phi} \cdot \boldsymbol{x}$ measurements using either BP, OMP and CBS algorithms.

The relationship expressed by Equation 6.11 can be graphically view in Figure 6.3. In order to create the lines represented in the figure, the coherence indicator was computed both for a Partial Fourier Transform Matrix (such as the one in Equation 6.6) and for a random matrix with normalized columns, as suggested in [91]. Recovery is possible in all cases where the blue line is below the red one (see Equation 6.11). As stated in [108], the best recovery performance for given matrix dimensions is achieved by a random matrix, which agrees with what is shown in the figures.

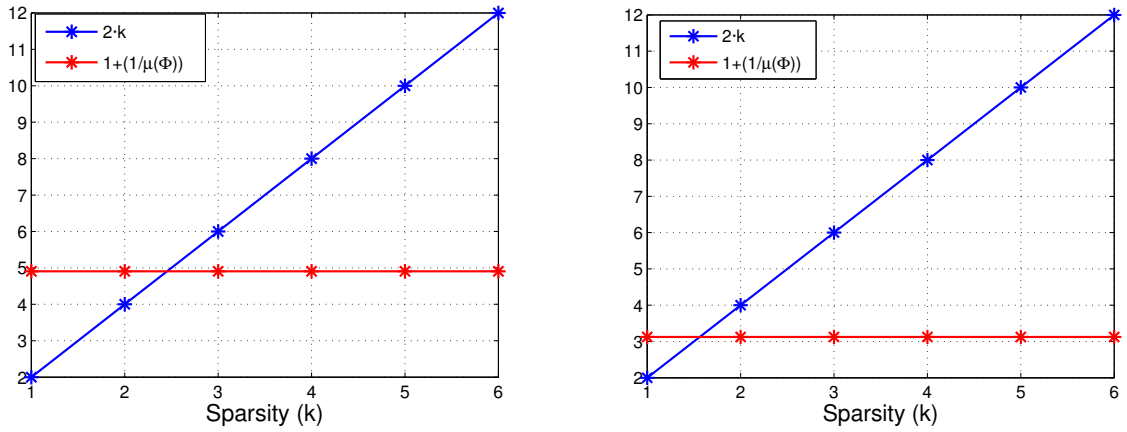

Figure 6.3: *Theoretical performance according to Equation 6.11. (a) 318x512 Random Matrix. (b) 318x512 Partial Fourier Transform Matrix.*

6.3.1.1 Numerical experiments

The aim of this subsection is to numerically quantify the recovery guarantees of the Orthogonal Matching Pursuit algorithm. To do so, simulations test the numerical performance of two configuration: a random and a partial Fourier transform matrix. The first configuration consists of an MxN matrix with random values, zero mean and normalised columns, whereas the partial Fourier transform matrix has also MxN dimension and is built as detailed in Section 6.3. The sparse vector to be recovered has dimension Mx1 and has k independent and identically distributed (i.i.d.) Gaussian values placed in random positions. The rest of the $k - M$ values are set to zero.

The OMP algorithm described in Algorithm 1 [97] (See Appendix A) is run with 500 repetitions using several values for the sparsity level (k) and for the measurements (M). A concrete implementation for this algorithm in Matlab code can be found in Appendix A.1.

Figure 6.4 shows the evolution of a concrete case when $N = 512$, $M = 318$ and $k = 3$ when using a partial Fourier transform matrix. The blue signal represents the sample signal whose sparsity wants to be extracted. The red stars represent the sparsity values reconstructed on every step of the OMP algorithm.

Figure 6.5 shows the recovery performance for all runs. This performance is computed based on the number of successful reconstructions divided by the number of repetitions, as suggested in [97]. A reconstruction is said to be successful when the euclidean difference between the reconstructed and the original vector is less than 0.1. With this, the performance curves in Figure 6.5 show the relationship between the number of measurements (M) and the sparsity level (k) that can be handled by the OMP algorithm.

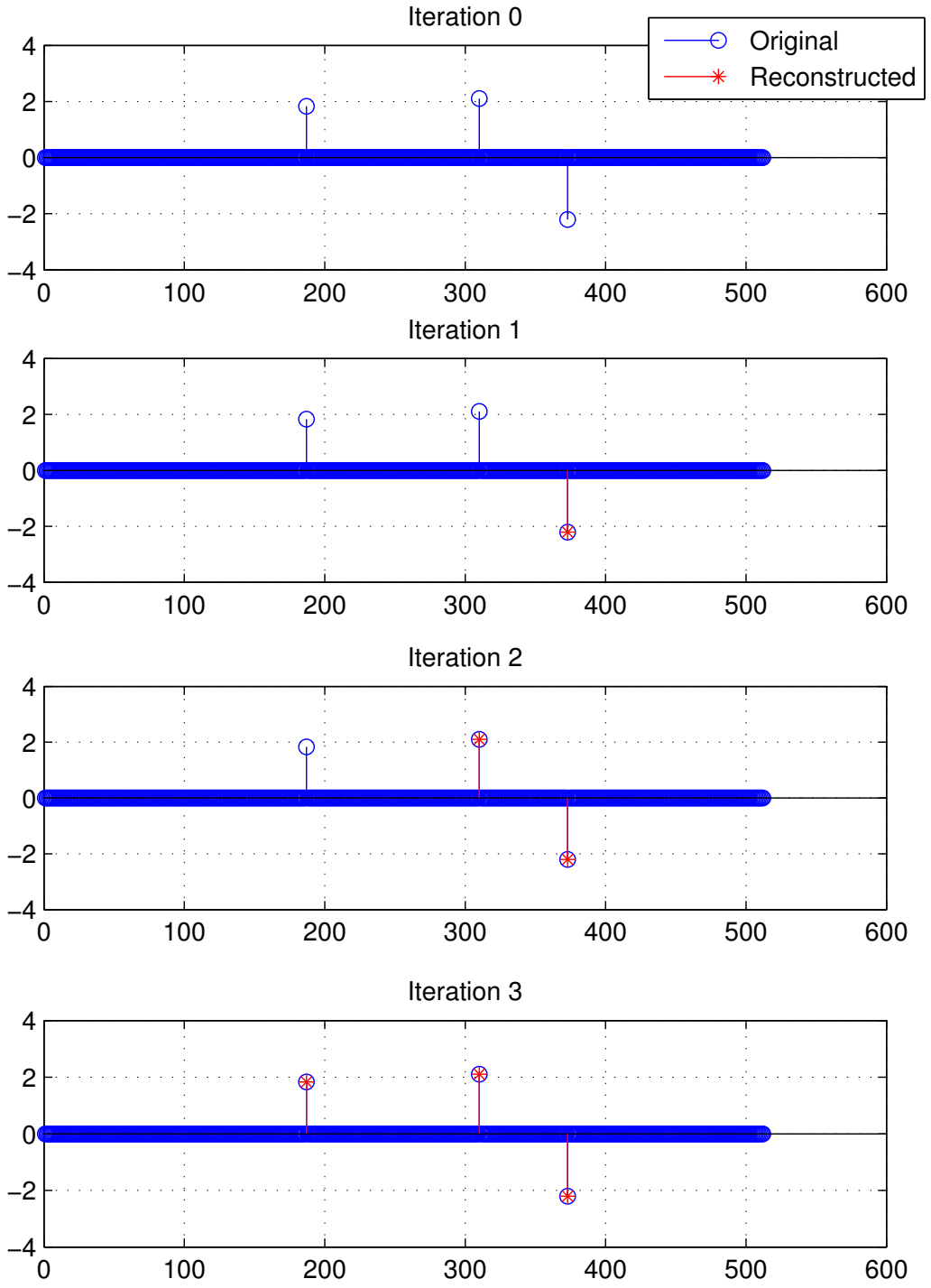

Figure 6.4: *Recovery evolution of a sparse signal with $N = 512$, $M = 318$ and $k = 3$ when using a partial Fourier transform matrix. A sparse sample is recovered on every iteration.*

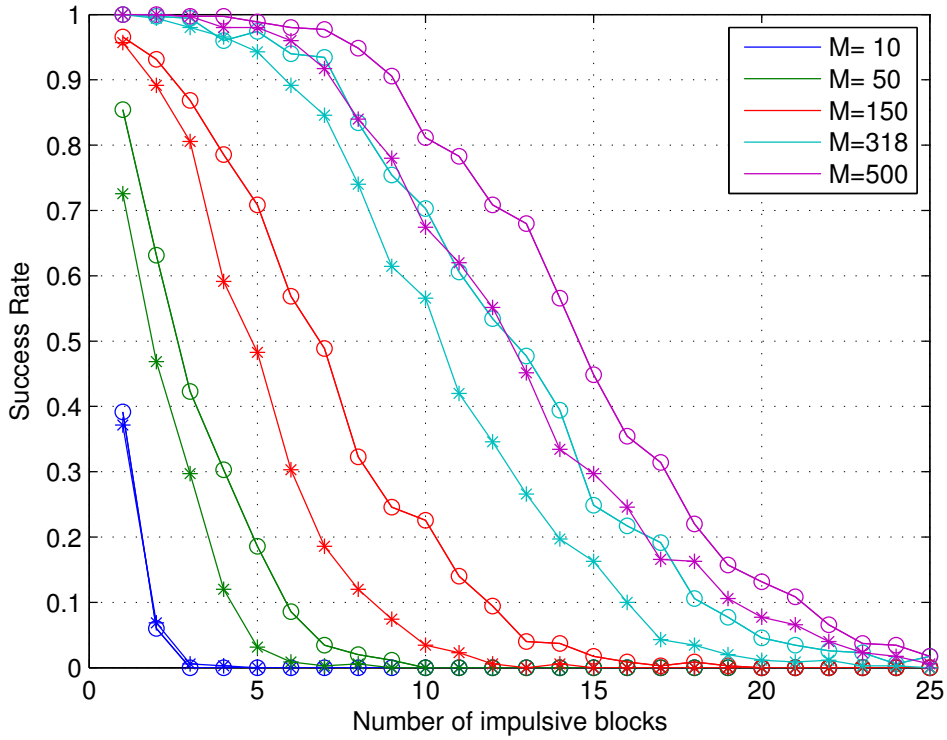

Figure 6.5: *Recovery performance using Orthogonal Matching Pursuit for $N = 512$ and different values for M and k. Stars and circles stand for the performance when using a partial Fourier and a random measuring matrix respectively.*

As it could be expected, a higher number of sparsity can be reconstructed when more measurements are available. This results are coherent with what was shown in Figure 6.4: a sparse signal with 3 samples different than zeros can accurately be reconstructed using $M \geq 318$ measurements.

Additionally, as it was already pointed out in Figure 6.3, using a random matrix for recovery provides a better performance than when using the partial Fourier transform one. However, due to the impulsive noise removal application that is being pursued in this thesis, a random sensing matrix could not be used because it does not provide the required mechanism to decouple the noise from the data, as it was discussed in Section 6.3. A partial Fourier transform matrix does provide this mechanism as it is depicted in Figure 6.1.

Moreover, it is worth mentioning that the performance achieved in the numerical experiment (Figure 6.5) clearly outperforms what could be expected from a theoretical point of view (Figure 6.3). This fact is in agreement with results shown in [92], where it is stated that recovery performances extracted from the theory (i.e. Equation 6.11) are more pessimistic than those extracted from numerical simulations (i.e. Figure 6.5).

6.3.2 Block recovery conditions

Previous sections dealt with recovering a sparse signal from an undersampled version of it. The final goal is to subtract the recovered signal from the received one as it was explained in Section 6.3. However, assuming that the impulsive noise is a plain sparse signal might be slightly idealistic. Noise impulses have certain duration which make them look as they appear in bursts or blocks. Even in situations where impulses are so narrow (or the sampling frequency is so low) that they only last for a single digital sample, the bandpass filter placed at the beginning of the receiver will make their energy spread over several time samples. This will make the noise adopt a *blocky* structure. This statement is also discussed in [35].

As reported in [35], [92] and [109] the recovery mechanism of compressed sensing can be improved if the sparsity of the signal occurs in clusters (i.e. it consists of sequences of consecutive non-zeros values). In the previously cited references, these kind of signal are referred to as block-sparse signal.

Mathematically, a block-sparse signal can be seen as a concatenation of several blocks of length d. If $\boldsymbol{x}[\boldsymbol{p}]$ stands for the p^{th} block in vector $\boldsymbol{x}$, it can be expressed as:

$$\boldsymbol{x} = [\underbrace{x_1, \cdots, x_d}_{\boldsymbol{x^T[1]}}, \underbrace{x_{d+1}, \cdots, x_{2d}}_{\boldsymbol{x^T[2]}}, \cdots, \underbrace{x_{N-d+1}, \cdots, x_N}_{\boldsymbol{x^T[L]}}]^T \tag{6.12}$$

where $N = L \cdot d$ and L is an integer which represents the number of blocks the vector is divided in.

The same procedure can be done for the measurement matrix ($\boldsymbol{\Phi}$) by dividing it in blocks of size Mxd:

$$\boldsymbol{\Phi} = [\underbrace{\boldsymbol{\phi_1}, \cdots, \boldsymbol{\phi_d}}_{\boldsymbol{\Phi[1]}}, \underbrace{\boldsymbol{\phi_{d+1}}, \cdots, \boldsymbol{\phi_{2d}}}_{\boldsymbol{\Phi[2]}}, \cdots, \underbrace{\boldsymbol{\phi_{N-d+1}}, \cdots, \boldsymbol{\phi_N}}_{\boldsymbol{\Phi[L]}}] \tag{6.13}$$

with $\boldsymbol{\Phi}[\boldsymbol{p}]$ being the p^{th} block of size Mxd.

In order to heuristically determine the reconstruction properties of a CS algorithm, analogously to Equation 6.10, the block-coherence is defined as [92]:

$$\mu_B = \max_{p,q \neq p} \frac{1}{d} \cdot \rho(\boldsymbol{\Phi}[\boldsymbol{p}, \boldsymbol{q}]) \tag{6.14}$$

where $\boldsymbol{\Phi}[\boldsymbol{p}, \boldsymbol{q}] = \boldsymbol{\Phi^H}[\boldsymbol{p}] \cdot \boldsymbol{\Phi}[\boldsymbol{q}]$. Note how $\boldsymbol{\Phi}[\boldsymbol{p}, \boldsymbol{q}]$ is the $(p, q)^{th}$ dxd block of the NxN matrix $\boldsymbol{\Phi^H}[\boldsymbol{p}] \cdot \boldsymbol{\Phi}[\boldsymbol{q}]$. As it could be expected, when block size is one ($d = 1$), the coherence and block-coherence have the same value (i.e. $\mu = \mu_B$).

Additionally, whereas the coherence measures global properties of the matrix $\boldsymbol{\Phi}$, local block properties are defined by the *sub-coherence* [92]:

$$\nu = \max_{l} \left[\max_{p,q \neq p} |\boldsymbol{\phi_p^H} \cdot \boldsymbol{\phi_q}| \right], \qquad \boldsymbol{\phi_p}, \boldsymbol{\phi_q} \in \boldsymbol{\Phi[l]} \tag{6.15}$$

where, in case of $d = 1$, ν is defined as 0.

Some of the main conclusions extracted from the previous derivations (deeper explained in [92]) is that, if $\boldsymbol{\Phi}$ has unit norm, the coherence (Equation 6.10), block-coherence (Equation 6.14) and sub-coherence (Equation 6.15) are in the interval $[0, 1]$. Additionally, in case the columns of $\boldsymbol{\Phi[l]}$ being orthonormal for each l, then $\nu = 0$. Moreover, as proved in [92], the block-coherence also satisfies $0 \leq \mu_B \leq \mu$.

One of the advantages of assuming block sparsity is the new reltion for the recovery conditions [92] (dual to Equation 6.11):

$$k_d \cdot d < \left(\frac{1}{\mu_B} + d - \frac{(d-1)\nu}{\mu_B} \right) \frac{1}{2} \tag{6.16}$$

This expression provides an upper bound of the number of blocks (k_d) of a given length (d) that can be recovered using a specific measurement matrix. Consequently, lower values of μ_B are translated into better reconstruction performance. It is worth mentioning that the sub-coherence metric is only dependent on the measurement matrix ($\boldsymbol{\Phi}$), so, the way to increase the number of blocks able to reconstruct, the effort needs to be put in the design of this matrix.

Recovery conditions expressed in Equation 6.16 are represented in Figure 6.6a and 6.6b for a random normalized and partial Fourier transform matrix respectively. Abscissas represents now block-sparsity, i.e. the number of blocks of size d that can be reconstructed. d is set to 2 for this concrete representation. When comparing with the performance shown in Figure 6.6, it can be seen how the total amount of non-zero samples that can be recovered has improved. This improvement is not very significant but, as mentioned before, the theoretical performance is rather pessimistic when compared to results in numerical experiments. Next section provides numerical results obtained when dealing with a block-sparse recovery.

6.3.2.1 Numerical experiments

The aim of this subsection is to quantify the recovery guarantees of the Block Orthogonal Matching Pursuit (BOMP) algorithm numerically. To do so, simulations test the numerical performance of two configurations: a random and a partial Fourier transform matrix. The first configuration consists of an MxN matrix with random values, zero mean and normalised columns whereas the partial Fourier transform matrix has also MxN dimension and is built as detailed in Section 6.3. The sparse vector to be recovered has dimension Mx1 and has k_d independent and identically distributed (i.i.d.) blocks of

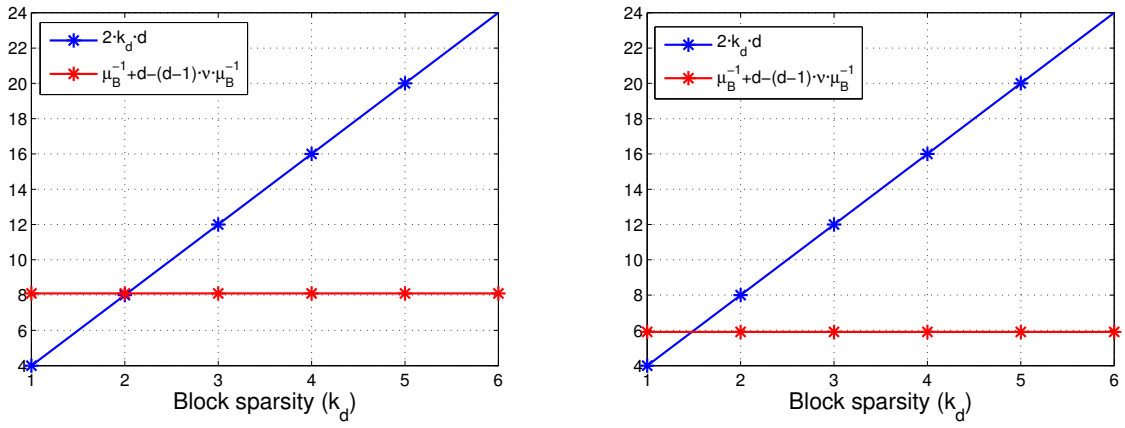

Figure 6.6: *Theoretical performance for $d = 2$ according to Equation 6.16. (a) 318x512 Random Matrix. (b) 318x512 Partial Fourier Transform Matrix.*

2 samples (i.e. $d = 2$) of Gaussian values placed in random positions. The rest of the $k_d \cdot d - M$ values are set to zero.

The BOMP algorithm described in Algorithm 2 [110] (See Appendix A) is run with 500 repetitions using several values for the sparsity level (k_d), for the measurements (M) and for a fixed block size of $d = 2$. A concrete implementation using Matlab can be found in Appendix A.2.

Numerical simulations when running the BOMP algorithm are shown in Figure 6.7. It can be seen how the overall number of impulses is improved when compared with results reported in Section 6.3.1.1. Note that, in Figure 6.7, each one of the abscissa values represents number of impulsive noise blocks of size d.

This shows how, assuming a block-sparsity nature of the impulsive noise, the reconstruction's performance of compressed sensing can be improved.

6.4 Improving compressed sensing's performance via difference sets

Previous section proved that assuming block-sparsity in the measured signal leads to an improvement in the reconstruction capabilities via compressed sensing. Nevertheless, it could be seen that the obtained improvement was not substantial. This subsection will combine this effect with some modification in the sensing matrix to further improve the achieved recovery performance.

As it was mentioned before, the reconstruction performance achieved by CS is directly related to its measurement matrix; as it is the only variable involved in the computa-

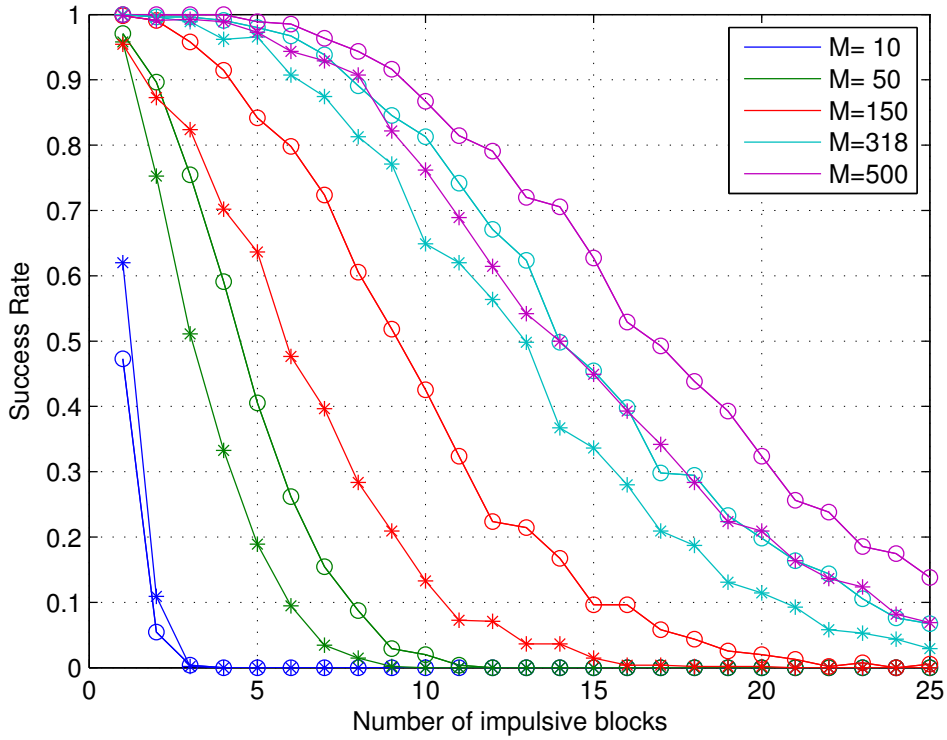

Figure 6.7: *Recovery performance with Block Orthogonal Matching Pursuit for $N = 512$ and different values for M and k_d when impulsive noise is grouped in blocks of $d = 2$. Stars and circles stand for the performance when using a partial Fourier and a random measuring matrix respectively.*

tion of the coherence, block-coherence and sub-coherence. Additionally, a specially good performance is achieved when blocks in $\mathbf{\Phi}$ (i.e. $\mathbf{\Phi}[\boldsymbol{p}]$) are linearly independent. This produces $\nu = 0$ and Equation 6.16 is simplified to:

$$k_d \cdot d < \frac{\mu_B^{-1} + d}{2} \tag{6.17}$$

which allows for a higher upper bound than the one in Equation 6.16. One way to achieve this incoherence is by using the scheme proposed in [111]. There, certain rows of a partial Fourier transform matrix are chosen to make the overall matrix incoherent in blocks. Additionally, since it is based on partial Fourier transform matrices, data sub-carriers can be decoupled from the received spectrum, as discussed in Section 6.3. This feature makes the scheme completely suitable for the impulsive noise application that is being pursued in this chapter.

The following definition can be found in [111]:

Definition 3. *A subset $\mathbb{U} = \{u_1, \cdots, u_{M_{DS}}\}$ of $\mathbb{Z}_{N_{DS}}$ is called a (N_{DS},M_{DS},λ)-Difference*

Set if the $M_{DS} \cdot (M_{DS} - 1)$ *differences*

$$(u_k - u_l) \ mod \ N_{DS}, \qquad k \neq l \tag{6.18}$$

take all possible non-zero values $1, 2, \cdots N_{DS} - 1$*, with each value exactly* λ *times.*

It is proved in [111] that, if the $\mathbb{U}$ subset is used to index the rows of a partial Fourier matrix, this matrix is incoherent in blocks (which produces $\nu = 0$) and Equation 6.17 holds. According to [111], this set of row indexes $\mathbb{V} = \{v_k\} \in \mathbb{Z}_{N_{DS}}$ is defined by:

$$\mathbb{V} = \{N_{DS} \cdot s + u_t : u_t \in \mathbb{U}\} \tag{6.19}$$

where $1 \leq t \leq M_{DS}$ and $0 \leq s \leq N_{DS} - 1$. Using the previously defined subset, Matrix $\boldsymbol{F^{(2)}}$ in Equation 6.9 can be re-written taking $\mathbb{V}$ indexes as:

$$\boldsymbol{F_{DS}^{(2)}} = \begin{bmatrix} 1 & \beta^{v_1} & \beta^{2v_1} & \dots & \beta^{(N_{DS}-1)v_1} \\ 1 & \beta^{v_2} & \beta^{2v_2} & \dots & \beta^{(N_{DS}-1)v_2} \\ \vdots & \vdots & \vdots & \ddots & \vdots \\ 1 & \beta^{v_{M_{DS}}} & \beta^{2v_{M_{DS}}} & \dots & \beta^{(N-1)v_{M_{DS}}} \end{bmatrix} \tag{6.20}$$

where $\beta = e^{-j\frac{2\pi}{N_{DS}}}/\sqrt{M_{DS}}$, $\boldsymbol{F_{DS}^{(2)}}$ is now a $M_{DS} \cdot N_{DS}$xN_{DS}^2 matrix and v_m are elements of $\mathbb{V}$ with $m = 1...M_{DS}$.

For the above mentioned matrix, the cross correlation of any two column vector can be expressed as [111]:

$$f(m) = |\phi_l^H \cdot \phi_{l'}| = \left| \frac{1}{M_{DS}} \sum_{i=1}^{M_{DS}} e^{j2\pi v_i (l-l')/N_{DS}} \right| \tag{6.21}$$
$$1 \leq m = (l - l')\text{mod}(N_{DS}) \leq N_{DS} - 1$$

As proved in [111,112], the cross correlation between any two vectors of $F_{DS}^{(2)}$ is either 0 or $\sqrt{N_{DS} - M_{DS}/M_{DS}(N_{DS} - 1)}$. In the following, an example is provided in order to help in the understanding of the effect that the Difference Sets have in the cross correlation of the measurement matrix's columns.

Let's consider the $(7, 3, 1)$ difference set with $\mathbb{U} = \{0, 1, 3\}$[1]. It creates a $M_{DS} \cdot N_{DS}$xN_{DS}^2 = 21x49 partial Fourier sensing matrix as the one in Equation 6.20 particularized by the set:

[1]Indeed this is a difference sets since $(0-1)\text{mod}(7) = 6$; $(0-3)\text{mod}(7) = 4$; $(1-0)\text{mod}(7) = 1$; $(1-3)\text{mod}(7) = 5$; $(3-0)\text{mod}(7) = 3$ and $(3-1)\text{mod}(7) = 2$ (i.e. all elements in $[1, 6]$ appear one time. See Definition 3).

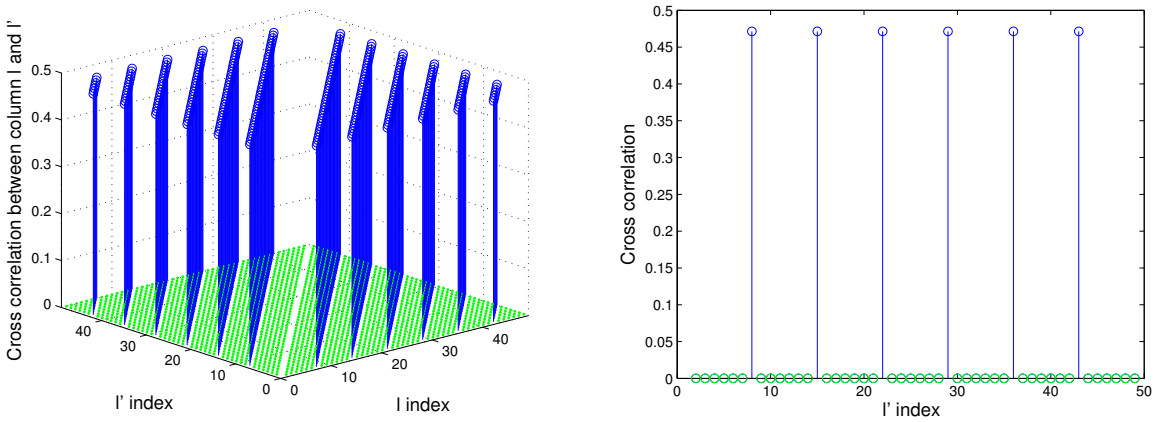

(a) **(b)**

Figure 6.8: *Cross correlation of columns for matrix in Equation 6.20. (a) Cross correlation for all possible combination of columns. (b) Cross correlation between column 1 and the rest.*

$$\mathbb{V}^{(DS-(7,3,1))} = \{0, 1, 3, 7, 8, 10, 14, 15, 17, 21, 22, 24, 28, 29, 31, 35, 36, 42, 43, 45\} \quad (6.22)$$

Cross correlations for the columnss of a partial Fourier matrix indexed by $\mathbb{V}^{(DS-(7,3,1))}$ are graphically displayed in Figure 6.8. There, Figure 6.8a shows the resultant cross correlation for all possible combinations of the columns in the sensing matrix (Equation 6.22). It can be seen how resultant values are only either 0 or 0.4714 (which corresponds to $\sqrt{N_{DS} - M_{DS}/M_{DS} \cdot (N_{DS} - 1)}$). Zero values are coloured in green for a better visualization. Additionally, Figure 6.8b shows a two-dimensional perspective with the computation of the cross correlation of the first column with the rest of the ones. From this last figure, it can more clearly be seen that only columns separated by a distance equal N_{DS} (i.e 7 for this concrete case) are different than 0, as proved in [111].

This feature has consequences in the computation of the sub-coherence. As defined in Equation 6.15, this parameter computes the maximum cross correlation inside a block of columns. As seen in previous figure, it is enough to choose a block smaller than N_{DS} to have a null sub-coherence. When this situation occur, Equation 6.16 holds and higher bound can be achieved in the reconstruction process.

A public repository of difference sets (DS) is available at [113]. There, values of M_{DS} and N_{DS} holding Definition 3 can be found as well as values for the corresponding $\mathbb{U}$ sets.

In order to work with similar dimension as in PRIME (512-length FFT), a value near 512 is chosen. According to the previous repository, the difference set ($N_{DS} = 23$, $M_{DS} = 11$, $\lambda = 1$) can be used to create a sensing matrix with dimensions $N_{DS} \cdot M_{DS}$ x N_{DS}^2 (i.e. 253 x 529) and defines the following subset: $\mathbb{U} = \{0, 1, 2, 3, 5, 7, 8, 11, 12, 15, 17\}$.

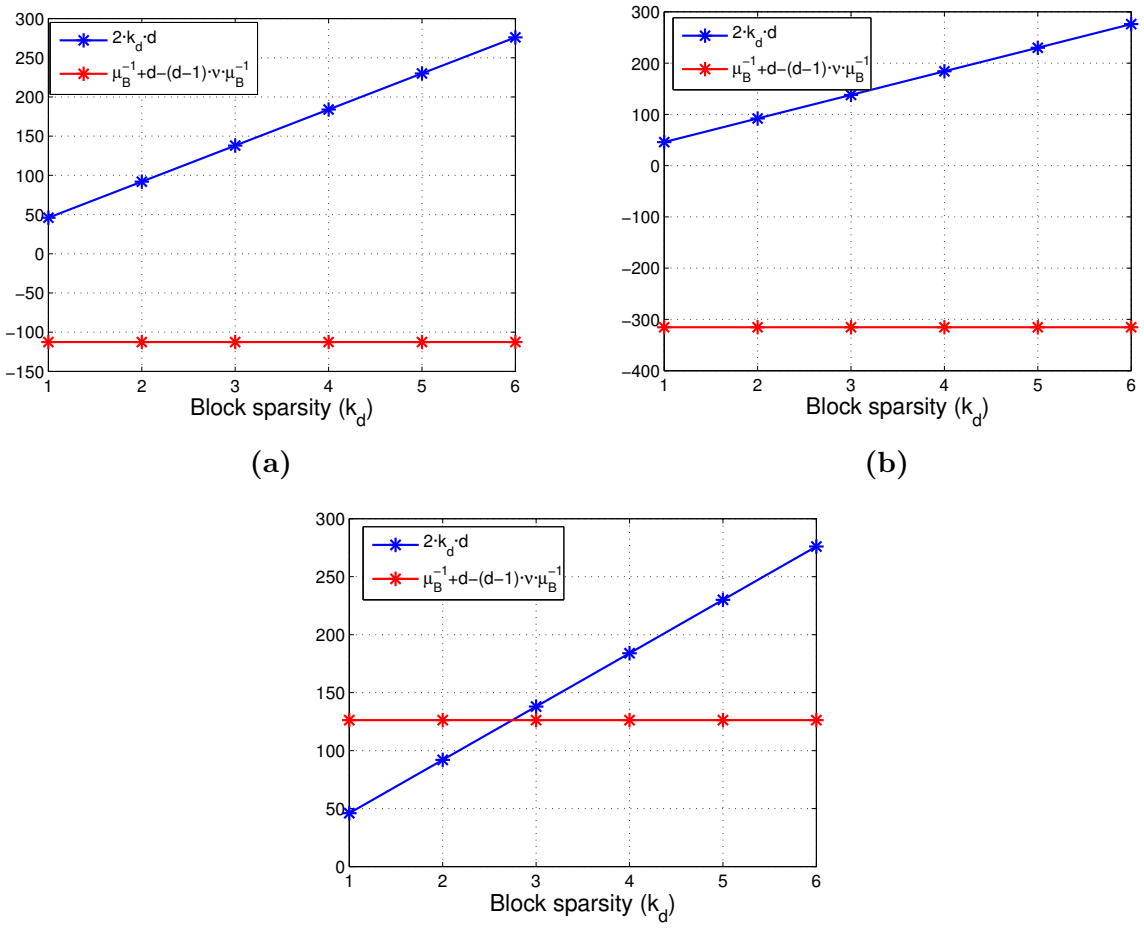

Figure 6.9: *Theoretical performance according to Equation 6.17. Block-sparsity is set to* $d = 23$. *(a) 318x512 Random Matrix. (b) 318x512 Partial Fourier Transform Matrix using original PRIME's null tones. (c) 253x529 Difference Sets-based Partial Fourier Transform Matrix.*

The corresponding frequencies for the $\boldsymbol{F}^{(1)}$ and $\boldsymbol{F}^{(2)}$ matrices can be found in Appendix C.

Theoretical recovery conditions are compared in Figure 6.9. The first figure (6.9a) shows the recovery when using a 318x512 random matrix. The same thing is done in the second figure (6.9b) using a 318x512 partial Fourier transform matrix that indexes the $86 + 147 + 85$ null tones defined by PRIME (see Figure 6.1). Finally, the ($N_{DS} = 23$, $M_{DS} = 11$, $\lambda = 1$) difference set is used to create a 253x529 partial Fourier transform whose recovery can be seen in Figure 6.9c. All three analysis use a block-sparsity of size $d = 23$. A clear conclusion is that using the proposed difference set considerably increases the recovery performances since it is able to recover two blocks of 23 samples. However, no blocks of that length can be recovered when using the other two cofigurations.

6.4.1 Numerical experiments

As it was done in the previous sections, some numerical simulations are provided. In this case, the experiment consists of reconstructing a block-sparse signal with block size $d = 23$. The reconstruction is done via the BOMP procedure described in Algorithm 2 and using three different measurement matrices. Two of them are the random and partial Fourier transform matrices used in previous section whereas the third one is a partial Fourier transform matrix indexed by a ($N_{DS} = 23$, $M_{DS} = 11$, $\lambda = 1$)-Difference Set (previously described). All three measurement matrices use $M = 318$ null tones available for noise sensing.

Figure 6.10 represents the simulated performances. The green and red lines stand for the performance when using a random and a partial Fourier transform matrix with the original PRIME' spectrum respectively. The blue line represents the success rate when using a PFT matrix and reordering the data tones according to the previous Difference Set. As the figure shows, the use of Difference Set-based compressed sensing allows for a better reconstruction since it can accurately estimate up to two blocks of impulses with size equal to 23.

The consequences of these results in terms of bit error rate improvement will more clearly be seen in the following sections.

6.5 Performance in a PLC channel

Sections 6.3.1, 6.3.2 and 6.4 focused on analysing the reconstruction capabilities of different compressed sensing configurations. However, the final objective pursued in this work is to apply compressed sensing technique in cancelling the impulsive noise present in power line channels. In order to do so, this section shows the results when applying

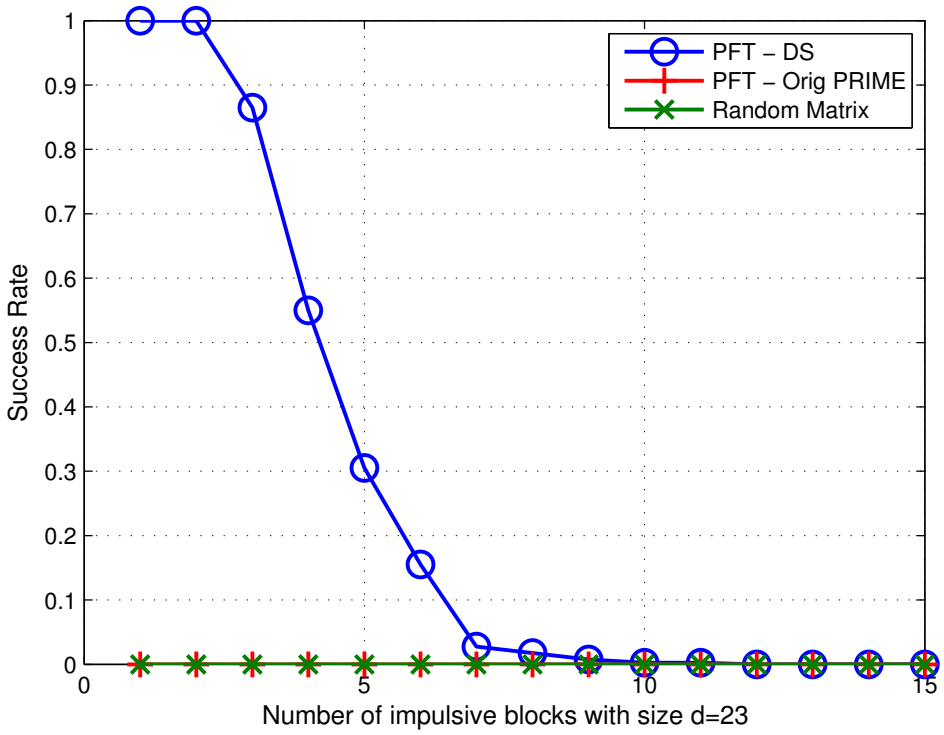

Figure 6.10: *Recovery performance when using different configuration of measurement matrices. All of them use* $M = 318$ *samples to reconstruct the impulses.*

the scheme proposed in Figure 6.2 to a PLC receiver. As in Chapter 4, the performance is measured in terms of the obtained BER for a given SNR.

Figure 6.11a shows the performance when applying compressed sensing cancellation using a 318x512 partial Fourier transform matrix. In order to provide some reference, blue and purple dashed lines are plot representing the theoretical performance in a background and impulsive scenario respectively.

Comparing Figures 4.7a and 6.11a, some improvement can be seen in the performance. In concrete, the most robust mode (DBPSK-FEC) has an improvement of around 9dB. This communication mode is the most likely to be used in such an impulsive scenario, due to its higher robustness.

However, this performance can be further improved by using the difference sets configuration for compressed sampling as explained in Section 6.4. To implement this configuration in the simulations, the transceiver was modified in order not to use carriers placed at $v_m \cdot F_s/N$ frequencies for data transmission (where F_s stands for the sampling frequency, N stands for the number of points considered in the FFT, and m runs from 1 to M_{DS}).

Setting variables N_{DS} and M_{DS} to 23 and 11 respectively creates a $\mathbb{V}$ set of 352

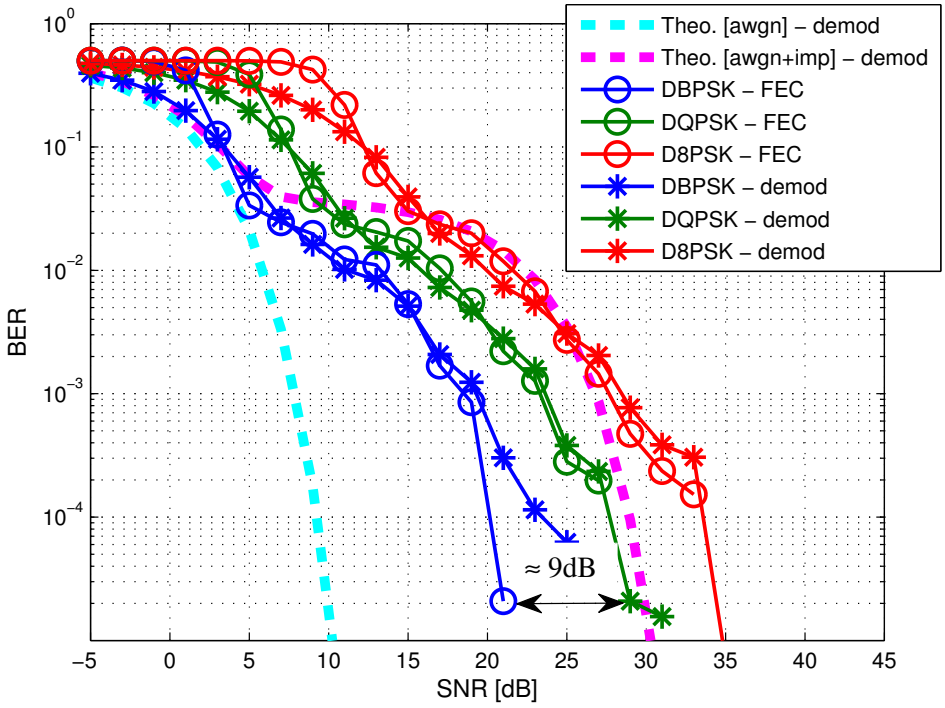

(a)

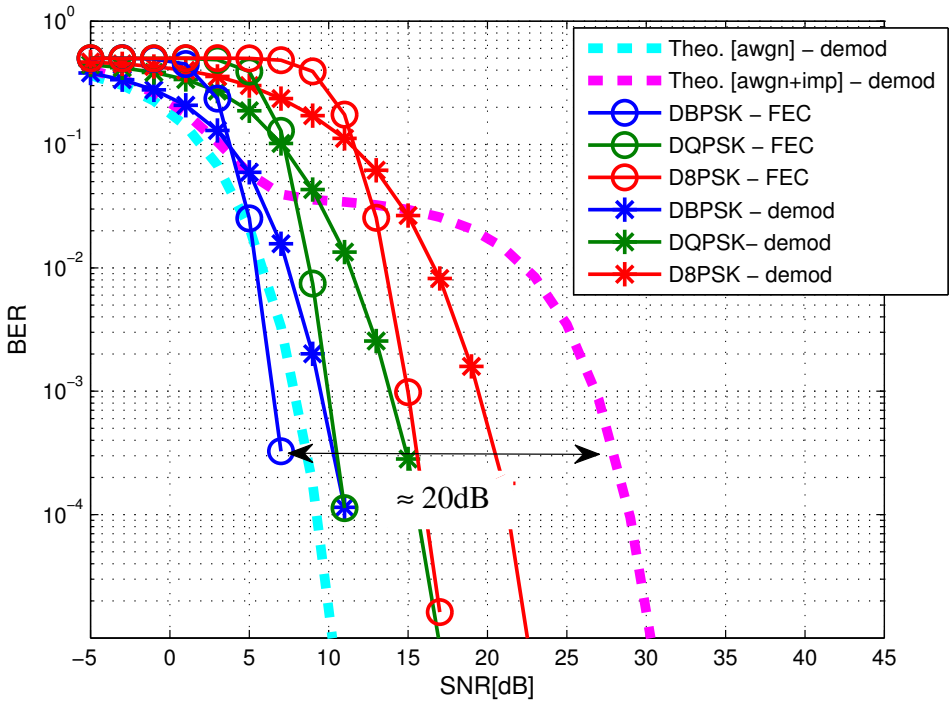

(b)

Figure 6.11: *Performances in Impulsive Noise Channel using compressed sensing cancellation. (a) Applying CS cancellation over the original spectrum. (b) Applying DS-based CS cancellation.*

components ($\hat{\mathbf{\Omega}}$, as referenced in Section 6.3). This leaves 276 sub-carriers available for data transmission ($\mathbf{\Omega}$, as referenced in Section 6.3), although only 97 of them were used in the simulations due to compatibility with PRIME.

The achieved performance when using Difference Sets-based Compressed Sensing is shown in Figure 6.11b. Since most of the impulses are correctly reconstructed from measurements done at null tones, the performance obtained is similar to the white Gaussian noise scenario (blue thick and dashed line in Figure 6.11b). There is an approximate gain of 20 dB for the most robust mode when using DS-based CS.

As explained in previous sections, the only modification needed in the transceiver to achieve this gain is (besides the introduction of the BOMP block) a re-mapping of the frequencies used for null and data tones.

Concrete values for this frequencies are provided in Appendix C. Note that they belong to the designated CENELEC band.

6.6 Conclusions

The present chapter has described an impulsive noise cancellation method based on a concrete configuration for compressed sensing. This specific configuration is based on the ideas presented in [92] and [93], where it is argued that the recovery properties of compressed sensing can be improved by using a partial Fourier matrix indexed by a subset based on Difference Sets.

To the best of authors' knowledge, no results have been published regarding the use of difference set-based compressed sensing for impulsive noise cancellation in OFDM systems. Thus, it is believed to be an original contribution for the severe problem of OFDM performance in impulsive noise environments.

In contrast with other recent proposed techniques [38, 114], simulations show that an almost complete cancellation of the impulsive noise effect is achieved when using DS-based CS.

An added value of the application of CS techniques to cancel the impulsive noise is that, since they are applied at the very beginning of the receiver chain, they can be used in already working systems with small modifications (basically the inclusion of the BOMP block). All the CS-related processing can be done in an external block before entering the PRIME receiver. Additionally, there is no reduction in the transmission rate since no redundancy is added in the message. This last feature makes this technique very suitable for systems which have traded off low robustness for high transmission speed, as it is the case of PRIME.

Moreover, in order to achieve an almost complete impulsive noise cancellation, difference set-based compressed sensing can be used. The adaptation to already working system is not as straight-forward as with plain compressed sensing, but it basically breaks down to a different mapping of the digitally modulated symbols to the DFT block (vice versa for the receiver). Consequently, no extra complexity is added with respect to the use of CS with an original PRIME' spectrum while a considerable gain in performance is achieved, as the last figure of this chapter shows.

Nevertheless, the proposed technique has some drawbacks. The use of difference set-based compressed sensing requires a more complex receiver than an original one. In concrete, if using the frequency mapping proposed in this chapter, a DFT with a length non-integer power of two is needed. A consequence of this is that typical Fast Fourier Transform (FFT) algorithms cannot be used. Nevertheless, some of the algorithms described in [115] can be used to perform this calculation efficiently.

Chapter 7

PLC network simulation tool

7.1 Introduction

One of the key Smart Grids' applications very suitable for using PLC as a communication medium is the Advance Metering Infrastructure (AMI). However, although previous chapters of this thesis have focused on the physical layer of PLC, the BER vs. SNR metric analysed cannot provide an estimation of how an AMI system would behave in a real environment. Considerations like connection-oriented communications, packet fragmentation, medium access strategy and network synchronisation play also an important role in the dynamics of such a system. This chapter describes the approach proposed in this thesis in order to model the main communication effects and obtain the performance achieved by the overall network.

The AMI generic scenario under consideration is the one shown in Figure 7.1: some utility company communicates with a Medium Voltage / Low Voltage (MV/LV) transformer through a dedicated line and this transformer acts as a gateway retransmitting all messages through the power lines. The communication architecture of this scheme is shown in Figure 7.2. The so called "bridge node" would be implemented at the MV/LV transformer and would have two communication interfaces: one of them would implement the internet layer stack to allow messages to be received from and transmitted to the utility' servers, whereas the other interface would be compatible with PRIME's specifications. As it can be seen, with this architecture, any application existing at the end-user or at the utility's can communicate with each other.

In contrast with other performance metrics analysed before, the key parameter of interest from a network's perspective is the communication's latencies between application layers. This parameter gives an upper bound on how often all devices inside an AMI network can be polled. This bound is an important design parameter for Demand Response (DR) applications, since it defines how long it takes for a command/request to be received by all the entities in the whole system and act according to it.

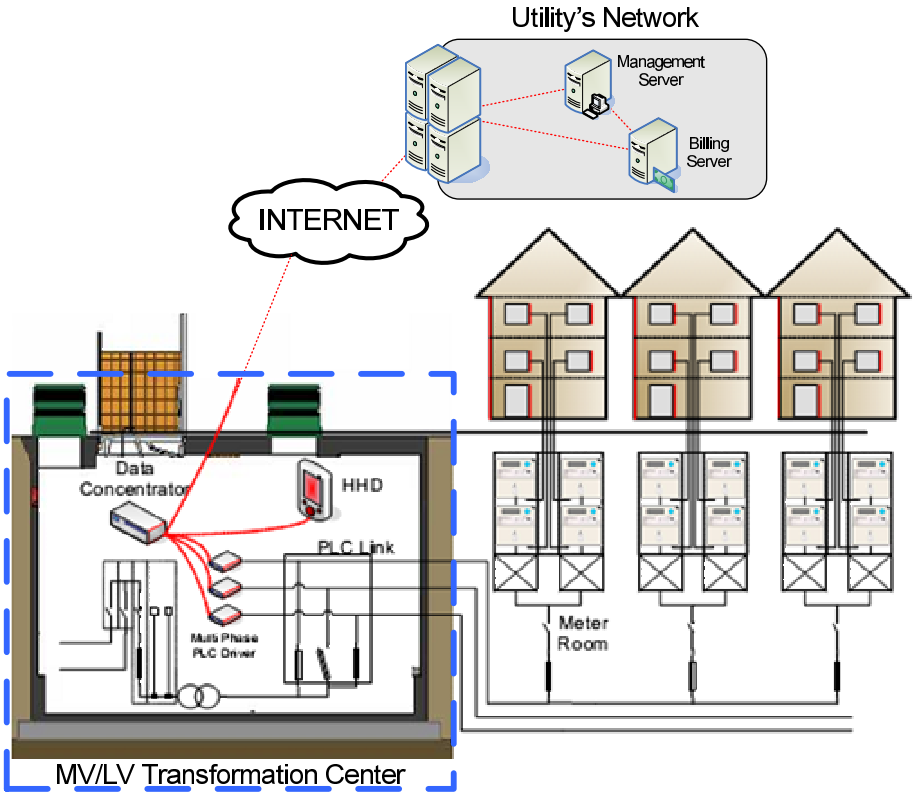

Figure 7.1: *Generic scenario for Advance Meter Infrastructure [10].*

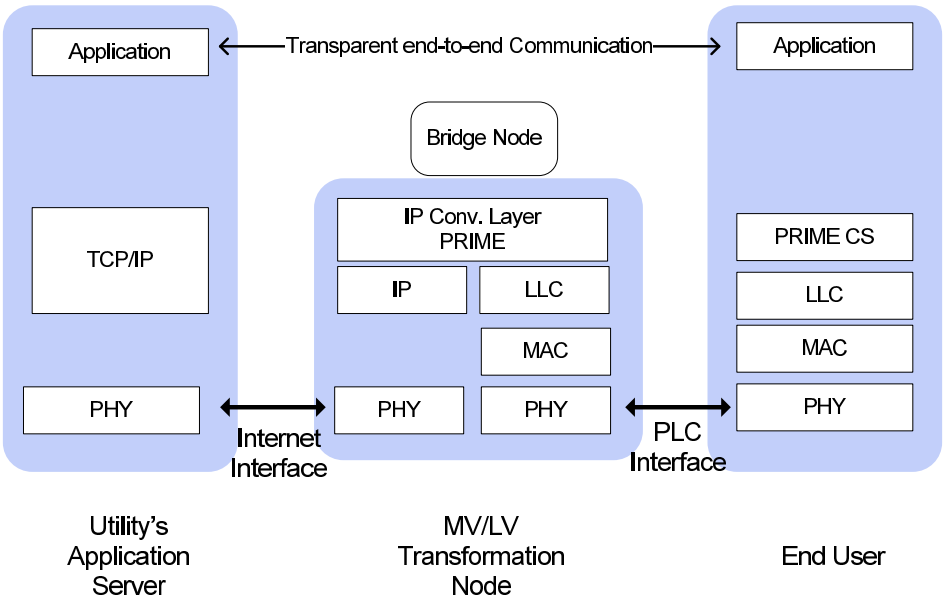

Figure 7.2: *Communication layer stack of the implemented scenario.*

As stated in [116], a simulation tool that could give a reference of the network's behaviour would be very useful for the AMI systems currently being deployed. Some examples of those systems are detailed in [117] and [12]. Knowing the expected communication latencies before hand will be very useful when gauging these AMI networks.

The present chapter details the proposed simulation framework to analyse network performances in such terms and provides simulation results for a general LV scenario.

After this introduction, Section 7.2 lists a survey of previous works in the literature that address the study of the performance of a LV PLC network. Section 7.3 details the main characteristics of the specification of PRIME's MAC layer so that the reader can have a general knowledge of its main features. Section 7.4 describes the architecture of the simulation framework developed and how each one of the communication processes is take into account. After this, results from a couple of cases of study under different channel environments are shown and discussed in Section 7.5. Finally, the chapter finishes underlining the main conclusions.

7.2 State of the art for PLC network simulators

There are several works in the literature which provide an analysis of the performance of PLC solutions [58, 85, 118] in different scenarios. However, although accurate, they only focus on the physical layer of the communication and their main output consists of bit error rate curves.

This section goes through the most up-to-date projects that have addressed the performance analysis of a PLC network.

In [119] an interesting analysis of the available throughput in multi-hop power lines is conducted. Nevertheless, no channel noise is added to the transmission, so no errors are modelled in the communication.

The study presented in [38] attempts to analyse the effective data rate achieved in a LV PLC network. However, the bit error rate in the communications is fixed for all nodes in the simulation independently of their position, which is not a realistic situation.

In [120], a method is proposed to abstract the PHY layer from the simulations by means of Packet Error Rate (PER) versus Signal to Noise Ratio (SNR) curves. However, when computing those curves, a fixed packet length is used, leading to a non realistic situation either. Results extracted from this study are later applied in [116] and [121] for a hardware-on-the-loop experiment with PRIME devices. This same tool is used in [122] to shown how useful this kind of simulations are to reproduce and improve the performance in real environments.

A similar study to the one presented in this paper is given by Zaballos et al. in [123]. They analyse the time required to read 100 meters over a 64 kbps channel. Packet loss probabilities are taken into account in simulations, however, no noise sources or channel attenuation are considered in the study.

Finally, a more theoretical approach is followed by Lazaropoulos in [39]. The link's capacity of a broad band PLC network is computed using Shannon's capacity equation for a medium and low voltage scenario in an additive white Gaussian noise channel. Additionally, the study is enhanced by analysing the optimal position of two repeaters in the network. Nevertheless, no networks effects (such as channel access, packet fragmentation, etc) are taken into account in the model.

The simulation framework proposed in this thesis models the physical, media access and logically link control layers of the LV PLC network. Effects like channel's transfer function, noise sources, transmission delays, fragmentation, connection set-up and medium access are taken into account in simulations to create a scenario as realistic as possible.

7.3 PRIME's data link layer

In order to provide to the reader a basic understanding of a PRIME's PLC network, the main feature of the data link layer (DLL) is briefly reviewed in this section. For a more detailed information, the reader is invited to access the G.9904 ITU-T recommendation where both PHY and DLL layers of PRIME are described [124]. In PRIME' standard, the data link layer is divided in two sublayers: the Medium Access (MAC) and the Logical Link Control (LLC).

With respect to the MAC sublayer, PRIME basically defines two kinds of nodes: **Base Node** and **Service Node**. The role of the Base Node (BN) is to manage the network resources and connections. Only one BN should exist per network and all the rest nodes must register to it in order to be able to transmit data. The BN is typically placed at the MV/LV transformer (See Figure 7.1).

Service Nodes (SN) act as leaves or branch points of the logical tree-structured network, as shown in Figure 7.3. The initial state of the SN is **Disconnected**. They may change to **Terminal** by registering to the network's BN and, only when they are in Terminal state, they can be promoted to **Switch**. While the objective of a node in Terminal state is to provide connectivity to the upper layers, Switch nodes are also responsible for forwarding traffic to and from other nodes. The evolution of the different states and the name of their processes are displayed in Figure 7.4.

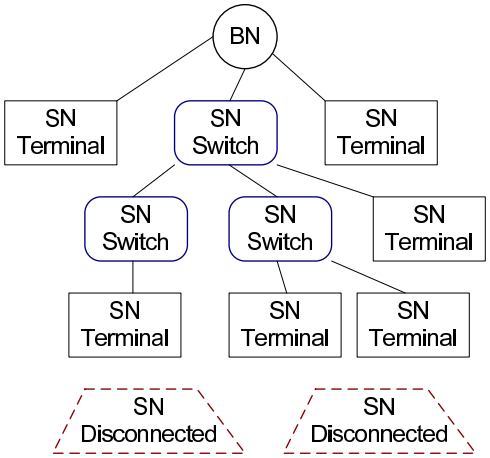

Figure 7.3: *Logical structure of a PRIME network.*

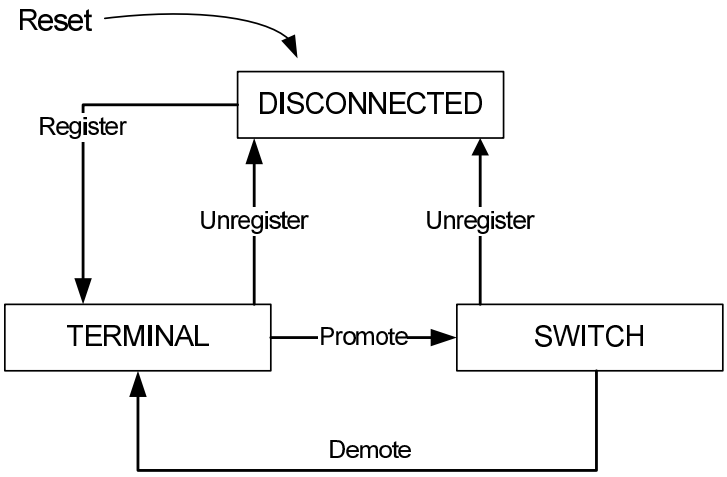

Figure 7.4: *Different states that a PRIME' SN node can reach.*

Additionally, the BN also performs network management functions. For instance, it polls all SN in the network to obtain an up-to-date state of all the devices that are connected to it. To do so, keep-alive messages are periodically sent. Another mission of the BN is to add some synchronism to the network so that every device has a chance to transmit, given the shared nature of the communication medium.

With respect to the LLC sublayer, it provides mechanisms to perform fragmentation and reassembling of the packets, flow control and automatic repeat request (ARQ) functions. The LLC sits on top of the MAC sublayer and below the convergence or application layer.

All these features and others that are considered as important for the understanding of a PRIME's network are described in the following subsections.

7.3.1 Addressing

Each PRIME node counts with several addresses, each one of them is used depending on the context of the communication.

All nodes have a universal 48-bits long MAC address formerly named as the EUI-48 address. Each manufacturer assigns this address during the assembling process and it can be used to universally identify a node.

Additionally, since each network has only one BN, the BN's EUI-48 is used to identify the whole network. This address is known as the Subnetwork Address (SNA).

Each Switch node also has a specific address within the network. This address is not hardcoded in the manufacturing process but it is assigned dynamically by the BN. This Switch address is known as Switch Identifier (SID) and is 8-bits long. A Switch is universally identified by its SID and the SNA of the networks where it exists. By default the SID of the BN is set to 0.

When a SN registers (i.e. promotes from Disconnected to Terminal), the BN provides him with a local address. This address is known as Local Node Identifier (LNID) and is 14-bits long. After this registration, all the exchanged messages between the SN and BN need to include the SN's LNID and the SID of the node they are registered through. This LNID-SID combination is also referred to as Node Identifier (NID) and identifies a node within a network. Once again, the LNID = 0 address is reserved for the BN.

Finally, during a connection establishment, another dedicated identifier is used to reference the current connection. It is a 9-bits long address known as Local Connection Identifier (LCID). The combination of NID and LCID is called Connection Identifier (CID) and identifies a connection within a network.

Previous structure is schematically summed-up in Figure 7.5.

To summarize, only EUI-48 addresses are pre-set in PRIME's nodes. The rest of them are dynamically assigned by the BN as the network evolves.

7.3.2 MAC frame structure and channel access

Given the physical characteristics of the power lines, the medium acts as a bus channel for all devices connected to it (i.e. the medium is shared and no more than one node can be transmitting at the same time). Another mission of the BN is to add some synchronism to the network so that every device has a chance to transmit. In order to do so, time is divided into slots known as MAC frames.

Additionally, MAC frames are divided into three sections: Beacons (BCN) period, where information about the network is transmitted; Shared Contention Period (SCP), where all nodes in the network contend to access the channel; and Contention Free Period

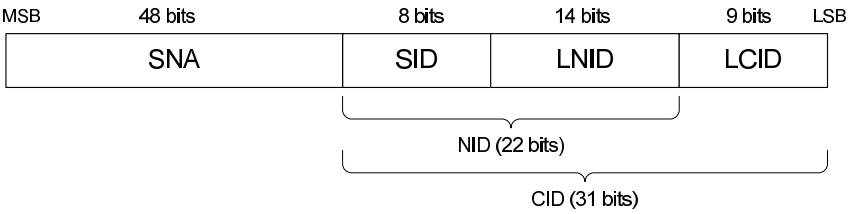

Figure 7.5: *Address structure in PRIME networks.*

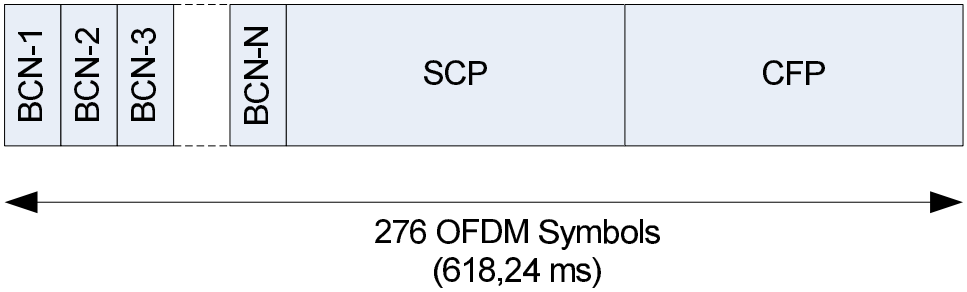

Figure 7.6: *MAC Frame scheme.*

(CFP), where only nodes which previously reserved a dedicated transmission time can use the channel. Moreover, Beacon frames can only be transmitted by the BN and Switches existing in the network.

The length of each MAC frame is constant and equal to 276 OFDM symbols (i.e. 618.24 ms). This value is referred in the standard with variable *MACFrameLength*. The length of the SCP and CFP varies dynamically depending on the network needs and their duration is specified in the beacon's information so that every device is synchronized.

The structure of the three period that a MAC frame consists of is shown in Figure 7.6. In the following, a more detailed description of each one of them is done.

7.3.2.1 Beacon period

Each instant of time when a Beacon Packet Data Unit (BPDU) is transmitted is referred to as beacon-slot. All beacon-slots are placed at the beginning of a MAC frame, as Figure 7.6 shows. The first one of the slots is reserved for the BN's beacon. The rest of the slots are assigned to the Switches present in the network. This assignation is done by the BN during the promotion process.

Among others, the information present in each BPDU is intended for network synchronization's purposes. It includes the number of beacon-slots that the current MAC frame contains (so that all nodes know when the SCP period starts, and they can contend for the channel access) and the BN and Switches' addresses (so that all nodes know who to contact in the registration process).

More details about the length and structure of a BPDU are given in Appendix D.

7.3.2.2 Shared contention period

As mentioned before, the Shared Contention Period is a time-slot where all devices in the network contend to access the channel in order to transmit. It starts immediately after the last BPDU's transmission is finished. The length of the SCP may vary from frame to frame depending on the number of BPDU being transmitted. However, its value cannot be lower than *MACMinSCPLength*, set to 64 OFDM symbols (i.e. 143.36 ms).

Since collisions are likely to happen during this period, a Channel Sense Multiple Access - Collision Avoidance (CSMA-CA) mechanism is used. The CSMA-CA algorithm implemented in PRIME's devices is described in Figure 7.7. The algorithm starts with a random back-off time which depends on the message's priority. The *rand_back_off* term in Figure 7.7 is computed with:

$$rand\_back\_off = min(2^{\text{priority}+\text{txAttempts}} + 1, \text{macSCPLength}/2) \tag{7.1}$$

Before the back-off period starts, the device must be sure that the transmitted message can fit into the remaining MAC frame, otherwise the transmission must be postponed to the next one.

After every completion of a *rand_back_off*, the channel is sensed. Channel must be sensed as idle for *macSCPChSenseCount* times before a transmission is made. Every time the channel is sensed as busy, the variable *txAttempts* is incremented. In case the channel is sensed as busy for a number of times equal to *macSCPMaxTxAttempts*, the current transmission is aborted.

The default value for all previous parameters is stated in the standard [124], however, their final values are left open for specific implementations.

7.3.2.3 Contention free period

In addition to the shared contention period, all devices have the possibility to request to the BN for a Contetion Free Period (CFP) to transmit information without contending for the channel. If no request is done, the CFP is left empty and the MAC frame only consists of the BPDUs and the SCP.

In case a CFP is requested from a SN which is not directly connected to the BN (i.e. it is connected through a Switch), it is the BN's duty to allocate a CFP for all the Switches that are in the same branch of the network. This way, the whole communication path counts with an effective period of time without any collisions.

BN's criteria to accept CFP requests from the SNs is not specified in the standard and it is left open for concrete implementations.

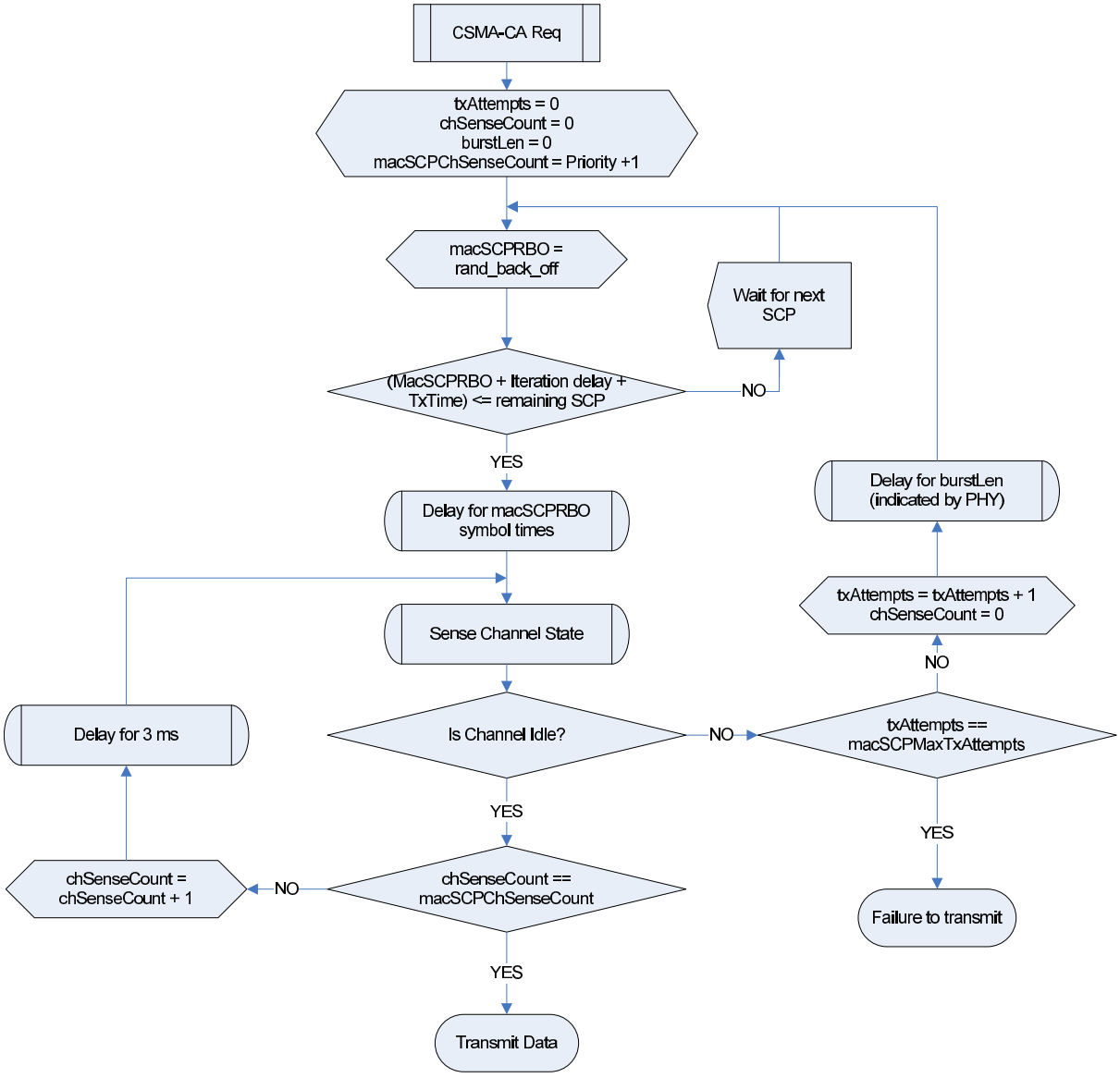

Figure 7.7: *CSMA-CA flow chart.*

Figure 7.8: *Generic scheme of the a MAC frame. Dashed lines stand for optional parts.*

7.3.2.4 MAC PDU structure

A PRIME's MAC frame may consist of several fragments of information depending on their purpose. As shown in Figure 7.8, the first part of a MAC frame is known as MAC Header and determines the information encapsulated in the following fields. Depending on its type it can be a Beacon PDU, a Promotion Needed PDU or Generic MAC header containing a generic packet. These three types are briefly described in the following:

- **Beacon PDU**. It can only be sent by the BN or a Switch node. Its purpose is to publish the addresses needed in the registration process (See Appnedix E). It also includes information needed for the network synchronisation. This kind of frames are identified with the HDR.HT field set to 2.

- **Promotion Needed PDU**. It is intended to be sent by SNs which do not receive beacon messages with enough power to interpret the encapsulated information. Whenever any of the SN in Terminal state receives a Promotion Needed (PRN) PDU, it should request to the BN for a Switch promotion. If the promotion is accepted, the new Switch would propagate the beacons to the disconnected node so that it can register (See Appendix E). This kind of frames are identified with the HDR.HT field set to 1.

- **Generic MAC PDU**. This kind of frame can be sent by all nodes in the PLC network and is intended for the rest of scenarios where Beacons and Promotion Needed PDU do not apply. These frames are identified with the HDR.HT field set to 0 and are subdivided in Control and Data packets to manage the network and transmit information respectively:

  - MAC Control Packets. This kind of packets fulfils the needs for sending control signalling between the BN to the Switches and SN and vice versa (to handle the registration process for instance). There are several types of control messages, each one of them is coded in the PKT.CTYPE field. MAC Control packets are identified with the PKT.C field set to 1.
  - MAC Data Packets. This kind of packets is used to encapsulate PDUs from higher layers. MAC Data packets are identified with the PKT.C field set to 0.

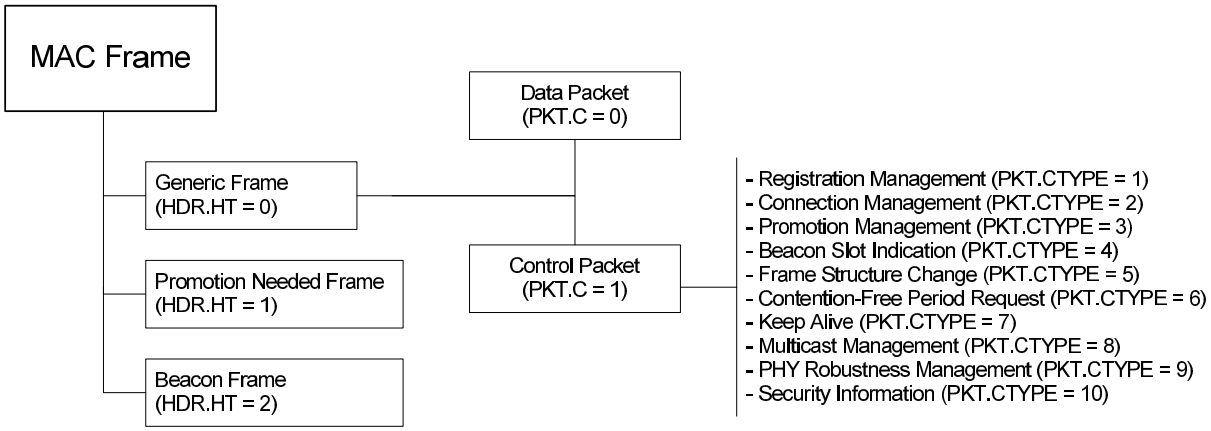

Figure 7.9: *MAC type of messages' hierarchy. Field's description is detailed in Appendix D.*

This hierarchy of the MAC frame is schematically shown in Figure 7.9, and all the information regarding the specific fields and length of each type of GPDU is detailed in Appendix D.

7.3.3 Switches and switching

Due to the severe attenuation suffered by the PLC channel, the BN cannot communicate directly with all nodes in the network. Because of this, some of the SN may promote to the state known as Switch. Should this occur, it is the Switches' mission to forward uplink and downlink messages from and to the part of the network that is not directly reachable by the BN. Additionally, switches are not simple repeaters, they only forward the traffic that comes from or goes to one of the nodes within their hierarchy. The rest of the traffic is directly discarded. A detailed description of the promotion process of a SN to become Switch is provided in Appendix E.

7.3.3.1 Switching process

In order to strictly forward traffic to and from nodes in its same branch, each switch node maintains a list of all the SNs that are connected to the network through it. Having this information in an up-to-date switching table is sufficient to implement the switching process.

At the beginning, switches star with empty tables. The switching table is updated with the promotion, demotion or registration messages in the network. In the following, conditions that must be met in order to switch a message are described.

For a downlink packet, switching must be done if any of the following conditions occurs:

- The destination of the packet is connected to the network through this switch.

- It is a broadcasting destination and this packet was sent by a node registered through this switch.

For an uplink packet, switching must be done if any of the following conditions occurs:

- The origin of the packet is connected to the network through this switch.
- It is a broadcasting destination and this packet was sent by a node connected to the network through this switch.

Following this criteria, the switching process is achieved without communication loops.

7.4 Simulation framework

As mentioned in the introduction of this chapter, one of the key features of the simulation framework proposed in this thesis is the binding of physical power line channel effects together with network's behaviour. To accomplish this objective, the simulation framework displayed in Figure 7.10 has been implemented.

As it can be seen in the figure, all effects related to the physical layer (PHY) of the communications have been taken into account via Matlab simulations; this includes attenuation and noise effects described in Chapter 3. Analogously, all the functionality defined by the PRIME's MAC and LLC layers have also been developed with OMNeT++ together with the application layer, implementing a Device Language Message Specification / Companion Specification for Energy Metering (DLMS/COSEM) protocol.

As seen in Figure 7.10, the interface between Matlab and OMNeT++'s workspace is the BER value and communication mode for a given transmitted signal. Matlab models the transceiver's behaviour in terms of BER as a function of the SNR and the communication mode. Therefore, when a message is generated in a node, it is transmitted with the maximum power defined in PRIME standard (-3 dBW). As the packet reaches all nodes in the network, its power is attenuated. Attenuation for each pair of nodes (transmitter and receiver) are pre-computed by Matlab using the transmission lines techniques described in Section 3.3.

When a message is received, the SNR (computed using the received signal power and the noise level of the current scenario) and the communication mode used in the transmission are extracted from the incoming packet. This two parameters are then used in the curves shown in Figure 7.11 (pre-stored in OMNeT++'s memory) to compute the BER for the received message. Depending on the BER and the message's length for the current transmission, the packet may be correctly received or dropped due to errors.

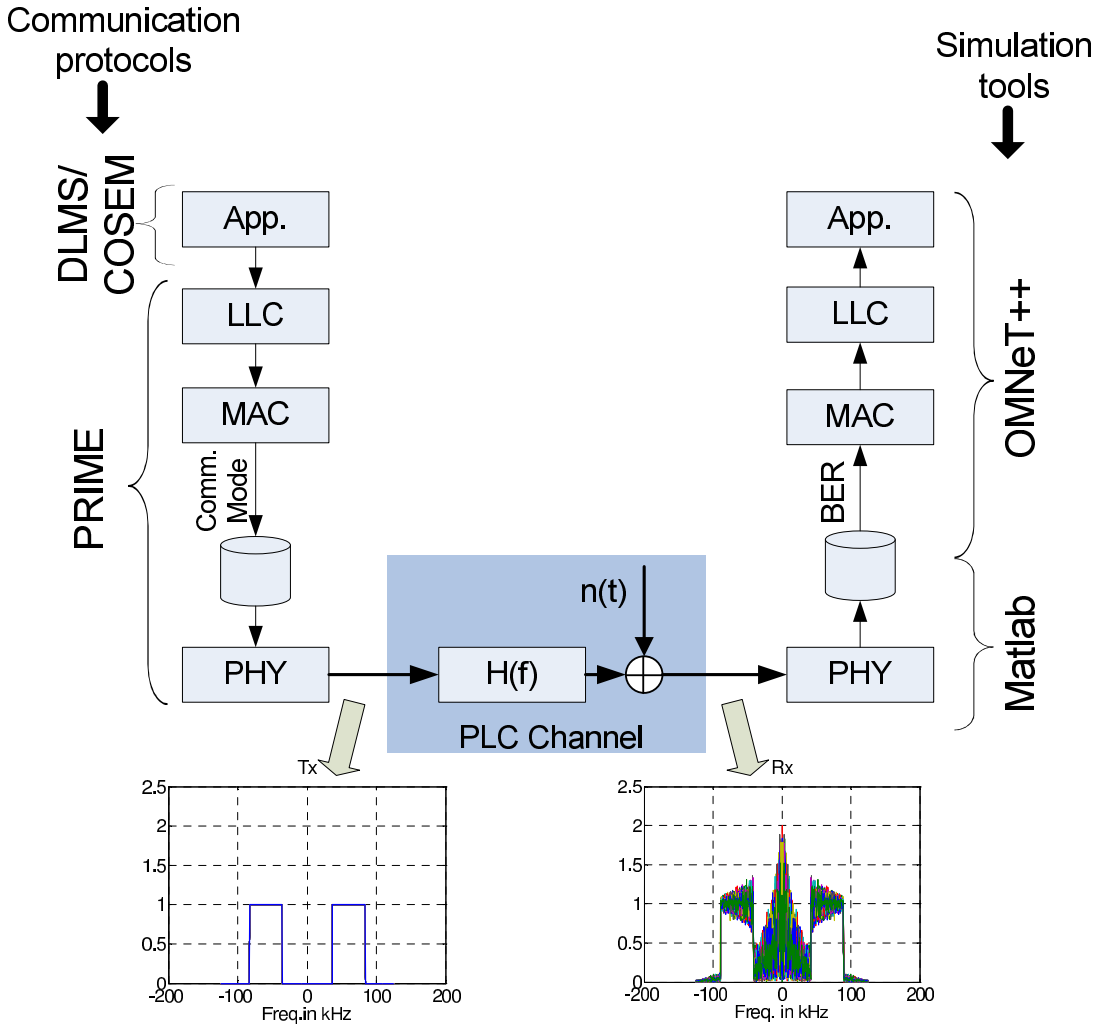

Figure 7.10: *Scheme of the simulation framework.*

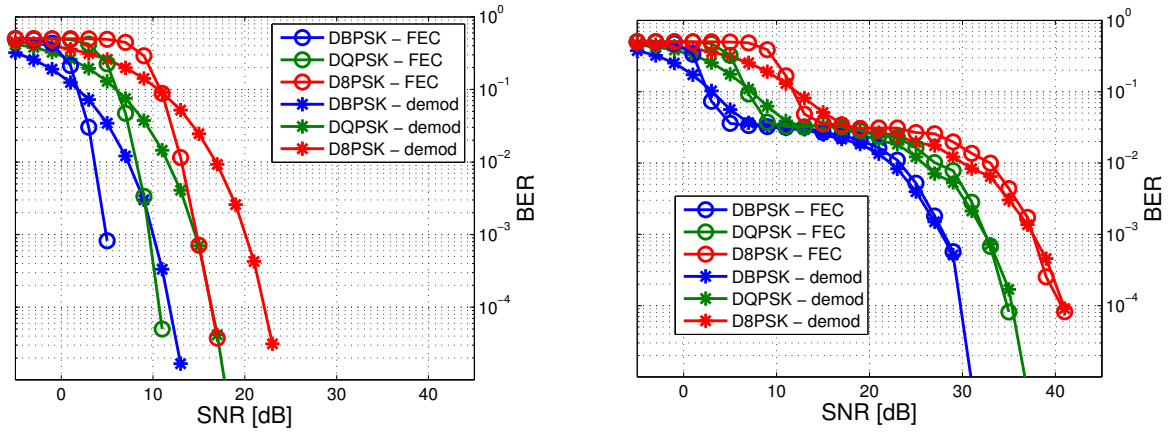

(a) **(b)**

Figure 7.11: *PRIME's performance in the presence of background and impulsive noise. Figure replicated from Chapter 4. (a) Background noise. (b) Impulsive Noise.*

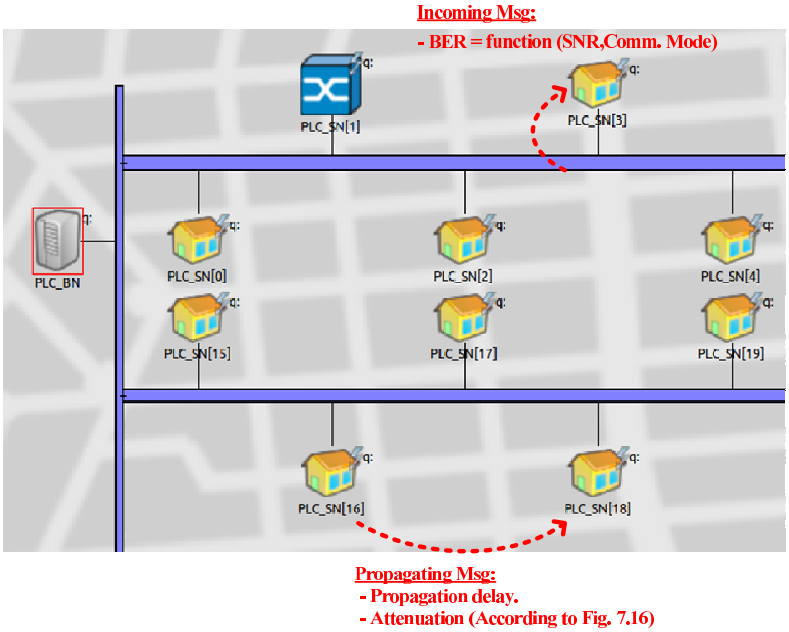

Figure 7.12: *Scheme of the communications effects taken into account in OMNeT++.*

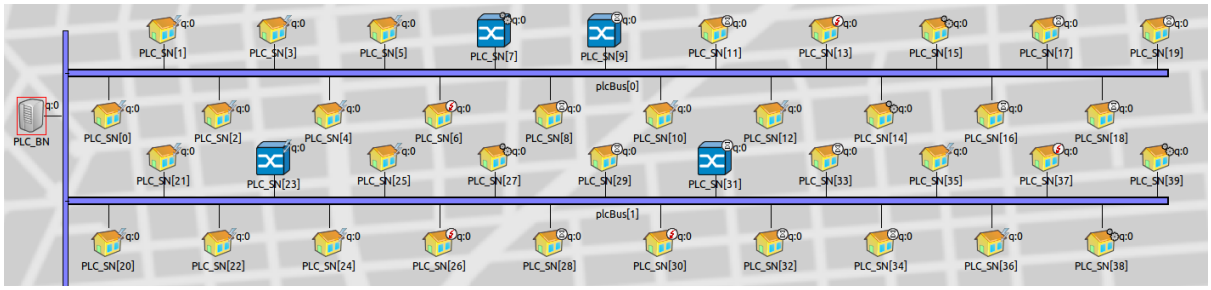

Figure 7.13: *Example of a two-branch simulation network implemented with OMNeT++.*

Moreover, the implementation also takes into account propagation delays between nodes. Delays are computed depending on the wires physical characteristics (which gives the propagation speed), the message lengths and the distance between nodes. All these effects are schematically shown in Figure 7.12.

Additionally, Figure 7.13 shows a screen-shot of an example PLC scenario built with the developed framework. It represents a two-branch LV network with one BN and twenty SNs per branch. Service nodes in Terminal state are represented by a house icon whereas those which were promoted to Switch are represented by a blue box with a white cross. It is also worth noticing the small icon that all SN have on their upper right corner, which represents the communication mode that each SN is currently using.

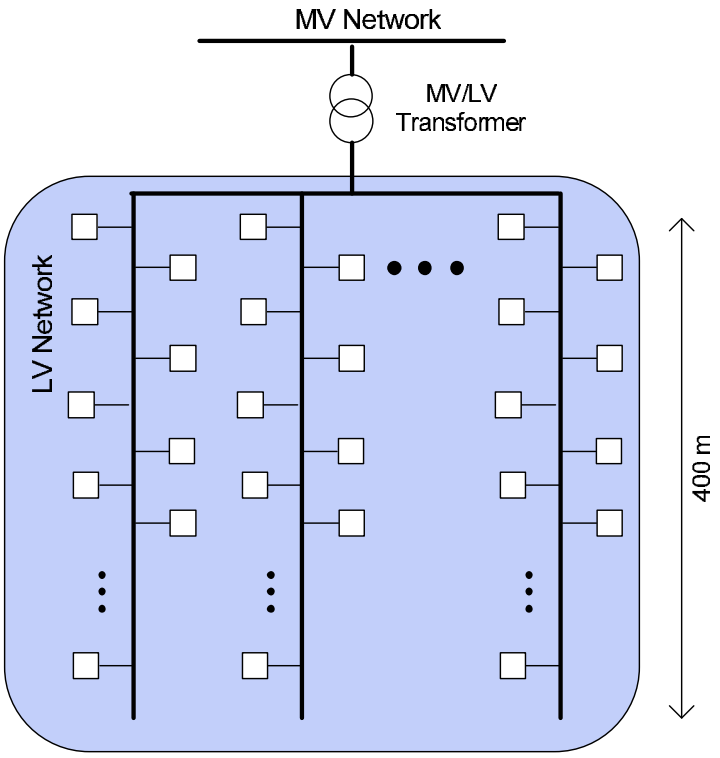

Figure 7.14: *Standard European LV distribution network. Adapted from [6].*

7.5 Performance results

This section describes the analysis carried out using the implemented framework. The case of study under analysis focuses on measuring communication's latencies between nodes in a LV PLC network. In concrete, as previously done in [123], the main output extracted from simulations is the time required by a BN to poll all SN in the network.

With respect to the physical topology of the LV network, Figure 7.14 shows a general scenario for a European's layout (taken from [6]). The European LV distribution network consists of a MV/LV transformer which serves one cell. As stated in [6], this cell gathers a number of distribution lines or branches where users are connected to. In urban environments these branches can be around 400 m long [9] and may have around 30 users per branch. Typically, there are 10 branches in the whole network, meaning that each transformer serves around 300 subscribers.

The following three subsections describe several experiments carried out in order to gain some insights of the network's performance. Section 7.5.1 conceptually describe the process to poll one SN. There, the connection mechanism implemented by PRIME is described for a better understanding of the reader. In Section 7.5.2, a more realistic experiment is carried out since simulations take into account all meters in the network. Experiments are done assuming different types of channel conditions (background and

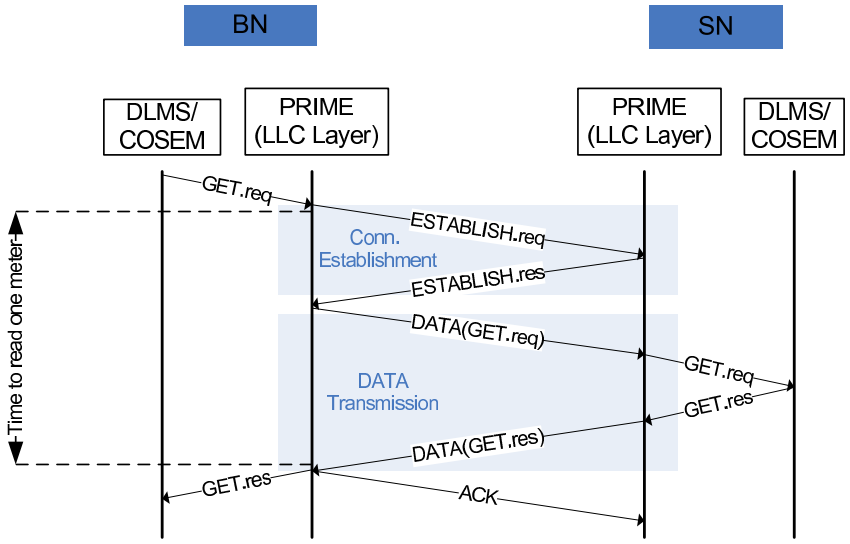

Figure 7.15: *DLMS/COSEM Data transmission diagram.*

impulsive noise) and different polling strategies (simultaneous and sequential). Finally, Section 7.5.3 analyses how the position of a Switch node in the network influences the overall system's performance.

7.5.1 Time to read one meter

The process required to read one meter, in accordance with the communication layer stack implemented (see Figure 7.10), is shown in Figure 7.15. Since PRIME is a connection-oriented protocol, a connection has to be established before sending the application request. The ESTABLISH.req message is triggered by the GET.req received from the Application layer, which implement a DLMS/COSEM protocol. The requested entity answers the ESTABLISH.req with the corresponding ESTABLISH.res to accept the connection.

Once the connection is established, application data is sent encapsulated in a LLC-layer frame (DATA(GET.req) message in Figure 7.15). The requested data values are included in a GET.res message by the SN. After the reception of a data frame at the BN, an acknowledgement message (ACK) is sent back to the transmitter to confirm the correct reception.

Given this message exchange, the time to read one meter (indicated in Figure 7.15) can be computed with:

$$T_{read1Meter} = \frac{ESTABLISH.req + ESTABLISH.res}{V_{TX_{CONTROL}}} + \\ + \frac{GET.req + GET.res + 2 \cdot LLC_{HEADER}}{V_{TX_{DATA}}} \tag{7.2}$$

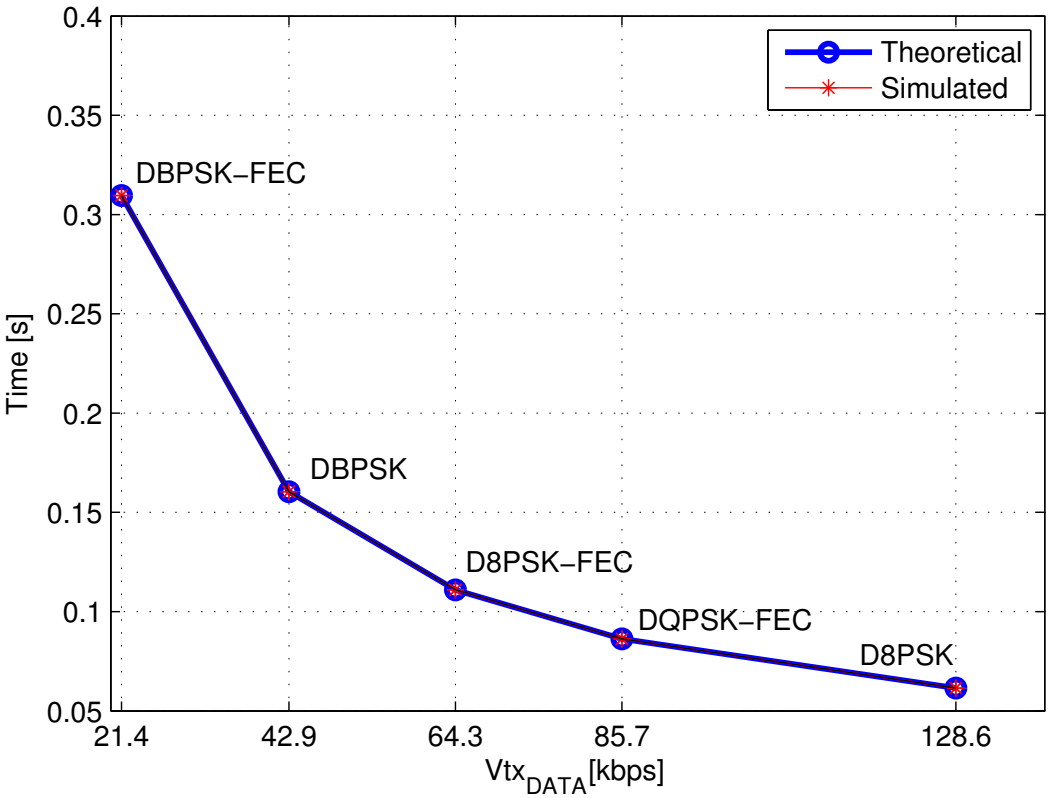

Figure 7.16: *Time required to read one meter for the different communication modes in PRIME. Theoretical versus simulated.*

where numerators stand for the bit length of each one of the messages and the denominators are the corresponding transmission speeds. It is worth mentioning that not all messages may be transmitted at the same speed. As defined in PRIME standard, all control messages (both the establish request and response in this case) must be transmitted using the most robust communication mode (DBPSK-FEC ON), which means 21.4 kbps. Frames containing data, however, can be sent using the most suitable communication mode given the channel conditions. Transmission speeds in those cases are described in Table 2.1.

Figure 7.16 shows the calculated and simulated time required to read one meter using all available communication modes. In this concrete simulation, additional processes, such as the back-off period before accessing the bus, have been omitted to facilitate comparison with Equation 7.2.

7.5.2 Time to read several meters

This section presents a study of the time required to read all meters in a network using the implemented framework. Results show this time as a function of the number of branches present in the network. In addition, this metric is compared with a 15 minutes reference, as suggested in [125].

In a real-life scenario, the network will contain messages from and to all nodes simultaneously. However, results cannot be extrapolated from a one-meter to a several-meter scenario for different reasons. One of them is, as explained before, the medium acts as a bus where all devices contend with each other for transmitting. This, on occasions, leads to collisions. The analytical study of the performance in such scenario is complex, therefore, simulations represent a more affordable approach.

In addition of the collision effect modelled by the simulations, the presented framework also takes into account the attenuation due to the propagation in the power lines. Figure 7.17 shows the values for each combination of transmitter and receiver nodes in one of the branches of a network such as the one in Figure 7.14. This computation has been carried out following the process described in Section 3.3.1. As it could be expected, attenuation grows when nodes are farther away from each other.

Two polling strategies are also studied: **simultaneous** and **sequential** polling. When using sequential polling, the BN waits for the response of the SN currently being polled before sending a new request. In the simultaneous case, the BN massively sends GET.req messages to all meters. The lengths of GET.req and GET.res messages are set to 254 and 144 bytes respectively in all simulations. The size of these messages would allow for a request for 22 measurement in a single message, which might be sufficient for any conventional application, as stated in [126].

Figure 7.18a shows the simulated times required to read all meters when using sequential polling. It can be seen that, in scenarios with up to five branches, the 15 minute threshold is only exceeded by a few outliers. Figure 7.18a shows how the time reference is sometimes overtaken when the network is composed of six or more branches.

Simulation results for the simultaneous polling experiment are shown in Figure 7.18b. In this case, the time required to read all meters increases up quickly with the number of branches. The 15 minute time limit is now clearly exceeded when the network has five branches.

As mentioned in Chapter 3, the PLC channel may be also impaired by impulsive noise interference. The consequences in terms of physical communication performance were discussed in Chapter 4. To understand how impulsive noise affects the network performance, OMNeT++ simulations are fed with the BER/SNR curves shown in Figure 7.11. As it can be seen from a physical layer's perspective, a direct consequence of the

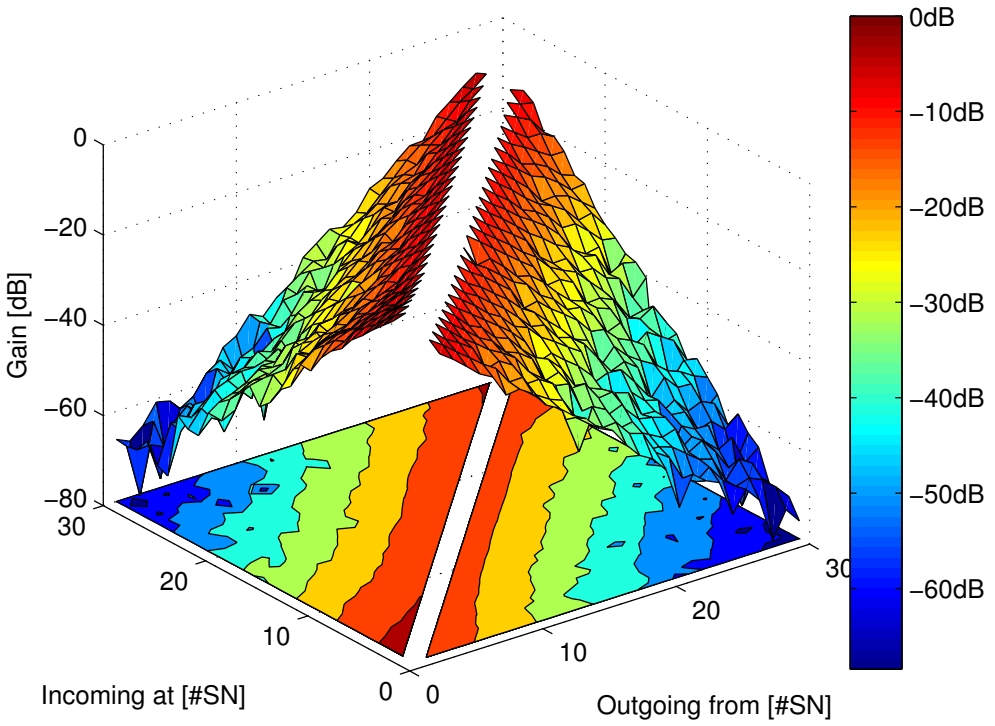

Figure 7.17: *Node to node attenuation for one branch.*

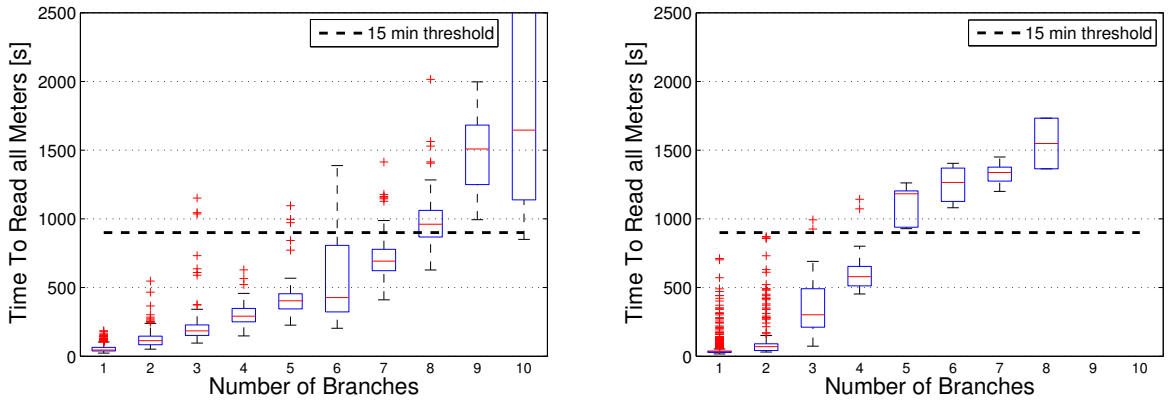

(a) **(b)**

Figure 7.18: *Time required to read all meters depending on the number of branches using sequential and simultaneous polling. (a) Sequential polling. (b) Simultaneous polling.*

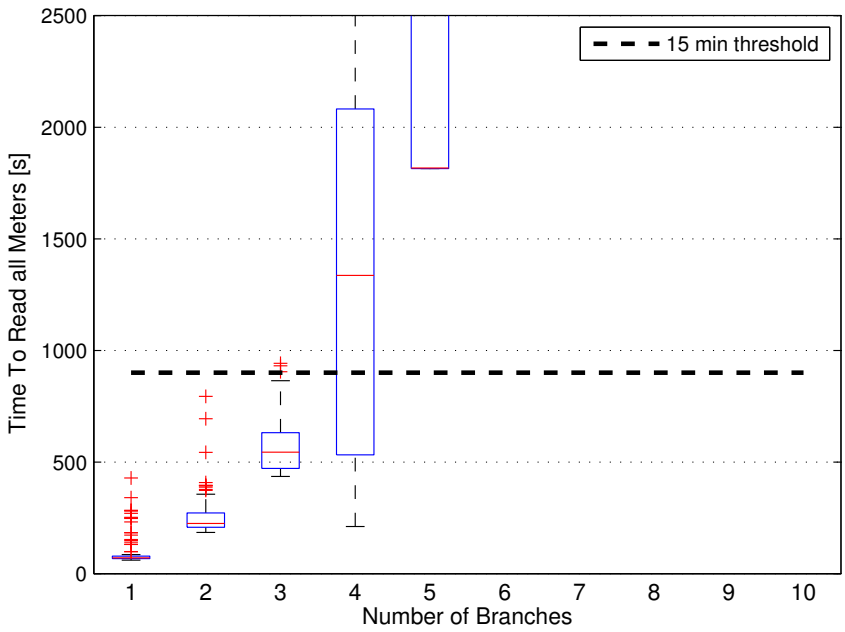

Figure 7.19: *Time required to read all meters depending on the number of branches using sequential polling in an impulsive noise environment.*

presence of impulsive noise is that nodes need a higher SNR to guarantee communications without errors. This is translated into a higher number of Switch nodes in the network, since the minimum received signal power is increased. This higher number of Switch nodes produces extra traffic due to re-transmissions and, therefore, the time required to read all meters is increased. Results are shown in Figure 7.19. When the network has six or more branches the amount of traffic is so high that the network cannot be set up, this is the reason why no latencies are plotted.

Figure 7.20 shows the median values of the Time To Read (TTR) all meters in the three analysed scenarios for a better comparison. It can clearly be seen how polling all nodes sequentially results in a better performance. Additionally, the figure shows how the dominant effect in the performance is the presence of impulsive noise in the channel.

Nevertheless, this poor performance in an impulsive noise environment can be improved by means of the techniques proposed in Chapter 6. Figure 7.21 includes the TTR as a function of the number of branches in the network when using compressed sensing with an original PRIME's frequency allocation and when using frequencies following a difference set approach. The improvement observed in Figure 6.11a in terms of SNR gain is now translated into a lower TTR. In addition, the use of difference set-based compressed sensing (Figure 6.11b) produces a result similar as the one with no impulsive noise present in the channel, as it could be expected.

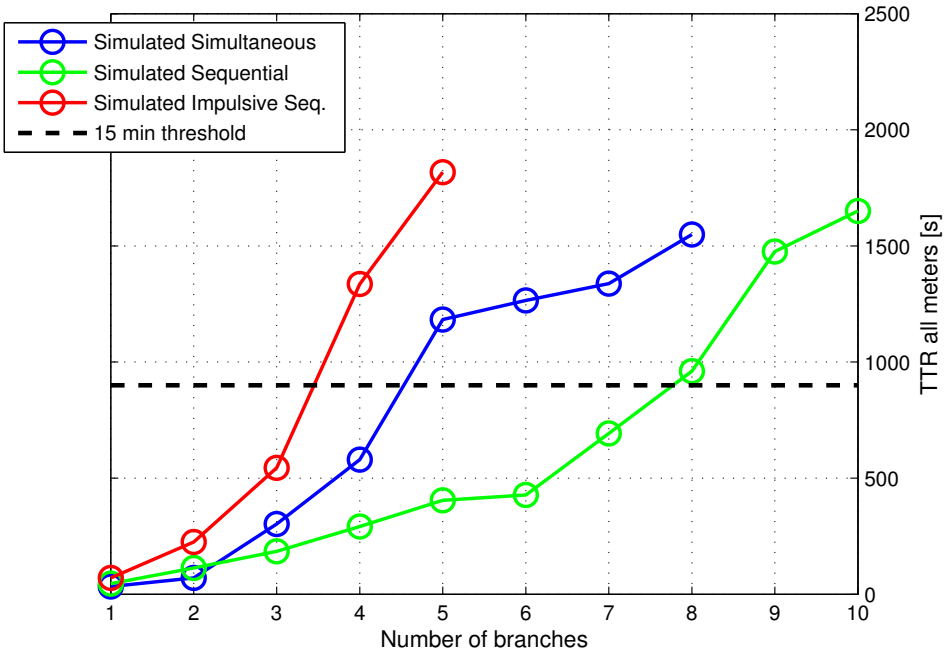

Figure 7.20: *Comparison of the time required to read all meters as a function of the number of branches. Median Values.*

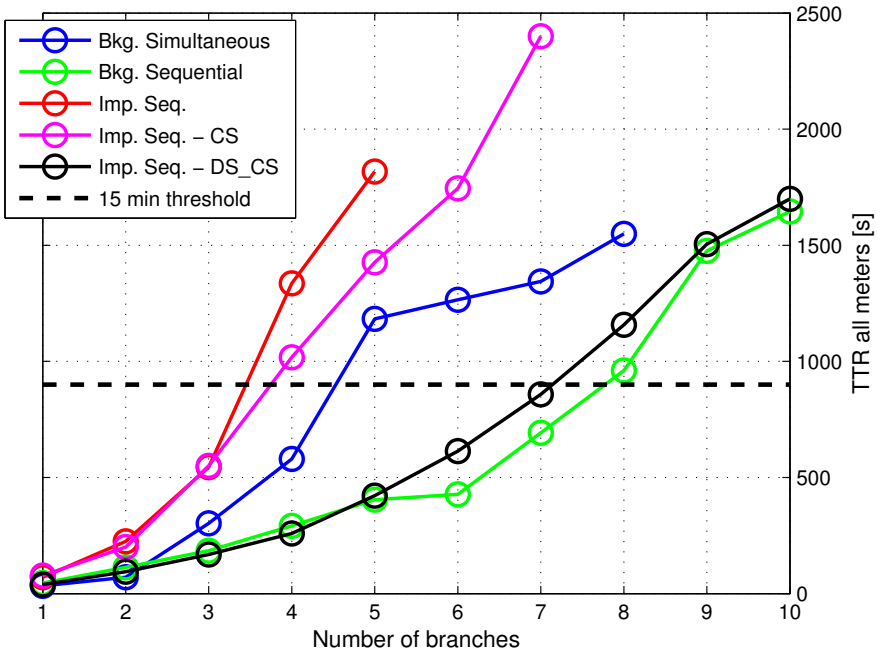

Figure 7.21: *Time required to read all meters with different kind of noise scenarios and cancellation methods. Median values.*

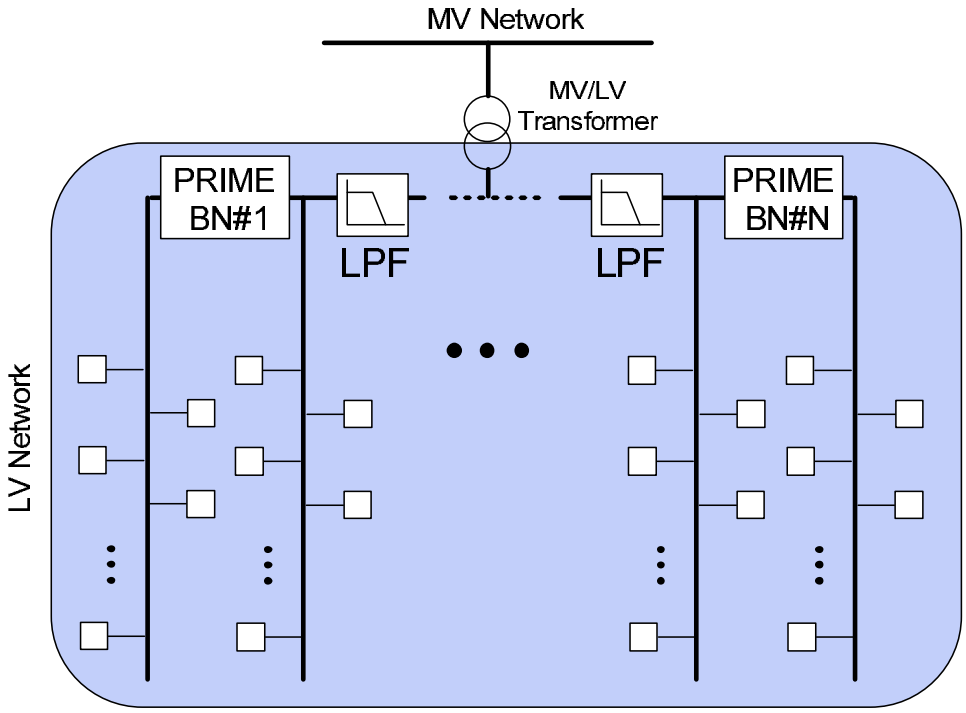

Figure 7.22: *Proposed topology in order to allow all meters in the network to be polled.*

Finally, simulations carried out reveal that a scenario with a low voltage network of ten branches cannot be managed with PRIME's PLC technology. A simple solution to enable PRIME's technology in European environments with such a high number of branches would have to use several BN's per network. This could be achieved by creating several subnetworks. Each of which would need to be isolated from the rest in order to prevent interference from PRIME's signals. A simple low-pass filter (LPF) would allow the transmission of power while blocking the high frequency communication. A scheme for this idea is shown in Figure 7.22.

With the proposed scheme, and looking at results shown in Figure 7.21, only one LPF would be needed, since a 5-branch network can already work below the 15 minutes threshold. This could be done for either a background noise scenario or for an impulsive noise scenario which includes the difference set-based compressed sensing improvement proposed in this thesis.

7.5.3 Switch location

As briefly described in Section 7.3, any SN may be promoted to Switch if the transmitted signal does not reach certain nodes. Should this occur, the new Switch will also transmit beacons to broadcast its information. It is the switch's function to re-transmit all messages from the SN that, due to attenuation, may not reach the BN with enough power, and vice-versa. All SN that use the Switch to re-transmit their messages may

also use the different communication modes defined by PRIME. Thus, those SN which are closer to the Switch will be able to communicate with it faster. In the same way, depending on how far the Switch is from the BN, it will be capable of using a faster or slower communication mode for the switched messages.

The promotion of a SN from Terminal to Switch is decided by the BN. However, the criteria used to choose which SN are promoted are not detailed in PRIME' specification. Nevertheless, it is reasonable to assume that the choice of SN will affect the performance of the overall network.

The experiment proposed in this subsection aims to study how the position of a Switch node in a PLC network influences its overall performance.

The experiment consists of studying the performance of a PLC network composed of a single branch of 400 m with 30 nodes. Several simulations have been run allowing only the existence of one Switch in the network. On each simulation, a node placed at different positions is forced to promote to Switch. In the first one, the Switch node is located at the minimum distance from the BN, and the last one at the maximum distance.

In addition, all simulations compute the time required to read all meters in the network in a sequential manner.

Figure 7.23 shows the result obtained from the experiment when the channel is impaired by background noise. The left axis represents the time required to read all meters, whereas the right axis represents the transmission speed used by the Switch when transmitting data packets to the BN. Abscissas represent which of the 30 SN has been promoted to Switch.

As it might be expected, as the Switch node is moved farther away from the BN (placed at position 0), it needs to change to a more robust (thus slower) communication mode to guarantee transmissions without errors. With respect to the time required to read all meters, it can be seen in Figure 7.23 that, when the Switch is placed too close to the BN, no value is shown. The reason for this is that beacons sent by both the BN and Switch do not reach nodes placed at the very end of the network with enough power. Hence, those nodes can neither register nor, obviously, be read. The same thing occurs when the Switch is placed too far from the BN. In this case, the Switch itself does not receive BN's beacons with enough power to register.

Figure 7.23 shows how, for the rest of the Switch's positions, the time required to read all nodes is minimized at certain locations. When zooming in on those positions (Figure 7.24), it can be seen how there is a small variation in performance. It might be expected that the best performance is achieved when the Switch uses a higher transmission speed when talking to the BN; however, in this case it communicates with the rest of the SN with a lower bit rate (since they are placed farther away). Therefore, not only the

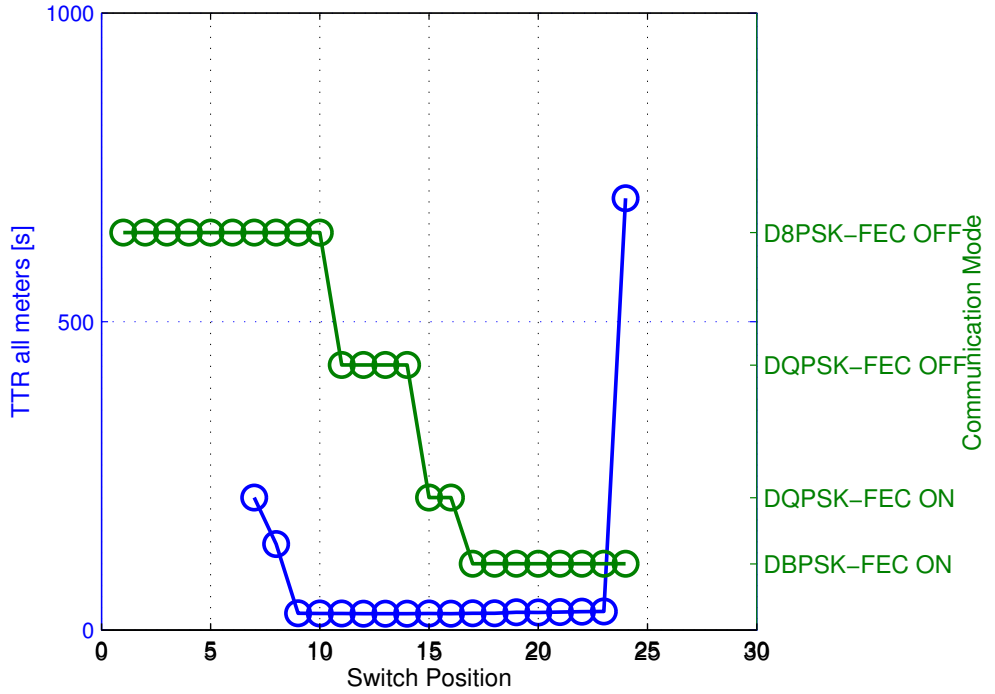

Figure 7.23: *Blue curve: time to read all meters depending on the Switch's position. Green curve: transmission speed achieved by the Switch Node when communicating to the BN.*

position of the Switch with respect to the BN effects the overall network's performance but the communication mode used to communicate with the farther placed SN also plays an important role.

This experiment shows that placing the Switch node in positions between 9 and 21 is sufficient to considerably improve the network's performance. Fine-tuning between these positions does not significantly decrease the required time, as seen in Figure 7.24.

Unfortunately, in the case of impulsive noise, the same kind of results are more complex to generate since more than one Switch is needed to interconnect all SN to the BN, as will be explained in the following.

In all simulations, PRIME's maximum transmitted power is set to -3 dBW (27 dBm) [124]. Additionally, the noise's power present in the channel is computed by integrating its power spectrum density between PRIME's transmission frequencies, what results in -54.3 dBW (-24.3 dBm).

The aim of the following analysis is to compute the maximum attenuation that two PRIME nodes can bare while transmitting without errors. Since BPSK - FEC ON is the most robust communication mode available in PRIME, it will be assumed that devices will use this mode when attenuation is high. BPSK - FEC ON mode requires a minimum SNR of 30 dB (See Figure 7.11b) to achieve zero BER in an impulsive noise environment.

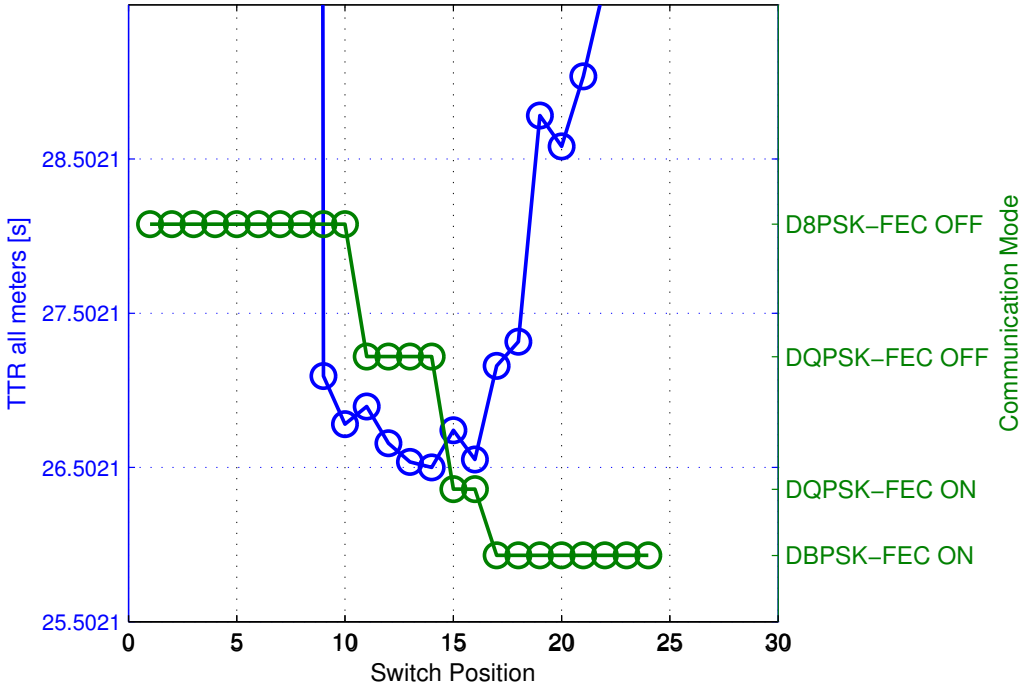

Figure 7.24: *Zoom of the time to read all meters as shown in Figure 7.23.*

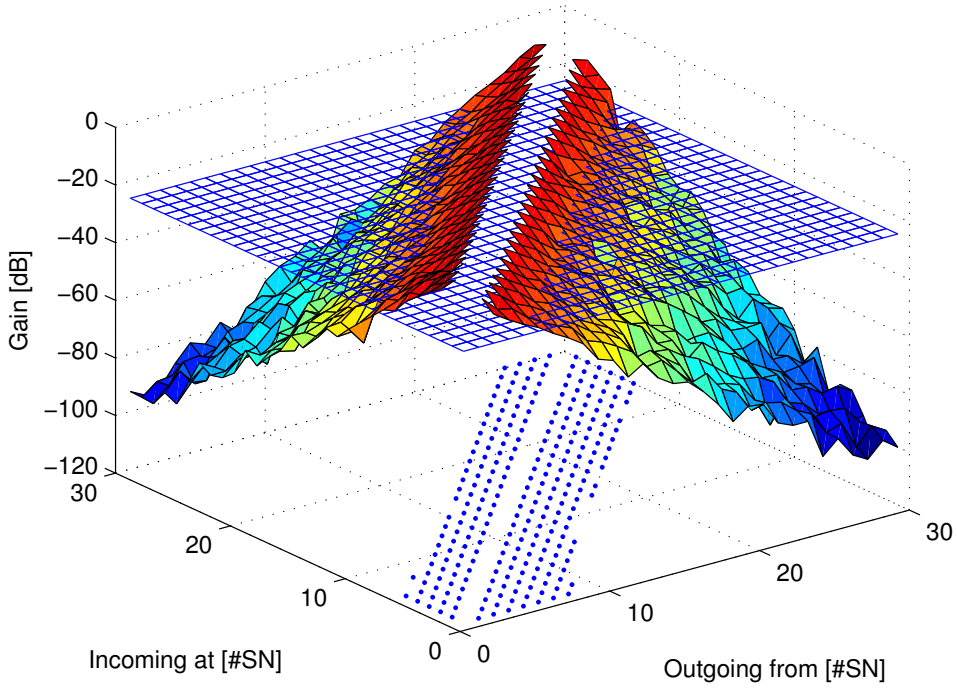

Figure 7.25: *Maximum attenuation for LOS in impulsive noise environment.*

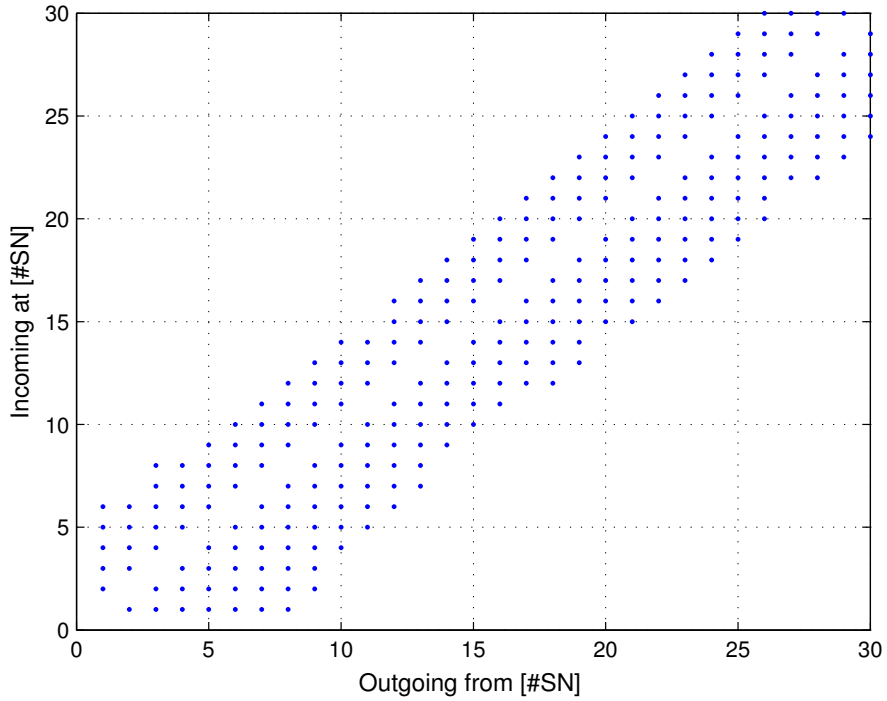

Figure 7.26: *Line Of Sight for SN's in impulsive environment.*

SNR is computed with expression:

$$SNR = Pot_{RX} - Pot_{noise} = Pot_{TX} - L - Pot_{noise} \tag{7.3}$$

where L stands for the mean channel attenuation and Pot_{TX}, Pot_{RX} and Pot_{noise} stand for transmitted, received and noise power respectively. All values are in decibels.

This allows for the computation of the maximum attenuation value so that two nodes can communicate without errors. This is elaborated in Equation 7.4:

$$L_{max} \leq Pot_{TX} - SNR_{min} - Pot_{noise} = -3 - 30 - (-54.3) = 21.3dB \tag{7.4}$$

The consequences of this for the communications of all nodes in the network can be seen in Figure 7.25. The roof-shaped figure represents the gain imposed by the channel when transmitting from one node ('Outgoing From(#BN)' axis) and receiving in another ('Incoming at(#BN)' axis).

The plane placed at −21.3dB shown in Figure 7.25 represents the maximum attenuation for direct communication, as derived previously in Equation 7.4. In principle, all nodes with a gain above this plane have 'Line Of Sight' (LOS). In order to clarify the figure, nodes with LOS are additionally marked with a blue dot on the base plane of the figure. This is more clearly shown in Figure 7.26. Obviously, there is an empty diagonal

that would represent transmitting and receiving in the same node. Using these dots, it can be seen how there is no node able to 'see' the base node and the last node in the network at the same time. In case that node existed, it would be a candidate for Switch. Therefore, more than one Switch are needed in an impulsive noise scenario. Due to the higher complexity of this analysis it is proposed as a future line of work.

7.6 Conclusions

This chapter describes a proposed simulation framework for emulating the communications' performance in PLC networks. In contrast to other studies, simulations carried out take into account all processes and effects in the communication layer stack.

Physical effects perturbing transmission, such as the different types of noise sources and the attenuation suffered by the signal, were modelled by Matlab simulations. The output of these simulations is then applied, in the form of BER/SNR curves, to a network simulation framework implemented with OMNeT++. There, processes related to the network topology were modelled.

The simulation framework shows how physical phenomena taking place in the channel are translated into the application layer in terms of time required to read a given number of devices.

The benefit of the approach presented is that, due to the decoupling of the physical effects on the networking, changes in the channel conditions (different types of noise sources for instance) or in the PHY layer (new transceiver designs) can be easily included in the simulation framework. Moreover, this approach also allows for the testing of other applications that could use PLC as a communication medium (as the IEC 60870-5-104).

This simulation framework can result in an interesting tool for utilities when deploying their smart grid solutions using Power Line Communications, as it is argued in [116]. With the use of this tool, aspects such as the maximum number of subscribers per area, the expected communication latency or the polling frequency can be estimated.

Simulation results show that a typical European low voltage network cannot be completely polled using a single Base Node. Additionally, the time required to read all meters increases considerably when the PLC network is affected by impulsive noise. A proposed solution would be the isolation of a group of branches to create smaller sub-networks.

Moreover, a study has been carried out regarding the effects of the Switch position within the PLC network. The influence of the distance of the Switch with respect to the BN has been shown in a simple experimental network. According to the results there is a range of position where the performance is substantially improved. However, no great gain is achieved when fine-tuning in values within that range. Nevertheless,

PRIME specification does not detail the criteria for deciding which nodes are promoted to Switch. The existence of several levels of Switches deteriorates the communications performance, since more re-transmissions are required to deliver a message. The design of algorithm able to optimize this task is an interesting topic for a future study.

Chapter 8

Summary, conclusions, contributions and future work

8.1 Introduction

This last chapter summarizes all the contents and conclusions that have been developed in this thesis, lists all main contributions, and proposes future lines of work that are left open for further research.

The chapter is structured in four different sections. Section 8.2 provides a qualitative summary of all the topics that have been treated in this document. Section 8.3 explains the main conclusions that can be extracted from the whole document. Section 8.4 details the main contributions that have been generated as a result of the research work. Finally, Section 8.5 proposes new lines of work that could be addressed in order to continue with the knowledge developed in this thesis.

8.2 Summary

This thesis can be divided in three main parts. The first one provides a qualitative description of the main narrowband power line communication' solution that have emerged since 2008. In addition to this, a mathematical description of the channel model, used to emulate the transmission's conditions, is given. Chapters 2 and 3 address these two issues.

The second part of the thesis focuses on the evaluation of two of the standards that have been endorsed by the industry: PRIME and G3-PLC (Chapter 4). There, a special sensitivity of PRIME in impulsive noise environments was detected. This PRIME's weakness motivates the study of the current state of the art of techniques to cancel impulsive noise effects in OFDM-based systems (Chapter 5). In addition to this, a proposal is made in order to enhance the impulsive noise cancellation capabilities of compressed sensing

(Chapter 6). The proposed enhancement is based on the modification of the structure of the subcarriers used to transmit information. Thanks to this reordering, an almost complete impulsive noise cancellation is achieved.

The last part of this thesis focuses on the implementation of a simulation tool to replicate the performance of a low voltage narrowband power line communication systems from a network's perspective (Chapter 7). Using physical layer's results from previous chapters, a simulation framework has been developed that implements PRIME's data link layer together with a generic application layer. Afterwards, this tool is used to simulate the behaviour of an Advanced Meter Infrastructure (AMI) system. Simulations are aimed to obtain the expected number of meters that can be read in a given period of time. This type of metric is in grand interest to the utility companies since it helps in the dimensioning process for the future AMI networks.

8.3 Main conclusions

All conclusions that have been drawn through out the chapters are summarised in the following paragraphs.

- It has been shown the poor performance that PRIME experiences in impulsive noise environments. Even using the FEC communication mode, the convolutional coder - interleaver combination does not improve the robustness due to the high power of the impulses and the design of the interleaver block. Comparing the performance of PRIME and G3-PLC, it could be seen how G3-PLC's design is more able to cope with the noise impulses thanks to its longer interleaver and two-stage enconding. All these differences produces that PRIME's performance is 25 dB lower than G3-PLC's for the normal communication mode.

- Due to the existence of null subcarriers in the transmitted spectrum, compressed sensing technique seems to be very suitable for impulsive noise cancellation in this kind of systems. As a matter of fact, this thesis has shown that using compressed sensing concepts to estimate the impulsive noise component can improve the performance achieved by around 9 dB. This mechanism has the advantage that it can be used in already working systems, since no modifications are required in the structure of the transmitted signal.

- An even higher improvement in the performance can be achieved by exploiting the reconstruction capabilities of compressed sensing. As it was shown in this thesis, reconstruction capabilities are maximized when indexing the measurement matrix

using a difference set. This indexing is physically translated into a number of frequencies that need to be free (i.e. not modulated with data). This reordering of the data and null subcarriers can significantly outperforms the impulsive noise estimation. As a matter of fact, when applied to a PRIME's transceiver, an SNR gain of 20dB is achieved. Furthermore, this reordering does not increase the message's length, thus transmission data bit rates are not decremented.

- Simulations from a network's perspective also showed that the amount of time required to read all devices in the network grows rapidly with the number of nodes. This effect is due to the higher probabilities of messages colliding in the channel. Additionally, the simulation model showed that physical layer's performance has a great impact on the networks' behaviour in terms of longer roundtrips. In concrete, in case the channel is being affected by impulsive noise, the time required to poll all devices increases exponentially as the number of nodes grow. The use of impulsive noise cancellation techniques proposed in the thesis considerably reduce this time.

- After analysing the roles that nodes can have in a PRIME's network, it has been observed that the position of the switch makes a considerable difference in the overall network's performance. However, criteria for promoting nodes to Switch are not detailed in PRIME' standard. Given its big influence, it seems reasonable that some research is needed in order to find what are the most significant parameters to be considered for an optimized network's performance.

8.4 Thesis contributions

The contributions achieved in this thesis are in accordance with the considered objectives. In the following, each one of the objectives, defined in Section 1.2, is assessed using the content of this document.

- **Objective:** Implement a transceiver simulation model for the two main NB-PLC technologies endorsed by the industry (PRIME and G3-PLC) according to their open specification.

  An implementation of both PRIME and G3-PLC transmitter and receiver has been developed that allows for the evaluation of both standards in different type of PLC scenarios. This implementation has been carried out with Matlab software.

- **Objective:** Perform a theoretical and simulation study of the performance of current narrowband power line communication technologies for transmitting information in the low voltage networks under different scenarios.

Chapter 4 provides detailed figures for the physical layer's performance of PRIME and G3-PLC, two of the main NB-PLC technologies that are currently being deployed as AMI solutions. The performance is evaluated in terms of bit error rate as a function of the signal to noise ratio at the receiver. Results from simulations are compared with theoretical derivations, resulting in good agreement.

This chapter also shows how impulsive noise is a major problem in the transmission through powerlines, specially in the case of transmissions using a PRIME transceiver. This fact justifies the need for the next contribution.

- **Objective:** Propose a mechanism for improving the performance of NB-PLC transmissions in environment where impulsive noise is dominant, while not decreasing its data bit rate.

  Chapter 6 explains how the performance of a recently applied technique for impulsive noise cancellation (Compressed Sensing) can be enhanced by a reordering of the subcarriers used for data transmission. This reconfiguration allows for a more accurate reconstruction of the impulsive noise component. In addition, since no redundancy is added into the message, no data bit rate reduction is required. Simulation results report an SNR gain of 20dB when applied to a PRIME's transceiver.

- **Objective:** Implement a simulation framework that emulates the behaviour of PRIME from a network's perspective taking into account physical (i.e. attenuations, reflections and noise sources) and telematic (i.e. connection establishment processes, channel access, packet fragmentation, etc) effects.

  Chapter 7 describes the implementation of a simulation framework able to simulate the communications in a PRIME's network while taking into account the required physical and telematic effects. This framework uses pre-computed parameters for the attenuation and bit error rate. With respect to the implementation, OMNeT++ network simulator was used.

- **Objective:** Obtain estimated values of the needed time to read all meters in a low voltage narrowband power line network using the developed simulation framework.

  Using the implemented framework, network simulations are performed in order to obtain the expected behaviour in a typical European low voltage network. These results are also given in Chapter 7. There, it is shown how the time to read all meters is highly increased when transmissions are impaired by impulsive noise. Additionally, an experiment shows how the position of Switch nodes (defined in PRIME standard) plays an important role in the overall network's performance.

Finally, the knowledge generated as a result of this thesis is in the scientific community's interest and, a proof for this is the number of publications that this work has entailed. The reader can find a list of those publications in Section 8.6.

8.5 Future work

The presented thesis leaves a number of open issues that are believed to be interesting for future research. Some of them are detailed in the following:

- A hardware implementation of the proposed difference set-based compressed sensing algorithm is very desirable since it could bring insights on the procedure and, at the same time, test its suitability in real conditions.
- Although it might not be easy to achieve, some kind of real-life scenario could be used in order to validate results from the PLC network simulator implemented. If real networks are difficult to access, perhaps a small testbed could be build that provide the validation up to some extend.
- As it could be seen in Chapter 7, the position of the Switch node in PRIME's PLC network plays an important role in the performance of the overall system. However, a detailed criteria for which SN to be promoted to Switch is not specified in the standard. A future line of work could address this issue by researching on which variables should be used for the optimal node in the network to be promoted in order to minimize the time needed to address all devices.

8.6 Published and under-review work

The published work produced as a consequence of the current research is shown in the following sections.

8.6.1 Conference presentations

- **Title:** Designing a narrow band PLC front-end platform.

  Authors: S. Alexandres, J. Matanza, C. Rodríguez-Morcillo and Jaime Ramírez-Angulo .

  Conference: Congreso de Diseño de Circuitos Integrados (DCIS). Donostia - San Sebastian, The Basque Country, Spain, 27-29 November 2013.

  Status: Accepted. It will be presented at the conference.

Abstract: Power Line Communications has been recently again seen by energy companies as a useful and natural technology for performing Automatic Meter Reading (AMR) within the currently smart grid network concept. This paper presents a hardware platform proposal for the physical communication layer using Power Line Communications technology and the PRIME parameters specifications. The hardware targets are ASIC and programmable logic devices. This platform aims also the assessment of the effects of different noise sources, main problem of power line technology.

The platform is focused on introducing solutions in hardware to mitigate impulsive noise reported for authors in literature. It is well know that the physical noise, such as background and impulsive noise sources, generate severe disruptions in the communication channel. The platform is a first step to evaluate the communication performance with hostile environments in the physical layer.

- **Title:** Compressive Sensing Techniques Applied to Narrowband Power Line Communications.

  Authors: J. Matanza, S. Alexandres and C. Rodríguez-Morcillo.

  Conference: IEEE International Conference on Signal Processing, Computing and Control - Networks and Communication (ISPCC). Shimla, India, 26-28 September 2013.

  Status: Accepted. It will be presented at the conference.

  Abstract: One of the most serious disturbances in Power Line Communications (PLC) is produced by the presence of impulsive noise sources in the transmission line. This paper analyses how impulsive noise affects the PLC communication's performance from a theoretical and simulation point of view and proposes a signal processing method to enhance its robustness.

  Authors focus on a popular narrowband PLC solution to evaluate the improvement: PRIME. A simulation framework based on Matlab was developed to assess PRIME's behaviour in an impulsive noise environment. In order to recreate a realistic scenario, narrowband noise parameters reported in the literature are used in a Middleton's Class-A noise model. The performance is measured in terms of Bit Error Rate (BER) as a function of the Signal to Noise Ratio (SNR).

  Additionally, compressive sensing (CS) techniques are proposed as a method to improve PRIME's performance in such environment. The application of this technique has only been proposed for broadband PLC technologies in the literature

before. Results from simulations report an SNR gain of 9dB for the most robust communication mode.

Moreover, since no modification is required in the transmitted signal, the proposed CS configuration can be applied to already existing systems and it is backwards compatible.

- **Title:** Automatic Meter-Reading Simulation through Power Line Communication.

  Authors: J. Matanza, S. Alexandres and C. Rodríguez-Morcillo.

  Conference: IEEE 21st International Symposium on Modelling, Analysis and Simulation of Computer and Telecommunication Systems. San Francisco, California, United States, 14-16 August,

  Status: Published and presented at the conference.

  Abstract: This paper proposes a simulation's architecture that allows for the analysis of the performance when using the Power Line Communication's technology, in concrete PRIME' standard, to send Automatic Meter Reading (AMR) messages through a low voltage network. In contrast with other studies, physical phenomena -such as background and impulsive noise sources, channel attenuation and multipath effect- are taken into account by Matlab simulations. Additionally, OMNeT++ network simulator is used to model the telematic effects that occur in the communication process.

  As an example of the kind of output that can be obtained by the proposed architecture, the paper analyses the end-to-end's performance at application layer in terms of round-trip latency. Several simulations are performed in a European low-voltage network topology to compute the number of meters that can be polled within 15 minutes. Additionally, one experiment tries to determine the optimal position of one of the key nodes in PRIME's networks: the SWITCH node.

- **Title:** PRIME Performance in power line communication channel.

  Authors: J. Matanza, S. Alexandres and C. Rodríguez-Morcillo.

  Conference: 15th IEEE International Symposium on Power Line Communications and its Applications - IEEE ISPLC 2011. Udine, Italia, 3-6 April 2011

  Status: Published and presented at the conference.

Abstract:

New communication schemes are being developed to be used for Automatic Metering Reading (AMR). For this AMR system, one of the most popular approach is using power lines as a communication medium to inject a narrow band spectrum. PRIME is a new Physical and Data Link layers specification for powerline communication in the last mile released in the last two years. The main problem that this technology has to deal with is the severe attenuation that signals suffer due to reflections and fadings. Another important handicap is the time varying response of the channel produced by impulsive noise. This paper focuses on PRIME's physical specification and describes its details and procedures to overcome the previously mentioned problems. A model, developed in Matlab, implements and integrates the Forward Error Corrections (FEC) and modulation techniques described in the standard. Together with the transmitter and receiver, a channel model was created following previous studies found in the literature. The study shows the performance of PRIME' solution on the severe conditions of a PLC channel.

- **Title:** PRIME Performance Under Impulsive Noise Environments.

  Authors: J. Matanza, S. Alexandres and C. Rodríguez-Morcillo.

  Conference: 16th IEEE International Symposium on Power Line Communications and Its Applications - IEEE ISPLC2012. Beijing, P.R. China, 27-30 March,

  Status: Published and presented at the conference.

  Abstract: The presented paper addresses the problem of impulsive noise interferences in Power Line Communication (PLC) systems. In order to provide a realistic scenario, a popular narrow band PLC solution has been chosen: PRIME. System's performance is evaluated under different impulsive noise environments.

  Simulations show how, even when the high-powerful time impulses hits a few signal samples, the noise energy corrupts most of the symbol in the OFDM spectrum. This affects directly the performance in terms of BER vs. SNR despite using the most robust communication mode in PRIME.

  Additionally, two common techniques are proposed to increase the performance under this kind of disturbances. The paper shows detailed figures with the improvement and a discussion of their usability.

8.6.2 Journals (peer-reviewed)

- **Title:** Performance Evaluation of Two Narrowband PLC Systems : PRIME and G3.

  Authors: J. Matanza, S. Alexandres and C. Rodríguez-Morcillo.

  Journal: Computer Standards& Interfaces. JCR impact factor 0.978 (2012)

  Status: Submitted on the 29$^{\text{th}}$ of July, 2011. Published.

  DOI: `http://dx.doi.org/10.1016/j.csi.2013.05.001`

  Abstract: The present work analyses and compares two of the most popular specifications for data transmission over power line networks: PRIME and G3. A complete and detailed description of the specifications together with simulation results of the performance of both solutions in a power line environment are presented. The simulation model has been built using the Matlab workspace.

  In order to create an accurate analogy of the disturbances present in the power line channel, frequency fading channels together with background and asynchronous impulsive noise are included. Both noise and channel response have been computed using previous results from literature and transmission matrix theory, respectively.

  Simulation results aim to show how PRIME and G3 behave in several frequency fading and noisy environments. Finally, with respect to PRIME, a proposal is made to increase its performance in a hardly impulsive noise channel.

- **Title:** Difference Sets-based Compressive Sensing as Denoising Method for Narrow-Band Power Line Communications.

  Authors: J. Matanza, S. Alexandres and C. Rodríguez-Morcillo.

  Journal: IET Communications. JCR impact factor 0.637 (2012).

  Abstract: The present work analyses the physical communication layer of two of the most popular specifications for data transmission over power line networks: PRIME and PLC-G3.

  Status: Submitted on the 13$^{\text{th}}$ of February, 2013. In print.

  DOI: `http://dx.doi.org/10.1049/iet-com.2013.0166`

  A simulation environment based on Matlab was developed to analyse PLC-G3 and PRIME's behaviour with special focus on impulsive noise channels. To model such an environment, Middleton's Class-A noise model was used in conjunction with

measured noise parameters reported in the literature for the narrow-band spectrum. The performance is measured in terms of bit error rate versus signal to noise ratio. Simulation results show how PLC-G3 outperforms PRIME when the channel is impaired by such type of noise.

Additionally, advance signal processing techniques are proposed to improve PRIME's behaviour. Especial effort is done in not adding extra redundancy in the message and, therefore, not reduce the effective transmission bit rates.

8.6.3 Papers under review

- **Title:** Simulation of Low-Voltage Narrow-Band Power Line Communication Networks to Propagate OpenADR Signals.

  Authors: J. Matanza, S. Kiliccote, S. Alexandres and C. Rodríguez-Morcillo.

  Journal: Journal of Communications and Networks. JCR impact factor 0.309 (2012).

  Status: Submitted on the 24$^{\text{th}}$ of February, 2013. Under review.

  Abstract: This study analyses the performance of powerline communications for sending open automated demand response (OpenADR) signals. In particular, we study main channel disturbances that can affect end-to-end communications and which have not been previously studied in detail.

  Our analysis takes into account physical phenomena, such as background and impulsive noise sources, channel attenuation, and multipath effects, and considers the physical, network, and applications layers of the communications structure. The performance of the physical layer is the basis for computing the packet error rate. In analysing application performance, we focus specifically on the latency in several communication environments. If a channel is impaired only by background noise, latencies are less than 40 seconds. With the addition of impulsive noise in the channel, this value increases as long as 68 seconds. Using these figures, we find that power-line technology is more suitable for "slow" demand programs, such as day-ahead or day-of curtailments, rather than ancillary services markets, which require near-real-time communication.

- **Title:** Improvements in PLC Transmissions via Difference Sets Schemes with Compressive Sampling.

  Matanza

Journal: International Journal of Electronics and Communications. JCR impact factor 0.588 (2012).

Status: Submitted on the 26th of February, 2013. Under review.

Abstract: The paper deals with the damaging effects produced by impulsive noise in PLC transmissions and proposes a cancellation scheme using difference-set-based compressive sensing.

Authors focus on a popular narrow-band PLC solution to evaluate its performance: PRIME. A simulation environment based on Matlab was developed to analyse PRIME's behaviour in an impulsive noise environment. To model the transmission channel, Middleton's Class-A noise model was used in conjunction with noise parameters reported in the literature for the narrow-banded spectrum. The performance is measured in terms of bit error rate versus signal to noise ratio.

Although the use of compressive sensing to cancel impulsive noise in communications has already been proposed in other studies, this paper details a modification based on Partial Fourier Matrix indexing according to difference sets. Results from simulations report an almost complete cancellation of the impulsive noise effects. The analysis is done studying the achieved bit error rate as a function of the signal to noise ratio at the receiver.

8.6.4 Seminars

- J. Matanza, "Power Line Communication as a Transmission Medium for OpenADR Signals", Environmental Energy Technologies Division Group at the Lawrence Berkeley National Laboratory, Berkeley (CA), USA. 14 December, 2011.

  Abstract: Power Line Communication (PLC) is currently considered an emerging technology and is attracting the attention of the scientific community due to the promise of new ways to transmit information. Since this transmission path reaches wherever electricity is present, one of the main motivations is its use in all kinds of energy-related applications. Some examples are: remote-metering, remote-control and demand management. However, not everything about PLC is advantageous, due to the fact that it uses a physical media, which was not designed for transmit information, and it suffers from several phenomena. The two main issues are reflections due to impedance mismatches and heavy noise environments.

  The seminar describes how the omnipresence of PLC networks could be integrated with the OpenADR infrastructure. The use of public and open PLC solution (PRIME) is proposed as a way to transmit OpenADR signals to end-users and

commercial buildings. A brief description about the characteristic of PRIME will also be provided.

This talk will also focus on evaluating the transmission of OpenADR signals using PRIME through a power line channel.

Available on-line at: `http://eetd-seminars.lbl.gov/seminar/power-line-communication-transmission-medium-openadr-signals`

Bibliography

[1] V. Gungor and F. Lambert, "A survey on communication networks for electric system automation," *Computer Networks*, vol. 50, pp. 877–897, May 2006. (Cited on page 1.)

[2] M. Daoud, "On the Communication Requirements for the Smart Grid," *Energy and Power Engineering*, vol. 03, no. 01, pp. 53–60, 2011. (Cited on page 1.)

[3] G. Bumiller, L. Lampe, and H. Hrasnica, "Power Line Communication Networks for Large-Scale Control and Automation Systems," *IEEE Communications Magazine*, no. April, pp. 106–113, 2010. (Cited on page 1.)

[4] A. Haidine, A. Tabone, and J. Muller, "Deployment of power line communication by European utilities in advanced metering infrastructure," *International Symposium on Power Line Communications and Its Applications*, pp. 126–130, Mar. 2013. (Cited on pages 1, 12, and 15.)

[5] K. D. Craemer and G. Deconinck, "Analysis of State-of-the-art Smart Metering Communication Standards," in *YRS*, (Leuven), pp. 1–6, 2010. (Cited on page 1.)

[6] H. C. Ferreira, L. Lampe, and J. Newbury, *Power Line Communications: Theory and Applications for Narrowband and Broadband Communications Over Power Lines*. John Wiley and Sons, 2010. (Cited on pages 2, 24, 25, 31, 47, 48, 57, and 99.)

[7] M. Zimmermann and K. Dostert, "A multipath model for the powerline channel," *IEEE Transactions on Communications*, vol. 50, no. 4, pp. 553–559, 2002. (Cited on pages 2 and 25.)

[8] M. Zimmermann and K. Dostert, "Analysis and Modeling of Impulsive Noise in Broad-Band Powerline Communications," *IEEE Transactions on Electromagnetic Compatibility*, vol. 44, no. 1, pp. 377–386, 2002. (Cited on pages 2 and 32.)

[9] G. Deconinck, "An evaluation of two-way communication means for advanced metering in Flanders (Belgium)," in *IEEE Instrumentation and Measurement Technology Conference Proceedings (IMTC)*, pp. 900–905, 2008. (Cited on pages 3, 11, and 99.)

[10] M. Bauer, W. Liu, J. Kallenberg, K. Dostert, L. Weilin, H. Hohl, G. Kmethy, D. Moneta, A. Arzuaga, O. Neumann, A. Wolff, M. Bittner, R. Denda, T. Schaub, W. Strabbing, and I. n. Berganza, "Identification of Research Needs from Bottom-Up Approach. Knowledge Gaps. - D2.3," tech. rep., OPEN Meter Consortium, 2009. (Cited on pages 3 and 86.)

[11] S. Galli, "Recent developments on the international standardization of Narrowband PLC for Smart Grid applications," in *IEEE International Symposium on Power Line Communications and Its Applications (ISPLC)*, (Beijing, P.R. China), pp. 1–24, 2012. (Cited on pages 3 and 22.)

[12] A. Sendin, I. Berganza, I. H. Kim, A. Arzuaga, and A. Pulkkinen, "Performance Results from 100 , 000 + PRIME Smart Meters Deployment in Spain," in *IEEE Third International Conference on Smart Grid Communications (SmartGridComm)*, no. Lv, pp. 145–150, 2012. (Cited on pages 3, 22, and 87.)

[13] L. Marrón, X. Osorio, and A. Sendin, "Low Voltage Feeder Identification for Smart Grids with Standard Narrowband PLC Smart Meters," in *International Symposium on Power Line Communications and its Applications*, pp. 120–125, 2013. (Cited on page 3.)

[14] N. Arcauz, A. Goñi, M. Adriansen, B. Roelofsen, T. Schaub, F. Tarruel, and B. Shumacher, "Smart Metering Market Overview: Open Meter Related Standards in Europe Smart Meter Roll-Outs Planned Until 2020," Tech. Rep. 226369, The OPEN meter Consortium, 2012. (Cited on page 3.)

[15] Institute for Research in Technology, "OPERA (Open PLC European Research Alliance)." (Cited on page 4.)

[16] European Commission, "eEurope 2005 - http://europa.eu/legislation_summaries/information_society/strategies/l24226_en.htm." (Cited on page 4.)

[17] Institute for Research in Technology, "Open PLC European research alliance for new generation PLC integrated network - Phase 2." (Cited on page 4.)

[18] Institute for Research in Technology, "Collaboration for design and development of the emulator channel system for integrated project OPERA-2," 2008. (Cited on page 4.)

[19] ENERGOS, "Energos Project." (Cited on page 4.)

[20] Institute for Research in Technology, "Project ENERGOS: technologies for automated and intelligent management of energy distribution networks of the future," 2012. (Cited on page 4.)

[21] ADDRESS, "ADDRESS Project." (Cited on page 4.)

[22] Institute for Research in Technology, "Active distribution networks with full integration of demand and distributed energy resources," 2013. (Cited on page 4.)

[23] Institute for Research in Technology, "IEC 61850 within the Framework DENISE (Intelligent, Secure and Efficient distribution of electricity)." (Cited on page 5.)

[24] H. Hosono, "Improved automatic meter reading and load control system and its operational achievement," in *4th Int. Conf. Metering, Apparatus, and Tariffs for Electricity Supply*, pp. 90–94, 1982. (Cited on page 11.)

[25] A. Usman and S. H. Shami, "Evolution of Communication Technologies for Smart Grid applications," *Renewable and Sustainable Energy Reviews*, vol. 19, pp. 191–199, Mar. 2013. (Cited on page 11.)

[26] CENELEC, "Signalling on low-voltage electrical installations in the frequency range 3 kHz to 148,5 kHz - 50065," 2011. (Cited on page 11.)

[27] Federal Communications Commission Office of Engineering and Technology Policy and Rules Division, "FCC Online Table for Frequency Allocations," 2012. (Cited on page 11.)

[28] R. van Nee and R. Prasad, *OFDM for Wireless Multimedia Communications*. Norwood, MA, USA: Artech House, Inc., 1st ed., 2000. (Cited on page 12.)

[29] IEEE Standards Committee Standards, "IEEE Draft Standard for Low Frequency (less than 500 kHz) Narrow Band Power Line Communications for Smart Grid Applications," 2013. (Cited on page 18.)

[30] ITU-T, "Narrowband orthogonal frequency division multiplexing power line communication transceivers for ITU-T G.hnem networks," tech. rep., 2012. (Cited on page 19.)

[31] B. Sklar, *Digital communications: fundamentals and applications*. Prentice Hall Communications Engineering and Emerging Technologies Series, Prentice-Hall PTR, 2001. (Cited on page 21.)

[32] H. Huynh and M. Lecours, "Impulsive noise in noncoherent M-ary digital systems," *IEEE Transactions on Communications*, vol. 23, no. 2, pp. 246–252, 1975. (Cited on page 21.)

[33] S. Haykin, *Modern wireless communications*. Pearson Prentice Hall, 2005. (Cited on page 23.)

[34] S. Galli, "A Review of Open Problems in Power Line Communications," in *IEEE Communication Theory Workshop*, (Mexico), 2010. (Cited on page 23.)

[35] L. Lampe, "Bursty impulse noise detection by compressed sensing," in *IEEE International Symposium on Power Line Communications and Its Applications (ISPLC)*, (Udine, Italy), pp. 29–34, Apr. 2011. (Cited on pages 25, 60, and 73.)

[36] H. Philipps, "Modelling of powerline communication channels," in *International Symposium on Power Line Communications and Its Applications (ISPLC)*, ISPLC, 1999. (Cited on page 25.)

[37] T. Banwell and S. Galli, "A Novel Approach to the Modeling of the Indoor Power Line Channel Part I : Circuit Analysis and Companion Model," *IEEE Transactions on Power Delivery*, vol. 20, no. 2, pp. 655–663, 2005. (Cited on page 25.)

[38] M. Korki, H. L. Vu, C. H. Foh, X. Lu, and N. Hosseinzadeh, "MAC Performance Evaluation in Low Voltage PLC Networks," in *ENERGY 2011, The First International Conference on Smart Grids, Green Communications and IT Energy-aware Technologies*, no. c, (Venice/Mestre, Italy), pp. 135–140, 2011. (Cited on pages 26, 45, 53, 64, 83, and 87.)

[39] A. G. Lazaropoulos, "Review and Progress towards the Capacity Boost of Overhead and Underground Medium-Voltage and Low-Voltage Broadband over Power Lines Networks: Cooperative Communications through Two- and Three-Hop Repeater Systems," *ISRN Electronics*, vol. 2013, pp. 1–19, 2013. (Cited on pages 26 and 88.)

[40] G. N. Srinivasa Prasanna, A. Lakshmi, S. Sumanth, V. Simha, J. Bapat, and G. Koomullil, "Data communication over the smart grid," *2009 IEEE International Symposium on Power Line Communications and Its Applications*, pp. 273–279, Mar. 2009. (Cited on page 26.)

[41] F. Aalamifar, A. Schl, D. Harris, and L. Lampe, "Modelling Power Line Communication Using Network Simulator-3," (Cited on page 26.)

[42] P. R. Clayton, *Analysis of multiconductor transmission lines*. Wiley-Interscience, 2008. (Cited on pages 26 and 29.)

[43] L. Lampe and A. Vinck, "On cooperative coding for narrow band PLC networks," *AEU - International Journal of Electronics and Communications*, vol. 65, pp. 681–687, Aug. 2011. (Cited on pages 30, 31, and 32.)

[44] J. Anatory, N. Theethayi, and R. Thottappillil, "Performance of Underground Cables that use OFDM Systems for Broadband Power-Line Communications," *IEEE Transactions on Power Delivery*, vol. 24, no. 4, pp. 1889–1897, 2009. (Cited on page 30.)

[45] K. Dostert, M. Zimmermann, T. Waldeck, and M. Arzberger, "Fundamental Properties of the Low Voltage Power Distribution Grid Used as a Data Channel," *European Transactions on Telecommunications*, vol. 11, pp. 297–306, May 2000. (Cited on page 31.)

[46] M. Babic, M. Hagenau, K. Dostert, and J. Bausch, "Theoretical postulation of plc channel model," Tech. Rep. 507667, The Opera Consortium, 2005. (Cited on page 32.)

[47] N. Andreadou and F. Pavlidou, "PLC Channel : Impulsive Noise Modelling and its Performance Evaluation under Different Array Coding Schemes," *IEEE Transactions on Power Delivery*, vol. 24, no. 2, pp. 585–595, 2009. (Cited on page 32.)

[48] J. Häring and A. J. H. Vinck, "Iterative Decoding of Codes Over Complex Numbers for Impulsive Noise Channels," *IEEE Transactions on Information Theory*, vol. 49, no. 5, pp. 1251–1260, 2003. (Cited on pages 32 and 56.)

[49] M. Korki, N. Hosseinzadeh, H. L. Vu, T. Moazzeni, and C. H. Foh, "Impulsive Noise Reduction of a Narrowband Power Line Communication Using Optimal Nonlinearity Technique," in *Australasian Telecommunication Networks and Applications Conference (ATNAC)*, (Melbourne, Australia), pp. 2–5, 2011. (Cited on page 32.)

[50] A. Mengi and A. H. Vinck, "Impulsive Noise Error Correction in 16-OFDM for Narrowband Power Line Communication," in *International Symposium on Power Line Communications and its Applications (ISPLC)*, (Desden, Germany), pp. 31–35, 2009. (Cited on pages 32 and 58.)

[51] O. Hooijen, "A channel model for the residential power circuit used as a digital communications medium," *IEEE Transactions on Electromagnetic Compatibility*, vol. 40, no. 4, pp. 331–336, 1998. (Cited on page 33.)

[52] D. Benyoucef, "A new statistical model of the noise power density spectrum for powerline communication," in *International Symposium on Power Line Communications and its Applications (ISPLC)*, (Kyoto, Japan), pp. 136–141, ISPLC2003, 2003. (Cited on page 33.)

[53] D. Middleton, "Statistical-Physical Models of Urban Radio-Noise Environments - Part I: Foundations," *IEEE Transactions on Electromagnetic Compatibility*, vol. EMC-14, pp. 38–56, May 1972. (Cited on page 34.)

[54] D. Middleton, "Statistical-Physical Models of Electromagnetic Interference," *IEEE Transactions on Electromagnetic Compatibility*, no. 3, 1977. (Cited on page 34.)

[55] D. Middleton, "Procedures for Determining the Parameters of the First-Order Canonical Models of Class A and Class B Electromagnetic Interference," *IEEE Transactions on Electromagnetic Compatibility*, vol. EMC-21, pp. 190–208, Aug. 1979. (Cited on page 34.)

[56] T. Q. Bui, *Coded Modulation Techniques with Bit Interleaving and Iterative Processing for Impulsive Noise Channels*. PhD thesis, University of Sask atchewan, 2006. (Cited on page 34.)

[57] A. Mengi, *On Combined Coding and Modulation*. PhD thesis, Universitat Duisburg-Essen, 2010. (Cited on pages 34, 58, and 64.)

[58] A. Mengi and A. J. H. Vinck, "Successive impulsive noise suppression in OFDM," in *International Symposium on Power Line Communications and Its Applications (ISPLC)*, pp. 33–37, 2010. (Cited on pages 34, 45, 55, 58, 64, and 87.)

[59] L. Berry, "Understanding Middleton's Canonical Formula for Class a Noise," *IEEE Transactions on Electromagnetic Compatibility*, vol. EMC-23, pp. 337–344, Nov. 1981. (Cited on page 34.)

[60] P. Glasserman, *Monte Carlo methods in financial engineering*. Applications of mathematics, Springer, 2004. (Cited on page 35.)

[61] F. Kural and M. Safak, "An Experimental Investigation of Impulse Noise on Low Voltage Powerlines," in *IEEE International Symposium on Power Line Communications and Its Applications (ISPLC)*, (Athenas, Greece), pp. 12–14, 2002. (Cited on pages 37, 38, and 45.)

[62] K. Wesolowski, *Introduction to Digital Communication Systems*. John Wiley & Sons, 2009. (Cited on page 42.)

[63] E. Tipsuwannakul, P. Johannisson, M. Sköld, E. Agrell, M. Karlsson, and P. A. Andrekson, "Performance Comparison of Differential 8-Ary Modulation Formats in High-Speed Optical," *Journal of Lightwave Technology*, vol. 29, no. 19, pp. 2954–2962, 2011. (Cited on page 42.)

[64] O. G. Hooijen, "A channel model for the residential power circuit used as a digital communications medium," *IEEE Transactions on Electromagnetic Compatibility*, vol. 40, no. 4, pp. 331–336, 2002. (Cited on page 45.)

[65] M. Nassar, K. Gulati, Y. Mortazavi, and B. L. Evans, "Statistical Modeling of Asynchronous Impulsive Noise in Powerline Communication Networks," in *IEEE Global Telecommunications Conference (GLOBECOM)*, pp. 1–6, Dec. 2011. (Cited on page 45.)

[66] Y. Kim, J. N. Bae, J. Y. Kim, and S. Member, "Performance of Power Line Communication Systems with Noise Reduction Scheme for Smart Grid Applications," *IEEE Transactions on Communications*, vol. 57, no. 1, pp. 46–52, 2011. (Cited on page 53.)

[67] H. A. Suraweera, C. Chai, J. Shentu, and J. Armstrong, "Analysis of Impulse Noise Mitigation Techniques for Digital Television Systems," *Proc. of 8th international OFDM Workshop*, 2003. (Cited on pages 53 and 58.)

[68] A. P. Nokes, Christopher Ryan Haffenden, Oliver Paul Mitchell, Justin David Robinson, J. H. Stott, and A. Wiewiorka, "Detection and removal of clipping in multicarrier receivers," 2000. (Cited on page 53.)

[69] S. V. Zhidkov, "Performance Analysis and Optimization of OFDM Receiver With Blanking Nonlinearity in Impulsive Noise Environment," *IEEE Transactions on Vehicular Technology*, vol. 55, pp. 234–242, Jan. 2006. (Cited on page 54.)

[70] S. V. Zhidkov, "Analysis and comparison of several simple impulsive noise mitigation schemes for OFDM receivers," *IEEE Transactions on Communications*, vol. 56, pp. 5–9, Jan. 2008. (Cited on page 54.)

[71] K. Al-Mawali, A. Z. Sadik, and Z. M. Hussain, "Time-Domain Techniques for Impulsive Noise Reduction in OFDM-Based Power Line Communications: A Comparative Study," in *Australasian Telecommunication Networks and Applications Conference*, pp. 368–372, 2009. (Cited on page 54.)

[72] K. S. Al-Mawali and Z. M. Hussain, "Adaptive-threshold clipping for impulsive noise reduction in OFDM-based power line Communications," *2009 International Conference on Advanced Technologies for Communications*, pp. 43–48, Oct. 2009. (Cited on page 54.)

[73] D. Dardari, V. Tralli, and A. Vaccari, "A Theoretical Characterization of Nonlinear Distortion Effects in OFDM Systems," *IEEE Transactions on Communications*, vol. 48, no. 10, pp. 1755–1764, 2000. (Cited on page 54.)

[74] G. Ndo, P. Siohan, M.-h. Hamon, and J. Horard, "Optimization of turbo decoding performance in the presence of impulsive noise using soft limitation at the receiver side," in *Global Telecommunications Conference*, pp. 1–5, IEEE, 2008. (Cited on page 54.)

[75] G. Ndo, P. Siohan, and M.-h. Hamon, "Adaptive Noise Mitigation in Impulsive Environment : Application to Power-Line Communications," *IEEE Transactions on Power Delivery*, vol. 25, no. 2, pp. 647–656, 2010. (Cited on pages 54 and 64.)

[76] D.-f. Tseng, R.-b. Yang, T.-r. Tsai, and Y. S. Han, "Efficient Clipping for Broadband Power Line Systems in Impulsive Noise Environment," in *International Symposium on Power Line Communications and its Applications*, pp. 362–367, 2012. (Cited on page 55.)

[77] V. N. Papilaya and a. J. H. Vinck, "Investigation on a new combined impulsive noise mitigation scheme for OFDM transmission," *2013 IEEE 17th International Symposium on Power Line Communications and Its Applications*, pp. 86–91, Mar. 2013. (Cited on pages 55 and 64.)

[78] X. Yibin and M. Okada, "Impulsive Noise Canceler for OFDM," in *International Symposium on Intelligent Signal Processing and Communication Systems*, no. Ispacs, pp. 465–468, 2009. (Cited on page 56.)

[79] J. Radic and N. Rozic, "Reconstruction of the Samples Corrupted with Impulse Noise in Multicarrier Systems," *IEEE Wireless Communications and Networking Conference*, pp. 1–5, Apr. 2009. (Cited on page 56.)

[80] J. Radić and N. Rožić, "Adaptive Impulse Noise Suppression in OFDM Systems," *Electronics and Electrial Engineering*, vol. 1, no. 1, 2010. (Cited on page 56.)

[81] P. Torio and M. G. Sanchez, "Method to cancel impulsive noise from power-line communication systems by processing the information in the idle carriers," *IEEE*

Transactions on Power Delivery, vol. 27, no. 4, pp. 2421–2422, 2012. (Cited on page 56.)

[82] J. Häring and A. Han Vinck, "OFDM transmission corrupted by impulsive noise," in *International Symposium on Power Line Communications and Its Applications (ISPLC)*, pp. 5–7, 2000. (Cited on pages 56 and 57.)

[83] H. Matsuo, D. Umehara, M. Kawai, and Y. Morihiro, "An iterative detection for OFDM over impulsive noise channel," in *International Symposium on Power Line Communications and its Applications (ISPLC)*, 2002. (Cited on page 56.)

[84] S. Zhidkov, "Impulsive noise suppression in OFDM based communication systems," *IEEE Transactions on Consumer Electronics*, vol. 49, pp. 944–948, Nov. 2003. (Cited on pages 57 and 58.)

[85] I. H. Kim, B. Varadarajan, and A. Dabak, "Performance Analysis and Enhancements of Narrowband OFDM Powerline Communication Systems," in *IEEE International Conference on Smart Grid Communications (SmartGridComm)*, pp. 362–367, 2010. (Cited on pages 58 and 87.)

[86] A. Hazmi, B. Sharif, and C. Tsimenidis, "Efficient Interleaving Technique for OFDM System over Impulsive Noise Channels," in *International Symposium on Personal Indoor and Mobile Radio Communications*, pp. 167–171, 2010. (Cited on page 60.)

[87] S. Nayyef, C. Tsimenidis, A. Al-Dweik, B. Sharif, and A. Hazmi, "Time- and Frequency-Domain Impulsive Noise Spreader for OFDM Systems," *IEEE 11th International Conference on Trust, Security and Privacy in Computing and Communications*, pp. 1856–1861, June 2012. (Cited on page 60.)

[88] T. Y. Al-naffouri, A. A. Quadeer, and G. Caire, "Impulsive Noise Estimation and Cancellation in DSL using Orthogonal Clustering," pp. 2841–2845, 2011. (Cited on page 60.)

[89] H. Nyquist, "Certain topics in telegraph transmission theory," *Transactions of the American Institute of Electrical Engineers*, vol. 90, no. 2, pp. 280–305, 1928. (Cited on page 63.)

[90] D. L. Donoho, "Compressed sensing," *IEEE Transactions on Information Theory*, vol. 52, pp. 1289–1306, Apr. 2006. (Cited on pages 63 and 66.)

[91] E. J. Candes and M. B. Wakin, "An Introduction To Compressive Sampling," *IEEE Signal Processing Magazine*, vol. 25, no. 2, pp. 21–30, 2008. (Cited on pages 64, 65, 66, and 69.)

[92] Y. C. Eldar, P. Kuppinger, and H. Bolcskei, "Block-Sparse Signals: Uncertainty Relations and Efficient Recovery," *IEEE Transactions on Signal Processing*, vol. 58, pp. 3042–3054, June 2010. (Cited on pages 64, 69, 72, 73, 74, and 83.)

[93] N. Y. Yu, "Deterministic Construction of Partial Fourier Compressed Sensing Matrices Via Cyclic Difference Sets," *arXiv.org*, pp. 1–16, 2010. (Cited on pages 64 and 83.)

[94] E. Candes, J. Romberg, and T. Tao, "Stable Signal Recovery from Incomplete and Inaccurate Measurements," *Communications on pure and applied mathematics*, vol. 40698, pp. 1–15, 2005. (Cited on page 66.)

[95] E. J. Candes and P. A. Randall, "Highly Robust Error Correction by Convex Programming," *IEEE Transactions on Information Theory*, vol. 54, pp. 1–22, 2007. (Cited on page 66.)

[96] E. J. Candes and T. Tao, "Decoding by linear programming," *IEEE Transactions on Information Theory*, vol. 51, no. 12, pp. 4203–4215, 2005. (Cited on page 66.)

[97] D. Needell, *Topics in Compressed Sensing*. PhD thesis, University of California Davis, 2009. (Cited on pages 66, 70, 139, and 141.)

[98] S. Jafarpour, *Deterministic Compressed Sensing*. PhD thesis, Princeton University, 2011. (Cited on page 66.)

[99] M. Nassar and B. L. Evans, "Non-Parametric Impulsive Noise Mitigation in OFDM Systems Using Sparse Bayesian Learning," in *IEEE Global Telecommunications Conference - GLOBECOM 2011*, pp. 1–5, Ieee, Dec. 2011. (Cited on pages 66 and 143.)

[100] J. Lin and B. L. Evans, "Non-parametric Mitigation of Periodic Impulsive Noise in Narrowband Powerline Communications," in *global Communications onference (GLOBECOM)*, (Atlanta, GA, USA), 2013. (Cited on page 66.)

[101] J. Wang, S. Kwon, and B. Shim, "Generalized Orthogonal Matching Pursuit," *IEEE Transactions on Signal Processing*, vol. 60, p. 12, 2012. (Cited on pages 66 and 143.)

[102] R. Gribonval and P. Vandergheynst, "On the Exponential Convergence of Matching Pursuits in Quasi-Incoherent Dictionaries," *IEEE Transactions on Information Theory*, vol. 52, no. 1, pp. 360–365, 2006. (Cited on page 69.)

[103] D. L. Donoho and M. Elad, "Optimally sparse representation in general (nonorthogonal) dictionaries via l minimization.," *Proceedings of the National Academy of Sciences of the United States of America*, vol. 100, pp. 2197–202, Mar. 2003. (Cited on page 69.)

[104] S. Mallat, "Matching pursuits with time-frequency dictionaries," *IEEE Transactions on Signal Processing*, vol. 41, no. 12, pp. 3397–3415, 1993. (Cited on page 69.)

[105] J. A. Tropp and S. Member, "Greed is Good : Algorithmic Results for Sparse Approximation," *IEEE Transactions on Information Theory*, vol. 50, no. 10, pp. 2231–2242, 2004. (Cited on page 69.)

[106] L. Welch, "Lower Bounds on the Maximum Cross Correlation of Signals," *IEEE Transactions on Information Theory*, pp. 397–399, 1973. (Cited on page 69.)

[107] M. A. Davenport, M. F. Duarte, Y. C. Eldar, and G. Kutyniok, "Introduction to compressed sensing," *Preprint*, 2011. (Cited on page 69.)

[108] M. Fornasier and H. Rauhut, "Compressive sensing," in *Handbook of Mathematical Methods in Imaging*, pp. 187–228, Springer, 2011. (Cited on page 69.)

[109] Y. C. Eldar and M. Mishali, "Robust Recovery of Signals From a Structured Union of Subspaces," *IEEE Transactions on Information Theory*, vol. 55, no. 11, pp. 5302–5316, 2009. (Cited on page 73.)

[110] W. Guo, X. Wang, Y. Lu, and W. Wang, "A Tree Based Recovery Algorithm for Block Sparse Signals," in *Proceedings of the 6th International ICST Conference on Cognitive Radio Oriented Wireless Networks and Communications (CROWNCOM)*, (Osaka, Japan), pp. 91–95, 2011. (Cited on page 75.)

[111] P. Xia, S. Member, and S. Zhou, "Achieving the Welch Bound With Difference Sets," *IEEE Transactions on Information Theory*, vol. 51, no. 5, pp. 1900–1907, 2005. (Cited on pages 76, 77, and 78.)

[112] N. M. Sriram, B. Adiga, and K. Hari, "Burst Error Correction using Partial Fourier Matrices and Block Sparse Representation," in *National Conference on Communications (NCC)*, no. 2, (Kharagpur, India), 2012. (Cited on page 77.)

[113] La Jolla, "La Jolla Difference Set Repository - http://www.ccrwest.org/diffsets/diff_sets/index.html," 2013. (Cited on page 78.)

[114] B. Sivaneasan and E. Gunawan, "Modeling and Performance Analysis of Automatic Meter-Reading Systems Using PLC Under Impulsive Noise Interference," *IEEE Transactions on Power Delivery*, vol. 25, pp. 1465–1475, July 2010. (Cited on page 83.)

[115] W. W. Smith and J. M. Smith, *Handbook of real-time fast Fourier transforms: algorithms to product testing*. IEEE Press, 1995. (Cited on page 84.)

[116] A. Sanz, P. J. Pinero, D. Montoro, and J. I. Garcia, "High-accuracy Distributed Simulation Environment for PRIME Networks Analysis and Improvement," in *IEEE International Symposium on Power Line Communications and Its Applications (ISPLC)*, (Beijing, P.R. China), pp. 108–113, 2012. (Cited on pages 87 and 111.)

[117] A. Arzuaga, I. Berganza, A. Sendin, M. Sharma, and B. Varadarajan, "PRIME interoperability tests and results from field," in *First IEEE International Conference on Smart Grid Communications (SmartGridComm)*, (New Delhi, India), pp. 126–130, 2010. (Cited on page 87.)

[118] K. Razazian, M. Umari, and A. Kamalizad, "Error correction mechanism in the new G3-PLC specification for powerline communication," in *International Symposium on Power Line Communications and its Applications (ISPLC)*, pp. 50–55, ISPLC2010, 2010. (Cited on page 87.)

[119] M.-s. Kim, D.-m. Son, Y.-b. Ko, and Y.-h. Kim, "A simulation study of the PLC-MAC performance using network simulator-2," in *IEEE International Symposium on Power Line Communications and Its Applications (ISPLC)*, vol. 2, pp. 99–104, Apr. 2008. (Cited on page 87.)

[120] K.-H. Kim, H.-B. Lee, Y.-H. Lee, and S.-C. Kim, "PHY abstraction methodology for the performance evaluation of PLC channels," in *IEEE International Symposium on Power Line Communications and Its Applications (ISPLC)*, pp. 28–32, 2010. (Cited on page 87.)

[121] A. Sanz, P. J. Pinero, S. Miguel, and J. I. Garcia-Nicolas, "Distributed Event-Driven Simulation Environment for Smart Metering Protocols Evaluation," in *IEEE Third International Conference on Smart Grid Communications (SmartGridComm)*, pp. 151–156, 2012. (Cited on page 87.)

[122] A. Sanz, P. J. Pinero, S. Miguel, and J. I. Garcia, "Real problems solving in PRIME networks by means of simulation," *2013 IEEE 17th International Symposium on Power Line Communications and Its Applications*, pp. 285–290, Mar. 2013. (Cited on page 87.)

[123] A. Zaballos, A. Vallejo, M. Majoral, and J. M. Selga, "Survey and Performance Comparison of AMR Over PLC Standards," *IEEE Transactions on Power Delivery*, vol. 24, no. 2, pp. 604–613, 2009. (Cited on pages 88 and 99.)

[124] ITU-T, "G.9904 : Narrowband orthogonal frequency division multiplexing power line communication transceivers for PRIME networks.," tech. rep., 2012. (Cited on pages 88, 92, and 108.)

[125] J. Lin, Y. Mortazavi, A. Dabak, I. H. Kim, and B. L. Evans, "Local Utility Power Line Communications in the 3-500 kHz Band: Channel Impairments, Noise, and Standards," *IEEE Signal Processing Magazine*, pp. 116–127, 2012. (Cited on page 102.)

[126] S. Feuerhahn, M. Zillgith, C. Wittwer, and C. Wietfeld, "Comparison of the communication protocols DLMS/COSEM, SML and IEC 61850 for smart metering applications," *2011 IEEE International Conference on Smart Grid Communications (SmartGridComm)*, pp. 410–415, Oct. 2011. (Cited on page 102.)

[127] A. Bjõrck, *Numerical Methods for Least Squares Problems*. Handbook of Numerical Analysis, Society for Industrial and Applied Mathematics, 1996. (Cited on page 143.)

Appendix A

Orthogonal Matching Pursuit algorithms

A.1 Orthogonal Matching Pursuit

Pseudo-code for Orthogonal Matching Pursuit Algorithm adapted from [97]:

Algorithm 1 Orthogonal Matching Pursuit

input : Measurement matrix Φ, measurement vector $y = \Phi x$
output: Reconstructed vector $\hat{x}$

//`Initialize variables`
$C = \emptyset$; $r(1) = y$; $iterCounter = 0$; $maxIter = 50$; $tol = 10^{-2}$;
//`Algorithm`
while $iterCounter < maxIter$ && $||r(iterCounter)||_2 > tol$ **do**
  //`Select the position` α `of the largest element in`
  // $\beta = \Phi^* \cdot r(iterCounter)$ `in absolute value.`
  $\beta = \Phi^* \cdot r(iterCounter)$;
  $\alpha = max\_pos(|\beta|)$;
  //`Add` α `to` C.
  $C \leftarrow C \cup \{\alpha\}$.
  //`Compute` Ψ `by indexing columns in` Φ `using` C.
  $\Psi = \Phi(C)$;
  //`Compute the reconstructed vector.`
  $\hat{x} = \Psi^\dagger \cdot y$;
  //`Update the residual.`
  $r(iterCounter + 1) = x - \Phi \cdot \hat{x}$;
  //`Increase counter for next iteration.`
  $iterCounter = iterCounter + 1$;

Maltab code for Orthogonal Matching Pursuit Algorithm:

```
function [xhat, residual] = OMP(Phi, y)

% Orthogonal Matching Pursuit — selection of group based on highest
% correlation of each column

% Input
% A = M x N  dimensional measurment matrix
% y = M dimensional observation vector

% Output
% s = estimated sparse signal
% r = residual

% Initialize variables
tol = 1e—2;
maxIter = 50;
xhat = zeros(size(Phi,2),1);
residual(:,1) = y;
i = 2;
C=[];

while (i < maxIter) && (norm(residual(:,end))>tol)

    beta = Phi'*residual;

    norma = sqrt(sum(abs(beta).^2,1));

    [value,posi]=sort(norma);

    C = [C posi(end)];

    Psi = Phi(:,Aind);
    xhat = lscov(Psi,y);
    yUpdated = Psi*xhat;
    residual = y — yUpdated;
    i = i + 1;

end
```

A.2 Block-Orthogonal Matching Pursuit

Pseudo-code for Block Orthogonal Matching Pursuit Algorithm adapted from [97]:

Algorithm 2 Block-Orthogonal Matching Pursuit

input : Measurement matrix Φ, measurement vector $y = \Phi x$
output: Reconstructed vector $\hat{x}$

//`Initialize variables`
$C = \emptyset$; $r(1) = y$; $iterCounter = 0$; $maxIter = 50$; $tol = 10^{-2}$; $d = 8$;
$nBlocks = N/d$;
//`Algorithm`
while $iterCounter < maxIter$ && $||r(iterCounter)||_2 > tol$ **do**
  //`Select the position` α `with the largest`
  //`absolute block coherence.`
  for $blockIter = 1{:}nBlocks$ **do**
    $\beta(blockIter) = \Phi[blockIter]^* \cdot r(iterCounter)$;
  $\alpha = max\_pos(|\beta|)$;
  //`Add indexes of block to` C.
  $C \leftarrow C \cup \{\alpha\}$.
  //`Compute` Ψ `by indexing columns in` Φ `using` C.
  $\Psi = \Phi(C)$;
  //`Compute the reconstructed vector.`
  $\hat{x} = \Psi^\dagger \cdot y$;
  //`Update the residual.`
  $r(iterCounter + 1) = x - \Phi \cdot \hat{x}$;
  //`Increase counter for next iteration.`
  $iterCounter = iterCounter + 1$;

Maltab code for Block-Orthogonal Matching Pursuit Algorithm:

```
function [xhat, residual] = BOMP(Phi, y, d)

% Block Orthogonal Matching Pursuit - selection of group based on highest
% correlation of each block

% Input
% A = M X N dimensional measurment matrix
% y = M dimensional observation vector


% Output
% s = estimated sparse signal
```

```
% r = residual

tol = 1e-2;
maxiter = 50;
xhat = zeros(size(Phi,2),1);
residual(:,1) = y;
i = 2;
numBlocks= size(Phi,2)/d;
C=[];


while (i < maxiter) && (norm(residual(:,end))>tol)
    beta = Phi'*residual;
    betaBlok = reshape(beta,d,numBlocks);
    normBetaBlock = sqrt(sum(abs(betaBlok).^2,1));
    [value,alpha]=sort(normBetaBlock);


    C = [C alpha(end)];

    PhiInd = length(C)*d; %Preallocation
    for Citer = 1:length(C)
        %Build indexes based on C and the block size
        PhiInd((Citer-1)*d+1:Citer*d) = (C(Citer)-1)*d+1:C(Citer)*d; %
    end

    Psi = Phi(:,PhiInd);
    xhat = lscov(Psi,y);
    yUpdated = Psi*xhat;
    residual = y - yUpdated;
    i = i + 1;
end
```

Appendix B

DS-based CS complexity analysis

B.1 Complexity for BOMP algorithm

This section provides some details on the amount of operations needed when using the BOMP algorithm for compressed sensing. According to [101], the algorithm described in Section 6.3.2.1 can be conceptually separated in the following parts: **Identification**, **Augmentation**, **Estimation** of $\hat{x}$ and **Residual Update**. The complexity of each step is summarised as follows:

- **Identification**. Here, a matrix-vector multiplication is performed ($\beta_{(k)} = \Phi^*_{(k)} \cdot r_{(k-1)}$), which requires $(2M-1)N$ flops (M multiplications and $(M-1)$ additions.
- **Augmentation**. Find the largest element in $\beta_{(k)}$, referred to as γ, and include its index to the collection of index (C). This sort operation requires N/d flops.
- **Estimation of $\hat{x}$.** $\hat{x}$ is obtained solving $\hat{x} = \text{argmin}_z ||y - \Phi_{(k)} \cdot z||_2$. To avoid the raw computation of the least square problem, a QR factorization can be made ($\Phi = QR$). This has a complexity of $\mathcal{O}(k^2 \cdot M)$ [127].
- **Residual update**. For the residual update, a matrix-vector multiplication is performed ($\Phi \cdot \hat{x}$) which is subtracted from the previous residual. Analogously to the Identification step, the matrix-vector multiplication requires $(2 \cdot d \cdot k - 1) \cdot M$ flops that need to be added to the M-long vector subtraction. In total this step involves $2 \cdot d \cdot k \cdot M$ floating point operations.

In total, the complexity when reconstructing a k-sparse vector can be expressed as $\mathcal{O}(k \cdot M \cdot N)$; in any case lower than the $\mathcal{O}(N^2 \cdot M)$ to $\mathcal{O}(N^3)$ complexity reported for Sparse Bayesian Learning [99].

Appendix C

Frequencies for difference set-based compressed sensing for a PRIME transceiver

The following table details the frequencies for the null and data tones used in the difference set-based compressed sensing technique described in Section 6.4.

Null Tones		Data Tones	
Index	Frequency [Hz]	Index	Frequency [Hz]
1	0.00	5	1893.94
2	473.48	7	2840.91
3	946.97	10	4261.36
4	1420.45	11	4734.85
6	2367.42	14	6155.30
8	3314.39	15	6628.79
9	3787.88	17	7575.76
12	5208.33	19	8522.73
13	5681.82	20	8996.21
16	7102.27	21	9469.70
18	8049.24	22	9943.18
24	10890.15	23	10416.67
25	11363.64	28	12784.09
26	11837.12	30	13731.06
27	12310.61	33	15151.52
29	13257.58	34	15625.00
31	14204.55	37	17045.45
32	14678.03	38	17518.94
35	16098.48	40	18465.91
36	16571.97	42	19412.88
39	17992.42	43	19886.36
41	18939.39	44	20359.85
47	21780.30	45	20833.33

48	22253.79	46	21306.82
49	22727.27	51	23674.24
50	23200.76	53	24621.21
52	24147.73	56	26041.67
54	25094.70	57	26515.15
55	25568.18	60	27935.61
58	26988.64	61	28409.09
59	27462.12	63	29356.06
62	28882.58	65	30303.03
64	29829.55	66	30776.52
70	32670.45	67	31250.00
71	33143.94	68	31723.48
72	33617.42	69	32196.97
73	34090.91	74	34564.39
75	35037.88	76	35511.36
77	35984.85	79	36931.82
78	36458.33	80	37405.30
81	37878.79	83	38825.76
82	38352.27	84	39299.24
85	39772.73	86	40246.21
87	40719.70	88	41193.18
93	43560.61	89	41666.67
94	44034.09	90	42140.15
95	44507.58	91	42613.64
96	44981.06	92	43087.12
98	45928.03	97	45454.55
100	46875.00	99	46401.52
101	47348.48	102	47821.97
104	48768.94	103	48295.45
105	49242.42	106	49715.91
108	50662.88	107	50189.39
110	51609.85	109	51136.36
116	54450.76	111	52083.33
117	54924.24	112	52556.82
118	55397.73	113	53030.30
119	55871.21	114	53503.79
121	56818.18	115	53977.27
123	57765.15	120	56344.70
124	58238.64	122	57291.67
127	59659.09	125	58712.12
128	60132.58	126	59185.61
131	61553.03	129	60606.06
133	62500.00	130	61079.55
139	65340.91	132	62026.52

140	65814.39	134	62973.48
141	66287.88	135	63446.97
142	66761.36	136	63920.45
144	67708.33	137	64393.94
146	68655.30	138	64867.42
147	69128.79	143	67234.85
150	70549.24	145	68181.82
151	71022.73	148	69602.27
154	72443.18	149	70075.76
156	73390.15	152	71496.21
162	76231.06	153	71969.70
163	76704.55	155	72916.67
164	77178.03	157	73863.64
165	77651.52	158	74337.12
167	78598.48	159	74810.61
169	79545.45	160	75284.09
170	80018.94	161	75757.58
173	81439.39	166	78125.00
174	81912.88	168	79071.97
177	83333.33	171	80492.42
179	84280.30	172	80965.91
185	87121.21	175	82386.36
186	87594.70	176	82859.85
187	88068.18	178	83806.82
188	88541.67	180	84753.79
190	89488.64	181	85227.27
192	90435.61	182	85700.76
193	90909.09	183	86174.24
196	92329.55	184	86647.73
197	92803.03	189	89015.15
200	94223.48	191	89962.12
202	95170.45	194	91382.58
208	98011.36	195	91856.06
209	98484.85	198	93276.52
210	98958.33	199	93750.00
211	99431.82	201	94696.97
213	100378.79	203	95643.94
215	101325.76	204	96117.42
216	101799.24	205	96590.91
219	103219.70	206	97064.39
220	103693.18	207	97537.88
223	105113.64	212	99905.30
225	106060.61	214	100852.27
231	108901.52	217	102272.73

232	109375.00	218	102746.21
233	109848.48	221	104166.67
234	110321.97	222	104640.15
236	111268.94	224	105587.12
238	112215.91	226	106534.09
239	112689.39	227	107007.58
242	114109.85	228	107481.06
243	114583.33	229	107954.55
246	116003.79	230	108428.03
248	116950.76	235	110795.45
254	119791.67	237	111742.42
255	120265.15	240	113162.88
256	120738.64	241	113636.36
257	121212.12	244	115056.82
259	122159.09	245	115530.30
261	123106.06	247	116477.27
262	123579.55	249	117424.24
265	125000.00	250	117897.73
266	-125000.00	251	118371.21
269	-123574.14	252	118844.70
271	-122623.57	253	119318.18
277	-119771.86	258	121685.61
278	-119296.58	260	122632.58
279	-118821.29	263	124053.03
280	-118346.01	264	124526.52
282	-117395.44	267	-124524.71
284	-116444.87	268	-124049.43
285	-115969.58	270	-123098.86
288	-114543.73	272	-122148.29
289	-114068.44	273	-121673.00
292	-112642.59	274	-121197.72
294	-111692.02	275	-120722.43
300	-108840.30	276	-120247.15
301	-108365.02	281	-117870.72
302	-107889.73	283	-116920.15
303	-107414.45	286	-115494.30
305	-106463.88	287	-115019.01
307	-105513.31	290	-113593.16
308	-105038.02	291	-113117.87
311	-103612.17	293	-112167.30
312	-103136.88	295	-111216.73
315	-101711.03	296	-110741.44
317	-100760.46	297	-110266.16
323	-97908.75	298	-109790.87

324	-97433.46	299	-109315.59
325	-96958.17	304	-106939.16
326	-96482.89	306	-105988.59
328	-95532.32	309	-104562.74
330	-94581.75	310	-104087.45
331	-94106.46	313	-102661.60
334	-92680.61	314	-102186.31
335	-92205.32	316	-101235.74
338	-90779.47	318	-100285.17
340	-89828.90	319	-99809.89
346	-86977.19	320	-99334.60
347	-86501.90	321	-98859.32
348	-86026.62	322	-98384.03
349	-85551.33	327	-96007.60
351	-84600.76	329	-95057.03
353	-83650.19	332	-93631.18
354	-83174.90	333	-93155.89
357	-81749.05	336	-91730.04
358	-81273.76	337	-91254.75
361	-79847.91	339	-90304.18
363	-78897.34	341	-89353.61
369	-76045.63	342	-88878.33
370	-75570.34	343	-88403.04
371	-75095.06	344	-87927.76
372	-74619.77	345	-87452.47
374	-73669.20	350	-85076.05
376	-72718.63	352	-84125.48
377	-72243.35	355	-82699.62
380	-70817.49	356	-82224.33
381	-70342.21	359	-80798.48
384	-68916.35	360	-80323.19
386	-67965.78	362	-79372.62
392	-65114.07	364	-78422.05
393	-64638.78	365	-77946.77
394	-64163.50	366	-77471.48
395	-63688.21	367	-76996.20
397	-62737.64	368	-76520.91
399	-61787.07	373	-74144.49
400	-61311.79	375	-73193.92
403	-59885.93	378	-71768.06
404	-59410.65	379	-71292.78
407	-57984.79	382	-69866.92
409	-57034.22	383	-69391.63
415	-54182.51	385	-68441.06

416	-53707.22	387	-67490.49
417	-53231.94	388	-67015.21
418	-52756.65	389	-66539.92
420	-51806.08	390	-66064.64
422	-50855.51	391	-65589.35
423	-50380.23	396	-63212.93
426	-48954.37	398	-62262.36
427	-48479.09	401	-60836.50
430	-47053.23	402	-60361.22
432	-46102.66	405	-58935.36
438	-43250.95	406	-58460.08
439	-42775.67	408	-57509.51
440	-42300.38	410	-56558.94
441	-41825.10	411	-56083.65
443	-40874.52	412	-55608.37
445	-39923.95	413	-55133.08
446	-39448.67	414	-54657.79
449	-38022.81	419	-52281.37
450	-37547.53	421	-51330.80
453	-36121.67	424	-49904.94
455	-35171.10	425	-49429.66
461	-32319.39	428	-48003.80
462	-31844.11	429	-47528.52
463	-31368.82	431	-46577.95
464	-30893.54	433	-45627.38
466	-29942.97	434	-45152.09
468	-28992.40	435	-44676.81
469	-28517.11	436	-44201.52
472	-27091.25	437	-43726.24
473	-26615.97	442	-41349.81
476	-25190.11	444	-40399.24
478	-24239.54	447	-38973.38
484	-21387.83	448	-38498.10
485	-20912.55	451	-37072.24
486	-20437.26	452	-36596.96
487	-19961.98	454	-35646.39
489	-19011.41	456	-34695.82
491	-18060.84	457	-34220.53
492	-17585.55	458	-33745.25
495	-16159.70	459	-33269.96
496	-15684.41	460	-32794.68
499	-14258.56	465	-30418.25
501	-13307.98	467	-29467.68
507	-10456.27	470	-28041.83

508	-9980.99	471	-27566.54
509	-9505.70	474	-26140.68
510	-9030.42	475	-25665.40
512	-8079.85	477	-24714.83
514	-7129.28	479	-23764.26
515	-6653.99	480	-23288.97
518	-5228.14	481	-22813.69
519	-4752.85	482	-22338.40
522	-3327.00	483	-21863.12
524	-2376.43	488	-19486.69
-	-	490	-18536.12
-	-	493	-17110.27
-	-	494	-16634.98
-	-	497	-15209.13
-	-	498	-14733.84
-	-	500	-13783.27
-	-	502	-12832.70
-	-	503	-12357.41
-	-	504	-11882.13
-	-	505	-11406.84
-	-	506	-10931.56
-	-	511	-8555.13
-	-	513	-7604.56
-	-	516	-6178.71
-	-	517	-5703.42
-	-	520	-4277.57
-	-	521	-3802.28
-	-	523	-2851.71
-	-	525	-1901.14
-	-	526	-1425.86
-	-	527	-950.57
-	-	528	-475.29
-	-	529	0.00

Table C.1: *Data and null subcarriers for Difference Set-based Compressed Sensing.*

Appendix D

Structure of main MAC messages

D.1 MAC PDU Format

There exist three different types of MAC PDU. The following section provide a brief overview of their main characteristics.

D.2 Generic MAC PDU

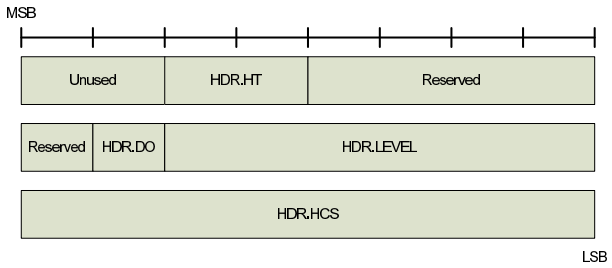

Figure D.1: *Generic MAC header structure.*

- **HDR.HT** - Header type. Either Generic Mac (0), Promotion Needed(1) or Beacon PDU (2).
- **HDR.DO** - Downlink/Uplink. To indicate which is the direction of the current message.
- **HDR.LEVEL** - Level. Level in the logical hierarchy of the current communication.
- **HDR.HCS** - Checksum. Checksum of the information encapsulated by the current message.

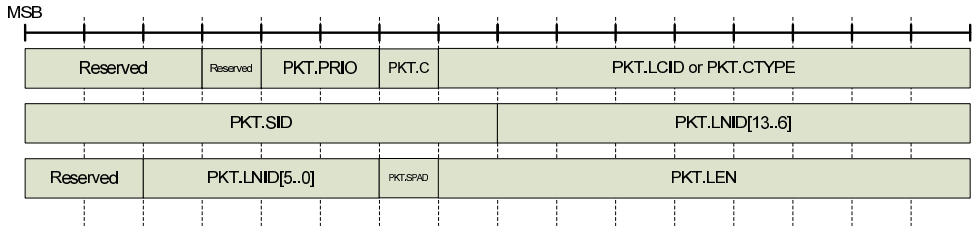

Figure D.2: *Packet header structure.*

D.3 Packet header structure

- **PKT.NAD** - No Aggregation. To indicate whether the packet may be aggregated with other packets at destination.
- **PKT.PRIO** - Priority. Indicates packet priority. It will affect on the number of times the channel is sensed before transmitting (see Figure 7.7). It can take values from 0 to 3.
- **PKT.C** - Control. To indicate whether it is a control or a data packet.
- **PKT.LCID/PKT.CTYPE** - Local Connection Identifier / Control Type. Depending on the type of packet, it indicates the local connection identifier of the type of control packet.
- **PKT.SID** - Switch Identifier. Depending on the direction of the packet it indicates the Switch Identifier of either the source or destination of the packet.
- **PKT.LNID** - Local Node Identifier. Depending on the direction of the packet it indicates the Local Node Identifier of either the source or destination of the packet.
- **PKT.SPAD** - Padding. It indicates if padding is inserted while encrypting payload.
- **PKT.LEN** - Length. Length of the payload in bytes.

D.4 Promotion needed PDU

- **HDR.HT** - Header type. Either Generic Mac (0), Promotion Needed(1) or Beacon PDU (2).
- **PNH.SNA** - network Address. The EUI-48 of the network the Service Node is trying to connect to.

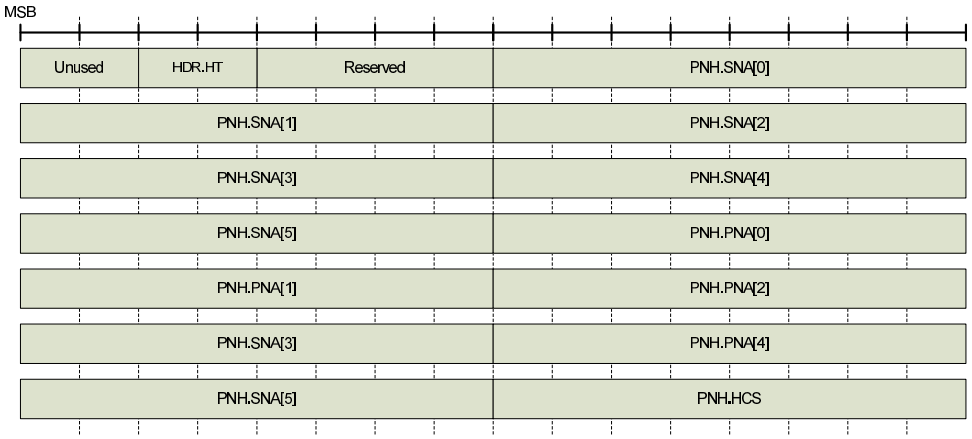

Figure D.3: *Promotion Needed structure.*

- **PNH.PNA** - Promotion Needed Address. The EUI-48 of Service Node that needs the promotion.
- **PNH.HCS** - Checksum. Checksum of the information encapsulated by the current message.

D.5 Beacon PDU

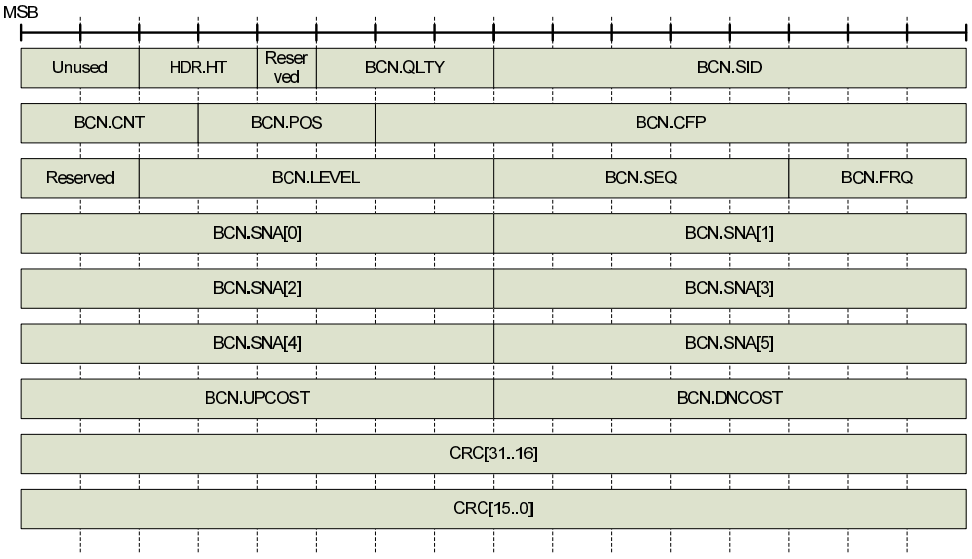

Figure D.4: *Beacon PDU structure.*

- **HDR.HT** - Header type. Either Generic Mac (0), Promotion Needed(1) or Beacon PDU (2).
- **BCN.SID** - Switch Identifier. Switch Identifier of the Switch that is transmitting the current beacon. In case of being the BN, the SID is set to 0.

- **BCN.CNT** - Count. Number of beacon slots per frame.
- **BCN.POS** - Position. Position of the current beacon within the beacon slots period. Position 0 is reserved for the beacon transmitted by the BN.
- **BCN.CFP** - Collision Free Period. Offset for the beginning of the Collision Free period, in case it exist.
- **BCN.SEQ** - Sequence. Sequence number of the current beacon in the beacon super-frame.
- **BCN.FRQ** - Frequency. Transmission frequency of the current beacon.
- **BCN.SNA** - network Address. Network identifier of the network where the current Switch resides.
- **BCN.UPCOST** - Uplink Cost. Total Uplink cost from the current Switch node to the Base Node.
- **BCN.DNCOST** - Downlink Cost. Total Downlink cost from the Base Node to the current Switch.
- **CRC** - Cyclic Redundancy Code. Cyclic Redundancy Code computed based on the Beacon PDU.

Appendix E

Registrantion and promotion process

This section details the MAC procedures that are indicated in PRIME' specification in order to perform a registration to the BN and promote a SN from Terminal to Switch state. This appendix provides a summarized version of what is said in the specification's document for the curious reader.

E.1 Registration process

After a node's boot, it shall start listening for beacon messages. Once it has received at least one beacon, it shall send a REG_REQ (Registration Request) message to the BN in order to get himself included in the subnetwork. Since no PKT.LNID (See Section D.3) has been assigned to it yet, it will send this field filled with digital ones. Additionally, the PKT.SID field must include the Switch the node is registering through.

Once the REG_REQ message arrives to the BN, it has to allocate a unique LNID and associate it to the node requesting the registration. The BN shall compose a REG_RES (Registration Response) message address to the SN including the corresponding LNID in the PKT.LNID field.

Since registration is a three-way process, the SN shall reply to the REG_RES message with a REG_ACK (Registration Acknowledgement). When receiving this third message, the BN considers the registration process as successfully concluded.

Figure E.1 shows the previously described process of a successful registration with all the required messages and including the action of a Switch in the communication diagram.

E.2 Promotion process

If , in contrast with the previous situation, a node is not able to receive any beacon message for a period of time, it shall send a Promotion Needed signal. All registered

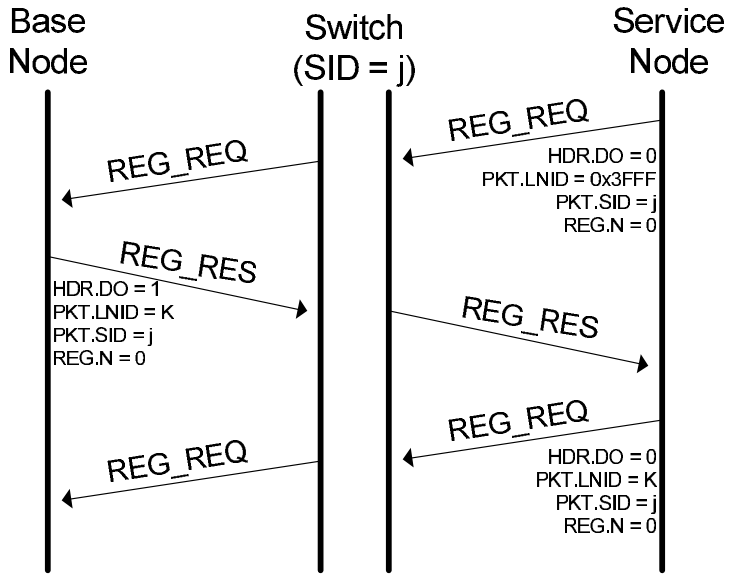

Figure E.1: *Messages exchanged during an accepted registration process of a SN.*

SN that listen to this message must send to the BN A PRO_REQ_S (Promotion Request from SN) message to ask for a promotion to Switch state. Among others, some of the information encapsulate in the promotion request is the quality of the received Promotion Needed message and the EUI-48 address of the disconnected node.

Upon the reception of the PRO_REQ_S message, the BN shall decide whether accept the promotion or not. In the case of receiving several request, it must also decide which one of them is accepted. Concrete criteria for the BN to accept/decline a given request is not detailed in PRIME' specification and is left open to the manufacturer's implementation.

The BN accept the promotion by replying with a PRO_REQ_B (Promotion Request from BN). This message includes the new Switch Identifier that will be used by the promoted node and that has been allocated by the BN.

As in the registration, the promotion process is a three-way handshake that concludes with a PRO_ACK from the new Switch node.

One of the new duties for the Switch is the broadcasting of its information via Beacon messages. However, to do so, some time slots have to be reserved for this purpose in the beacon period. This process is managed with the exchange of BSI (Beacon Slot Information) messages, where the BN indicates to the new Switch which position in the Beacon period it must use.

Figure E.2 shows the previously described process from the Promotion Needed message to the transmission of beacons by the recently promoted Switch.

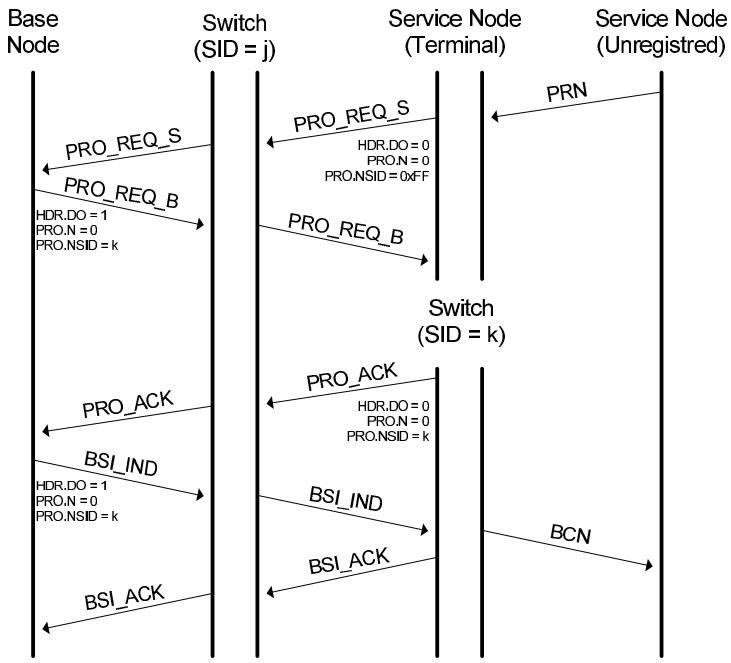

Figure E.2: *Messages exchanged during an accepted promotion process of a SN.*